OUT-OF-PLANE STRENGTH AND BEHAVIOUR OF MASONRY INFILL WALLS

by

Andrew H Smith

Submitted in partial fulfilment of the requirements for
the degree of Master of Applied Science

at

Dalhousie University
Halifax, Nova Scotia
September 2018

TABLE OF CONTENTS

Page

LIST OF TABLES

Table Page

LIST OF FIGURES

Figure Page

ABSTRACT

It has been shown in previous studies that masonry infills with rigid supports through boundary frames display greater out-of-plane strength than their flexural wall counterparts. This increase in strength is due to a mechanism often referred to as “arching action”, where an infill is considered as a three-hinged arch after initial cracking separates the infill into two rotating segments under out-of-lane loading. Any further rotation is restrained by the boundary supports, resulting in in-plane compressive forces and delaying further cracking. The failure mechanism is changed from tension controlled to the inherently stronger compression-controlled failure. The literature review on arching action, however, yielded limited available research results in terms of experimental testing and numerical studies. For design, the current Canadian masonry design standard CSA S304-14 specifies that the first principle mechanics be used for calculating the out-of-plane strength of infills without providing explicit equations. The American masonry standard MSJC 2013, on the other hand, adopts a semi-empirical equation for out-of-plane strength of regular infills.

This study is part of an on-going research study to gain understanding on the out-of-plane strength and behaviour of masonry infills in general and in particular, on the effect of several influential design parameters on the infill strength. The previous phases (Phase I and II) of the study focused on the testing of RC framed concrete masonry infills whereas this study dealt with the steel bounding frames and the design parameters considered were more representative of this frame type. A total of seven steel framed concrete masonry infills were subjected to out-of-plane loading to failure and design parameters included boundary frame condition, prior damage, interfacial gap, and presence of vertical loading. The experimental results were obtained and discussed in terms of load vs. displacement curves, cracking pattern, failure mode, and the vertical and horizontal displacement profiles. The experimental results were then used to evaluate the design parameter effects and determine the adequacy of the existing analytical models.

The experimental results showed that a steel framed infill sustained a significantly lower out-of-plane capacity than a RC framed infill. This is attributed to lower friction at steel to infill interface as evidenced by top infill slip-out that initiated a pre-mature failure that was observed in multiple test specimens. The presence of top beam-to-infill gap resulted in a reduction in strength as the two-way arching was not fully developed as evidenced by different cracking pattern and failure mode observed in the test. Prior in-plane damage caused a reduction in the out-of-plane strength of infills and more severe the prior damage, the greater the reduction. Further, the reduction is more pronounced when the loading causing the damage was maintained during the out-of-plane loading stage. The presence of a vertical load applied on the infill through the frame beam resulted in a reduced out-of-plane strength.

The existing analytical methods were shown to provide inconsistently strength estimate for specimens with RC frames vs. steel frames as none of the models considered the difference in interfacial friction between two materials. In general, the analytical models under-predicted the strength of RC framed infills while over-estimating the strength of the steel framed infills.

LIST OF ABBREVIATIONS AND SYMBOLS USED

ABBREVIATIONS

ASTM	American Society for Testing and Materials
CMU	Concrete Masonry Unit
COV	Covariance
CSA	Canadian Standards Association
HSS	Hollow Structural Section
FEMA	Federal Emergency Management Agency
LVDT	Linear Variable Differential Transformer
MSJC	Masonry Standards Joint Committee
RC	Reinforced Concrete

SYMBOLS

A	Area of diagonal compressive strut
A_b	Area of beam of surrounding frame
A_c	Area of column of surrounding frame
A_e	Effective infill area
C	Compressive thrust force from arching action
d	Length of diagonal compressive strut
E_f	Modulus of elasticity of frame
E_m	Modulus of elasticity of masonry
F_{app}	Maximum applied in-plane load
f'_c	Constant compressive stress in arching action
f'_j	Compressive strength of mortar cubes
f'_m	Compressive strength of infill
f_t	Tensile strength of masonry
f_v	Vertical stress applied to infill
G	Shear modulus
g_o	Deflection in the direction of arching due to axial shortening or gaps

h	Height of the infill
I_b	Moment of inertia of the beam
I_c	Moment of inertia of the column
J	Torsional constant
k_{cr}	Out-of-plane stiffness of infill at the first major crack load
k_i	Out-of-plane stiffness of infill at initial cracking load
k_{ult}	Out-of-plane stiffness of infill at ultimate load
l	Length of the infill
M_r	Moment resistance through arching action
M_{yh}	Moment resistance for horizontal arching (Klingler et al. 1996)
M_{yv}	Moment resistance for vertical arching (Klingler et al. 1996)
P_{cr}	Out-of-plane pressure at the first major crack stage
P_i	Out-of-plane pressure at initial cracking stage
P_f	Axial load applied to infill
P_r	Compressive force introduced due to arching action
P_{res}	Out-of-plane pressure at failure of the infill
P_{ult}	Ultimate pressure of the infill
q_{ult}	Ultimate pressure that an infill can resist
R_1	Reduction factor to account for the prior in-plane damage (Angel 1994)
R_2	Reduction factor for the bounding frame stiffness (Angel 1994)
r	Moment arm between compressive loads in arching action
S	Section modulus
t	Thickness of CMU
w_{eff}	The effective width of diagonal compressive strut as defined by CSA S304-14
w_f	Factored pressure imposed on the infill
x_{yh}	Displacement of the infill corresponding to horizontal arching at failure (Klingler et al. 1996)
x_{yv}	Displacement of the infill corresponding to vertical arching at failure (Klingler et al. 1996)
α_s	Factor which accounts for the relative stiffness of the boundary columns

β_s	Factor which accounts for the relative stiffness of the boundary beams
β_y	Moment coefficient for the moment resistance parallel to the bed joints in elastic plate analysis
β_{y1}	Moment coefficient for the moment resistance normal to the bed joints in elastic plate analysis
γ	Factor accounting for the contact area during arching action
Δ_{cr}	Deflection at the center of the infill at the first major crack stage
Δ_i	Deflection at the center of the infill at initial cracking stage
Δ_o	Additional mid-span deflection due to gaps and axial shortening in arching action
Δ_{res}	Deflection at the center of the infill at failure
Δ_{ult}	Deflection at the center of the infill at peak load
δ	Maximum infill drift
δ_{app}	In-plane deflection at maximum applied in-plane loading
δ_{cr}	Infill drift corresponding to occurrence of first crack
δ_{ult}	In-plane deflection at the peak load
ϕ_m	Safety factor for the reliability of masonry
φ_{st}	Safety factor in determining the stiffness of an infill. CSA S304-14
λ_s	Empirical parameter that is a function of the wall slenderness
θ	Angle between the base of infill wall and the diagonal

ACKNOWLEDGEMENTS

None of this could have been possible without all the hard work, support, encouragement and love by my wife. Thank you for everything and keeping me on the right track.

I would like to express sincere gratitude to my thesis advisor, Dr. Yi Liu. Thank you for believing in me and giving me the opportunity to achieve my academic goals. This thesis would not have been possible without your guidance and patience.

I wish to recognize the financial contributions received from the Canadian Concrete Masonry Producers Association.

Thank you to Brian Kennedy the department technician for not only all his work to build the test specimens, but also for teaching me the skills to build it alongside him.

I would finally like to acknowledge the support I have received from my family; work ethic is hereditary!

CHAPTER 1 INTRODUCTION

1.1 BACKGROUND

Masonry has been used in construction of structures dating back to ancient Egypt pyramids and Roman coliseums. Masonry materials used in construction have developed from early times of natural stone, cut stone, mud brick, to later times of various clay brick products. With the introduction of concrete in the 1900s, masonry was ushered into a new era where concrete block masonry products became a popular choice for construction due to their being more cost efficient than cut stones and less labor intensive than clay brick masonry. In addition, hollow cells unique to concrete block units have allowed the introduction of steel reinforcing in masonry, which allowed masonry to remain competitive with other building materials in both the residential and commercial construction.

The first document dealing with masonry design was introduced in 1953 by the American National Standards Institute, ANSI 41.1 (1953), which formed the basis for conventional design or empirical design of masonry. With development of knowledge of masonry behaviour enabled through more elaborate testing, in the next 30 years till 1980s, masonry design evolved from empirical design largely based on “rules of thumb” to engineering design where forces, moments, and stresses were considered in design rules. From 1980-90s, the “engineered masonry” was designed using Working Stress Design (WSD) approach, also known as Allowable Stress Design (ASD) in both Canada and the US. In the WSD approach, resistance of masonry structures was calculated based on an allowable limit. In 2004, the Canadian masonry design standard S304.1-2004 was published with significant technical changes and limit states based design was adopted where the concept

of load and resistance factor was introduced. In 2005, the American masonry design standard MSJC also adopted limit states based design. The current governing standard for masonry design in Canada is CSA S304-14, whereas in the US the governing standard is MSJC 2013.

1.2 OUT-OF-PLANE BEHAVIOUR OF MASONRY INFILLS

A masonry infilled frame refers to a frame system either made of steel or reinforced concrete with a masonry wall built within. These masonry walls are commonly referred to as masonry infills and they fulfill the function of either partitions for dividing spaces or exterior cladding for completing a building envelope. Previous research (B. Gabrielsen, Kaplan, & Wilton (1975); Hendry (1981)) has shown that when the masonry wall is built tight against the bounding frame, the interaction between the frame and the infill wall will change the behavioural characteristics of the masonry infill. Out-of-plane strength of a masonry wall without tight confinement is dependent on the masonry tensile strength. The confinement around the masonry wall creates a phenomenon called “arching action” in which the bending of the wall introduces an in-plane compressive force which delays cracking and additional arching of the wall. Out-of-plane capacity through “arching action” relies on the compressive strength of masonry as opposed to its tensile strength. The inherently higher compressive strength of masonry than its tensile strength results in much greater out-of-plane capacity of masonry infills than their flexural wall counterparts. While existing studies (Anderson (1984); Angel (1994); Dawe & Seah (1989); R. Flanagan & Bennett (1999); McDowell et al. (1956)) showed the effects of aspect ratio and slenderness ratio of the infill, and the bounding frame rigidity on this arching action, the number of

studies and variations in parameters in each study were insufficient to establish any definable correlations. Several analytical methods were proposed for the calculation of out-of-plane strength of infills, but they were mainly developed based on a limited number of data points and their application in a wide range of infilled frame situations was found to be incomplete.

For design practice, the Canadian masonry design standard CSA S304-14 does not contain any design provisions for the out-of-plane strength of a masonry infill wall, it does however suggest using first principle mechanics for analysis. The American masonry design standard MSJC 2013, on the other hand, employs a semi-empirical strength equation calibrated with limited rest results for the out-of-plane strength of masonry infills. However, the efficacy of the equation in application of various situations of infills and bounding frames has not been thoroughly examined.

More research is in need to provide reliable experimental results that could be used to further understand arching action on the behaviour and strength of masonry infills under out-of-plane loading.

1.3 RESEARCH OBJECTIVES

A multi-phased research program is being conducted at Dalhousie University to investigate the out-of-plane behaviour and strength of masonry infills. This research is a continuation of the work conducted by Sepasdar (2017) and Wang (2017) on reinforced concrete (RC) frames to further the investigation to include steel boundary frames. This research involved an experimental investigation on masonry infills bounded by steel frames with a focus on

the effect of prior in-plane damage, concurrent loading, and boundary support condition on the behaviour of infills. The objectives to be accomplished by this study are as follows:

1. To perform experiment on masonry infilled steel frame specimens subjected to the out-of-plane pressure along with auxiliary tests needed to evaluate the required material properties of the specimen.
2. To analyze the effect of prior in-plane damage, concurrent loading, interfacial gaps, boundary support, and vertical loading on the out-of-plane strength of the masonry infills.
3. To evaluate the difference in behaviour and strength between steel and RC frames by comparing the test results to the previous studies conducted by Sepasdar (2017) and Wang (2017).
4. To assess the adequacy of current analytical models.

1.4 SCOPE

This thesis is comprised of six chapters. Chapter 1 contains the introduction along with research objectives. Chapter 2 presents the literature review on the out-of-plane behaviour of masonry infill walls including experimental analysis, analytical models, and the research conducted thusly at Dalhousie University. Chapter 3 describes the experimental program in detail, including the auxiliary tests, the construction of the masonry infilled streel frames, and the in-plane and out-of-plane test set-ups. Chapter 4 presents the results from both the auxiliary tests performed and the seven, steel framed masonry infilled test specimens. Chapter 5 discusses both the effects of the different infill parameters and comparison of

test results to existing analytical models. Chapter 6 summarizes the findings of the research and recommendations for future work.

CHAPTER 2 LITERATURE REVIEW

2.1 GENERAL

This chapter presents an overview of out-of-plane behaviour, current code practice for design of infills, and previous research on both experimental testing and analytical model development on masonry infills. While this research is focused on steel bounding frames, the literature review included research on both RC and steel bounding frames.

2.2 OUT-OF-PLANE BEHAVIOUR OF MASONRY INFILLS

2.2.1 Arching action

A conventional unreinforced masonry flexural walls (without confinement), when subjected to out-of-plane loading, derives its resistance through the tensile strength of masonry. As the masonry is weak in tension, the flexural strength of such walls is small. In the case of masonry walls bounded by relatively rigid frames, when subjected to out-of-plane loading, the initial crack usually occurs around the mid-height where moment is maximum as it deflects. The crack separates the wall into two rigid segments, with each segment rotating about its end while the other end is rotated to butt against the boundary support, forming a three-hinge arch. **Figure 2.1** illustrates the behaviour of an infill wall supported on two boundaries, creating one-way arching (or also known as a three-hinged arch). If the bounding frame is stiff enough to restrain outward movement of the wall in its plane, in-plane compressive forces are induced (P) as the wall bends out-of-plane. The

external load is then resisted by the internal couple formed by these thrust forces, changing the tension-controlled mechanism for flexural walls to a compression-controlled mechanism for masonry infills. This mechanism, relying on thrust forces generated at two boundaries with the frame, can then be considered as one-way arching action. The arching action has shown to lead to an ultimate capacity, several times greater than that predicted by flexural analysis for masonry infills, see **Appendix A** for detailed flexural strength calculations.

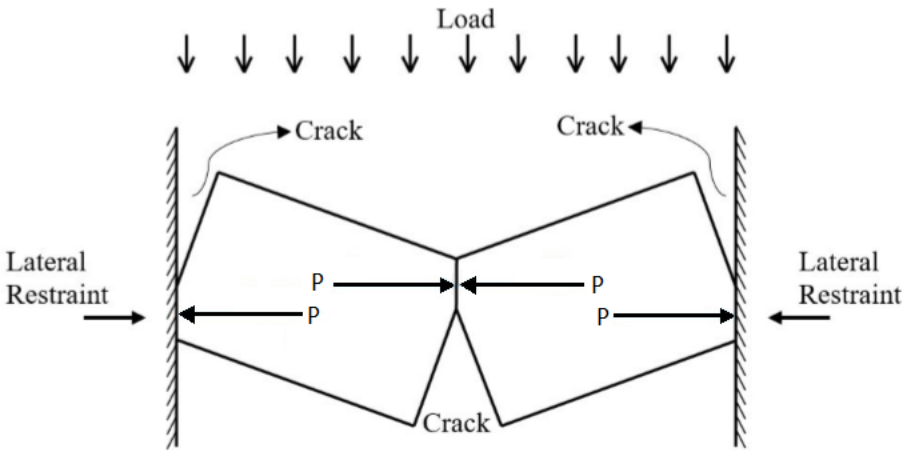

Figure 2.1 Arching action illustration: Three-hinged arch

2.2.2 Analytical models for arching action

While there are several analytical methods developed by various researchers to compute the out-of-plane strength of masonry infills, a close examination indicated that they were more or less derived from two main methodologies. One is based on the first principle mechanics as described previously and mainly for one-way arching. The other methods are empirical or semi-empirical in nature, developed mainly using curve-fitting on either experimental data or numerical simulation results considering two-way arching.

An example based on first principle mechanics of arching is the method proposed by McDowell et al. (1956). Based on simple equilibrium of three-hinged arch, he proposed that the moment resistance (M_r) comes from the moment arm between the internal thrust forces and is as follows:

$$M_r = Cr \qquad [2.1]$$

In which C is the compressive force and r is the moment arm between them. The thrust force, C, can be calculated as a summation of constant stress (f_c) in the compression zone over a contact area of $(1-\gamma)t$ where γ is the percentage of block thickness not in compression and t is the block thickness as shown in **Figure 2.2**.

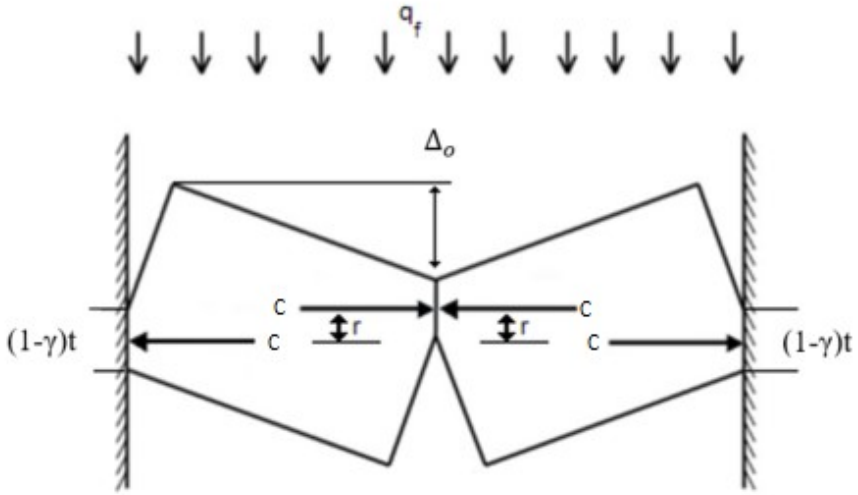

Figure 2.2 Mechanics of rigid arching

$$C = f_c(1-\gamma)t \qquad [2.2]$$

British Design Standard, BS 5628 "Code practice for use of masonry: Structural use of unreinforced masonry" (2005), suggested γ of a value of 0.9, indicating that 0.1t width is in compression. Thus, the ultimate out-of-plane pressure a vertically spanning infill can resist can be calculated as follows Drysdale (2005):

$$w_f = \frac{8C}{h^2}(\gamma t - \Delta_o) \qquad [2.3]$$

Where Δ_o is the wall deflection that may account for gaps between the infill and the frame, axial shortening of the infill, and any movement of supports. The deflection Δ_o due to axial shortening and gaps can be calculated using the following:

$$\Delta_o = \frac{g_o l}{4\gamma t} \qquad [2.4]$$

Where g_o is the axial shortening of the masonry infill in addition to any gaps between the infill and the surrounding frame. Geometry states that the maximum allowable gap between the infill and the surrounding frame for arching to close the gap and undergo arching is as follows:

$$g \leq \frac{4(\gamma t)^2}{l} \qquad [2.5]$$

In the case of two-way arching, the out-of-plane capacity is simply considered as the addition of arching in each direction. This can be achieved by using Eqns [2.2-2.4] to find the capacity in both directions assuming the deflection at the mid-span remains constant. A sample calculation is shown in Appendix A.

While the equation is simple to use, disparities observed between its analytical value and existing experimental results suggested that its inadequacies are attributed to several assumptions used in the method in terms of compression area, wall deflection, and two-way action.

The semi-empirical methods developed mainly in 1980s and 1990s applied the arching action concept to yield line analysis of panels with boundary supports. These methods were developed based on more complex failure modes observed in testing than just a three-hinged arch and thus are considered more advanced. One representative method was developed by Dawe & Seah (1989). They tested nine large-scale unreinforced infill walls bounded by a steel frame. Results from the tests and followed numerical studies led to the development of two semi-empirical relationships. The first relationship is for infills supported on three sides and free at the top (eqn. [2.6]), while the second relationship is for infills supported on all four sides (eqn. [2.7]).

$$q_{ult} = 800(f'_m)^{0.75} t^2 \alpha_s / L^{2.5} \quad [2.6]$$

$$q_{ult} = 800(f'_m)^{0.75} t^2 \left\{ \frac{\alpha_s}{l^{2.5}} + \frac{\beta_s}{h^{2.5}} \right\} \quad [2.7]$$

Where f'_m is the masonry compressive strength (*MPa*), l and h are the length (*mm*) and height (*mm*) of the infill respectively. The gross cross-section thickness of the infill is represented by t, and α_s and β_s account for the relative stiffness of the boundary columns and beams.

$$\alpha_s = \frac{1}{h}(EI_c h^2 + GJ_c th)^{0.25} \leq 50 \quad [2.8]$$

$$\beta_s = \frac{1}{l}(EI_b l^2 + GJ_b tl)^{0.25} \leq 50 \quad [2.9]$$

Where E and G are the elastic and shear modulus of masonry (MPa); I is the moment of inertia (mm^4), and J is the torsional constant (mm^4) of the column or beam denoted by c and b respectively.

This model was later modified by Flanagan & Bennett (1999) through calibration with additional test results from Angel et al. (1994), Flanagan & Bennett (1999), and Frederiksen (1992) as follows:

$$q_{ult} = 729(f'_m)^{0.75} t^2 \left\{\frac{\alpha_s}{l^{2.5}} + \frac{\beta_s}{h^{2.5}}\right\} \quad [2.10]$$

In which the parameters α_s and β_s are simplified as follows

$$\alpha_s = \frac{1}{h}(EI_c h^2)^{0.25} \leq 50 \quad [2.11]$$

$$\beta_s = \frac{1}{l}(EI_b l^2)^{0.25} \leq 50 \quad [2.12]$$

Flanagan & Bennett (1999) recommended that for frame members commonly encountered in practice, their torsional property values are much smaller than their flexural rigidity values and thus simplification of α and β terms is acceptable. Further, for walls with low slenderness ratios, (i.e. less than 8), the thickness of the infill should be taken as 1/8 of the infill height. The test results also led to empirical relationship for the deflection of the

center of the infill wall at peak load for different slenderness ratios and is expressed as follows:

$$\frac{\Delta_{ult}}{h} = \frac{0.002(h/t)}{1+\sqrt{1-0.001(h/t)^2}} \quad [2.13]$$

Based on the yield line analysis, Klinger et al. (1996) expanded a model proposed by Cohen & Laing (1956) on one-way arching to include the effects of two-way arching. The proposed expression for out-of-plane pressure is as follows:

$$q = \frac{8}{h^2 l}\left\{M_{yv}[(l-h)+h\ln(2)] + M_{yh}\left(\frac{x_{yv}}{x_{yh}}\right)\ln\left(\frac{1}{1-h/2}\right)l\right\} \quad [2.14]$$

In which M_{yv} is the moment resistance for vertical arching and is calculated as:

$$M_{yv} = \frac{0.85f'_m}{4}\left(t - x_{yv}\right)^2 \quad [2.15]$$

Where x_{yv} is the displacement of the infill corresponding to vertical arching at failure and is calculated as:

$$x_{yv} = \frac{tf'_m}{1000E\left[1-\frac{h}{2\sqrt{(h/2)^2+t^2}}\right]} \quad [2.16]$$

The moment resistance for horizontal arching and the displacement of the infill corresponding to horizontal arching are denoted by h instead of v. These values can be calculated by using Eqn. [2.15] and Eqn. [2.16] by replacing h with l.

Moghaddam & Goudarzi (2010) proposed two equations for calculating the out-of-plane strength of infills as the lesser of masonry crushing at boundaries (q_{cr}) and transverse instability (q_{max}). It was proposed that the strength q_{cr} was a function of the infill slenderness ratio, masonry compressive strength and elastic modulus, and the ratio of the frame stiffness to the masonry stiffness denoted as (α). The transverse instability is the resulting failure from large transverse deflection.

$$q_r = min\left(\begin{array}{c} q_{cr} = \left[0.85 - \left(0.12 + \frac{0.045}{\alpha}\right)\frac{f'_m}{E_m}\lambda^2\right]\frac{f'_m}{\lambda^2} \\ q_{max} = \frac{0.18E_m}{\left(0.12 + \frac{0.045}{\alpha}\right)\lambda^4} \end{array}\right) \qquad [2.17]$$

where α is shown in [2.18] and the support frame stiffness (K) is shown in [2.19]. The remaining terms are as defined before.

$$\alpha = \frac{K}{(E_m t l/h)} \qquad [2.18]$$

$$K = \frac{384E_f I_b}{l^3} \qquad [2.19]$$

2.2.3 Experimental studies

The following sections focus on reviewing experimental studies in the available literature that investigated parameters either similar or relevant to this research.

2.2.3.1 Masonry infilled frames with gaps

Frederiksen (1992) tested sixteen clay brick infills bounded by a steel frame under out-of-plane loading. The purpose of the experimental program was to study the effect of the infill-to-frame interfacial conditions. Instead of using mortar at the infill-frame interface, multiple different materials were used. The test results showed that the boundary interface filling with different materials does not influence the out-of-plane strength and cracking pattern as long as the infill is in tight contact with the surrounding frame.

Gabrielsen et al. (1975) investigated the effect of top beam-to-infill gap on the out-of-plane strength of masonry infills by testing two infills with a top gap. Two gap sizes of 0.1 *in* (2.54 *mm*), and 0.2 *in* (5.08 *mm*) were considered. When compared with specimens without gaps, it was found that gapped infills were still stronger than flexural walls or cantilevered walls. However, the presence of the gap caused the infills to resist 17% and 12.5% of the pressure resisted by an infill without gaps.

Dafnis et al. (2002) studied the effect of gaps on arching behaviour and stability using an experimental program consisting of six specimens loaded through a shake table. It was reported that the relative displacement of the gapped specimens was greater than non-gapped specimens, but for top gaps 3 *mm* or smaller arching action was still achieved.

Wang (2017) conducted two tests on masonry infills bounded by a RC frame with interfacial gaps. One specimen had a 10 *mm* top gap between the infill and the top boundary beam whereas the other had 5 *mm* gaps on both the left and right column to infill boundaries. The presence of the top gap on the RC framed specimen resulted in a 72% reduction in ultimate capacity as well as a severe reduction in initial stiffness. The deformation of the infill did not close the gap, therefore no vertical arching occurred. The reduction in ultimate capacity for the side gapped specimen was 45% and there was a reduction in initial stiffness but not to the same extent as the top gap. The specimen demonstrated one-way arching in the vertical direction. These results suggested that the presence of gap can alter the failure mechanism; the vertical arching provides more strength and stiffness than the horizontal arching; and thus top gap is more detrimental to infill strength than side gap.

2.2.3.2 Masonry infilled frames with prior damage

Angel (1994) studied the effect of prior in-plane damage on the out-of-plane strength of masonry infills. The experimental program consisted of seven masonry infilled RC frames. The specimen was loaded to a designated damage level under in-plane loading first and loading was removed. The out-of-plane loading was then applied to failure of the specimen. He proposed using a reduction factor to account for the prior in-plane damage. Based on analysis of the test results through curve-fitting, the final model including effect of prior damage and slenderness ratio is expressed as follows:

$$q = \frac{2f'_m}{\left(h/t\right)} R_1 R_2 \lambda_s \qquad [2.20]$$

Where λ_s is a dimensionless empirical parameter that is a function of the wall slenderness, R_1 is the prior in-plane damage reduction factor and R_2 is a reduction factor for the bounding frame stiffness obtained from:

$$R_1 = \left[1.08 - 0.015\left(\frac{h}{t}\right) - 0.00049\left(\frac{h}{t}\right)^2 + 0.000013\left(\frac{h}{t}\right)^3\right]^{\frac{\delta}{2\delta_{cr}}} \quad [2.21]$$

$$R_2 = 0.357 + 2.49 \times 10^{-14} EI \leq 1.0 \quad [2.22]$$

In which δ is the maximum drift the infill has previously sustained and δ_{cr} is the drift corresponding to the occurrence of the first crack in the infill under in-plane loading. The parameter λ for infills with a slenderness ratio between 10 and 30 can be calculated as:

$$\lambda_s = 0.154 exp\left(-0.0985\frac{h}{t}\right) \quad [2.23]$$

This method for determining the out-of-plane strength of an infill with prior in-plane damage was adopted by Federal Emergency Management Agency (FEMA 273) as shown:

$$q = \frac{0.7 f'_m}{\left(h/t\right)}\lambda \quad [2.24]$$

This formulation removes the two reduction factors by presenting a lower-bound strength equation since FEMA 273 is for seismic rehabilitation and there would be no data for story drifts.

Flanagan & Bennett (1999) tested a single-story clay tile infilled steel frame for a multitude of parameters including under in-plane loading, out-of-plane loading, and the combination

of both. The results showed that prior in-plane loading damage resulted in strength reduction and greater deflections for out-of-plane loading. However, it was noted that arching action was still achieved which allowed the infill to maintain a higher capacity than a flexural wall. On the other hand, the out-of-plane loading increased the in-plane stiffness of the infill while leaving the strength relatively unaltered.

Morandi et al. (2014) studied the response of RC framed masonry clay brick infills to cyclic out-of-plane loading using six hydraulics jacks spread out over the wall. It was confirmed that the out-of-plane strength of an infill was affected by in-plane damage although no relationship was provided.

Furtado et al. (2016) investigated the effect of prior in-plane damage to the out-of-plane strength of RC framed masonry infills. The experimental program consisted of three specimens and it was found that an undamaged infill had four times greater strength than the damaged specimens. The prior in-plane damage resulted in significantly lower initial stiffness and affected the cracking pattern and failure mode in specimens.

Sepasdar (2017) tested two RC framed concrete masonry infills with prior damage as the phase one of this research framework. The units and mortar were of similar properties to this study. One specimen was an out-of-plane test conducted with prior in-plane damage. The specimen was loaded in-plane to the occurrence of first major diagonal crack which was at the 75% of its ultimate in-plane capacity. The load was then removed, and the out-of-plane load was applied. Results showed that the prior in-plane damage resulted in a 33% reduction in the out-of-plane capacity. The second specimen was an in-plane test conducted with out-of-plane damage. The prior out-of-plane damage was caused by loading the

specimen to 40% of its out-of-plane capacity generating a horizontal crack at the infill mid-height. Results showed that the out-of-plane damage occurred at 40% its out-of-plane capacity, had little effect on the in-plane strength.

As the phase two of this research framework, Wang (2017) conducted a test on a RC framed concrete masonry infill with prior in-plane loading up to its ultimate in-plane capacity before being tested for its out-of-plane strength. In this case, the specimen which has reached its ultimate in-plane capacity still showed about 57% strength remaining when subjected to out-of-plane loading.

2.2.3.3 Masonry infilled frames subjected to vertical loading

There have not been studies on vertical loading effect in the exact context of masonry infills subjected to out-of-plane loading. One relevant literature found was on work conducted by Griffith et al. (2007) who studied eight clay brick masonry wall specimens subjected to an out-of-plane pressure to study the horizontal arching. The specimen was fix-supported on the sides and simply supported at the top and bottom. Four of the test specimens had different levels of axial load applied to a timber beam resting on the masonry wall. During the loading, the specimen was intended to develop arching in the horizontal direction. The results showed that the axial loads resulted in an increase in the out-of-plane strength.

2.2.3.4 Slenderness ratio

Anderson (1984) ran an experimental program in which he tested masonry wall panels subjected to out-of-plane loading to a variety of slenderness ratios. It was determined that the out-of-plane strength decreased with rising slenderness ratios. Masonry panels with

slenderness ratios in the range of 35-40 failed due to panel instability, whereas lower slenderness ratios had a failure mode of boundary crushing due to arching action.

Angel (1994) tested multiple masonry infilled RC frames with both clay brick and concrete masonry blocks. Two of his specimens were designed to test the influence of slenderness ratios. He concluded that when the slenderness ratio (*h/t*) was reduced from 34 to 14 (50% reduction) the out-of-plane strength increased by more than a factor of seven. He also determined that when the slenderness ratio was greater than 30, arching action did not have a strong influence on the strength of the infill.

2.2.3.5 Frame rigidity

Qualitative experiments by both Gabrielsen & Wilton (1974) and Monk (1958) concluded that a flexible boundary frame resulted in a reduced out-of-plane strength as compared to infills with a rigid boundary frame.

Dawe & Seah (1989) investigated the effect of frame stiffness in steel framed masonry infills and, in particular, different column stiffnesses as they applied out-of-plane pressure using an airbag system. They determined that both the flexural stiffness and the torsional stiffness of the columns had an effect on the out-of-plane strength of the infills. They used this alongside with other experimental results to propose an equation that includes the effects of flexural and torsional stiffness.

Flanagan & Bennett (1999) did an analysis on the analytical model proposed by Dawe and Seah (1989) using test results and determined that the flexural rigidity of the boundary

frame has a much greater impact on the out-of-plane strength than the almost negligible torsional rigidity.

Angel (1994) investigated the influence of boundary frame stiffness on the out-of-plane strength of infills using numerical simulations. What he determined was that a stiffer boundary frame will benefit the strength of the infill but that when a boundary frame stiffness (EI) exceeds $2.6\text{x}10^{13}$ *N-mm*^{2} the added benefit in negligent. Angel (1994) used these simulations to develop a flexural stiffness reduction factor.

2.2.4 Design standards

As mentioned previously, the current Canadian masonry design standard CSA S304-14 does not contain any design provisions for the out-of-plane strength of a masonry infill wall, it does however permits use of first principle mechanics for analysis.

The American masonry design standard, MSJC 2013, adopts the out of plane capacity of masonry infills proposed by Flanagan & Bennett (1999) which was originally developed by Dawe & Seah (1989), as follows:

$$q_{ult} = 105(f'_m)^{0.75} t^2 \left\{ \frac{\alpha}{l^{2.5}} + \frac{\beta}{h^{2.5}} \right\} \qquad [2.25]$$

Where α and β are defined by Eqn. [2.11] and Eqn. [2.12] but now both have an upper limit of 35 instead of 50. The thickness of the infill is limited to *h*/8. It must be noted that in these equations, imperial units are used (*psf*, *lb* and *in*).

CHAPTER 3 EXPERIMENTAL PROGRAM

3.1 GENERAL

As mentioned earlier, this study is the continuation of an ongoing research project on the behaviour and strength of masonry infilled frames subjected to out-of-plane loading. The overall objective of this research is to quantify the effect of arching action on the strength of masonry walls in the context of steel/RC framed masonry infills that have a wide range of geometric and material properties. Under this framework, two phases of study have been completed. Phase one of this research conducted by Sepasdar (2017) was focused on the behaviour of RC framed masonry infills with parameters of infill openings and prior in-plane damage. The second phase conducted by Wang (2017) continued to focus on the RC framed masonry infills but extended the range and variation of parameters of infill openings and prior in-plane damage, and also added interfacial gaps as a parameter. One specimen with a steel framed masonry infills was also tested. Built upon the information and results obtained thus far, this study is focused on steel framed masonry infills and expanding parameters to include interfacial gap, prior in-plane/out-of-plane damage, concurrent lateral and out-of-plane loading, combined vertical and out-of-plane loading, and boundary condition of bounding frames.

In addition to the masonry infilled frame specimens, the experimental program also included auxiliary tests to determine the material properties of concrete masonry units (CMU), masonry mortar, masonry prisms, and steel sections used for the frame. The

following sections present a detailed description of the infill specimens, test set-up, test procedure, as well as auxiliary tests conducted on the materials.

3.2 INFILLED FRAME SPECIMENS

Table 3.1 presents a summary of the test specimens with description of their parameters. A total of seven infilled frame specimens were tested in this program (labelled 2 to 7). Note that Specimen 1 was tested by Wang (2017) as a control specimen and was included in the table for comparison purpose in later sections.

Table 3.1 Summary of steel frame concrete masonry infill specimens

Number	Spec. ID	Parameter Description
1	IF-S-C*	Control specimen
2	IF-S-FS	Bounding frame bottom beam fully supported
3	IF-S-SW	Bounding beams with stiffeners
4	IF-S-TG	10 *mm* top gap (to the frame top beam)
5	IF-S-D1	Out-of-plane test with prior in-plane damage
6	IF-S-D2	In-plane test with prior out-of-plane damage
7	IF-S-CC	Concurrent in-plane and out-of-plane loading
8	IF-S-VL	Concurrent vertical and out-of-plane loading

Specimens 1 to 3 were used to investigate the effect of boundary conditions of bounding frames. It was thought that for steel bounding frames made up of W sections, the stiffness of bounding frames may be more easily affected by boundary conditions, in comparison to a concrete solid section, which in turn will affect the infill strength. Specimen 1 had the

frame bottom beam supported only at the two column locations whereas Specimen 2 had the frame bottom beam fully supported along its length. Specimen 3 added web stiffeners to frame beams based on Specimen 2's setup. Specimen 4 (IF-S-TG) had a 10 *mm* gap employed at the infill-to-frame-top-beam interface. This specimen was used to 1) evaluate the interfacial gap effect on the infill strength and 2) compare with a RC specimen with a 10 *mm* top gap tested by Wang (2017). Specimens 5 and 6 were used to study the effect of prior in-plane/out-of-plane damage on the out-of-plane/in-plane capacity of infilled frames. In this case, an in-plane/out-of-plane load was first applied to a prescribed level to generate the desired damage in the infill and then the load was removed, the out-of-plane/in-plane loading was subsequently applied to the failure of the infilled specimens. Specimens 7 and 8 were used to investigate the effect of loading application on the infill strength. For Specimen 7, an in-plane load was applied first to a level same as for Specimen 5 but was then held constant while the out-of-plane loading was applied to the failure of the specimen. This specimen can be compared with Specimen 5 to gain insights on how damage as well as additional stresses from the in-plane loading, affect the infill out-of-plane strength. For Specimen 8, a vertical loading was applied first to the infill through the bounding frame top beam to a designated level and was held constant while the out-of-plane loading was applied till the failure of the specimen. This specimen was used to study the effect of presence of vertical gravity loading on the infill out-of-plane strength.

3.2.1 Specimen geometry

The steel frame for all infill specimens consisted of four weld-connected W150x30 (G40.21 350W) sections. The physical dimensions of W150x30 (width and height) are

similar to the concrete members used in the case of RC frames and thus was selected to construct steel frames. As well, to compare with previous results obtained for RC framed infills, the geometry of infills was kept the same and the resulting dimensions of the steel framed specimens is shown in **Figure 3.1**.

The concrete masonry infills were constructed using custom made half-scale standard 200 *mm* CMUs laid in a running bond. All the concrete masonry infills were un-reinforced and un-grouted. The infill geometry yielded a slenderness ratio (h/t) of 10.9 and a height to length aspect ratio of 0.726. The measured average dimensions of the half scale CMUs in the form of a stretcher and end block are shown in **Figure 3.2**. All of CMUs were fabricated at a custom concrete block manufacturing plant in Ontario and they have also been used in the first two phases of the research.

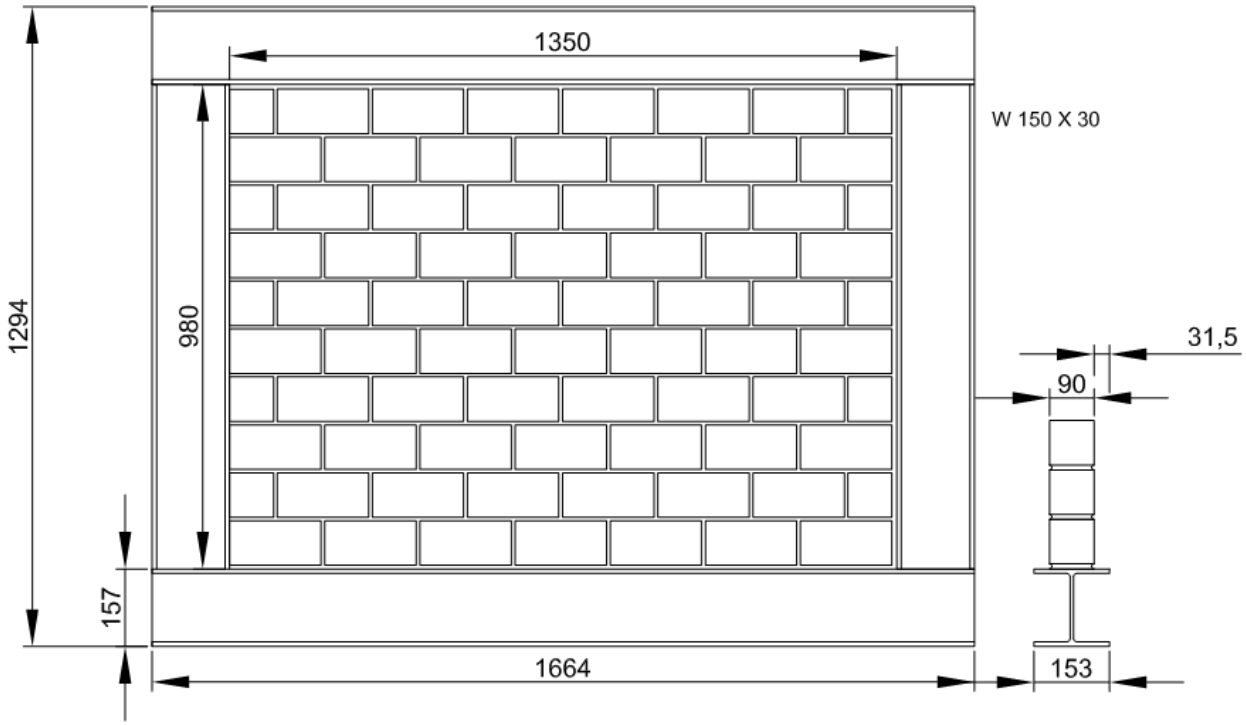

Figure 3.1 Out-of-plane test specimen dimensions

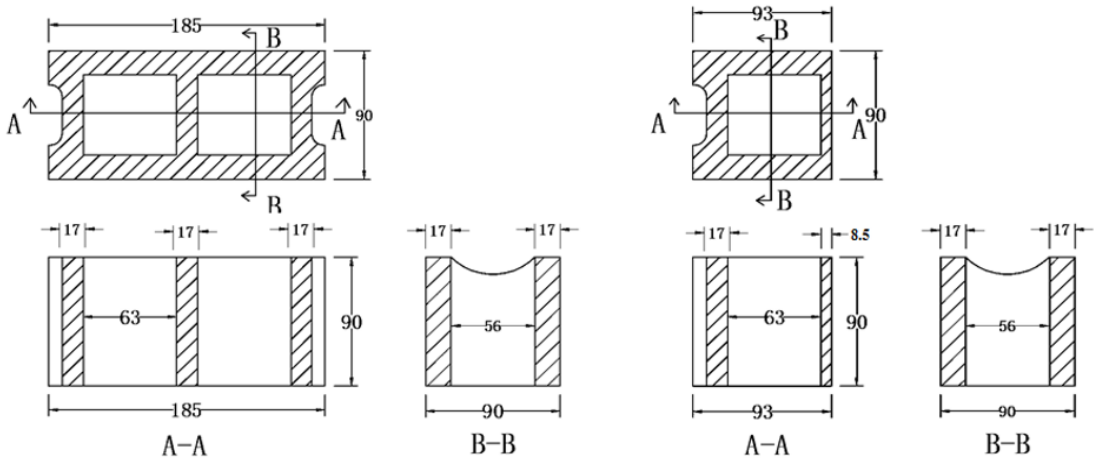

Figure 3.2 Measured average dimensions of half-scale CMU *(dimensions in mm)*

3.2.2 Construction of the steel frame and masonry infill

The infilled specimens were constructed in the Heavy Structures Laboratory in the Department of Civil and Resource Engineering. The steel frames were constructed first. As seen in **Figure 3.3(a) and Figure 3.3(b)**, the columns were placed and secured between the top and bottom beams and welded in place using a 6 *mm* fillet weld on both side of the column web. **Figure 3.3(c)** shows bolt holes that were cut in the top and bottom beam web with a plasma cutter and these holes were used to enable connection with the reaction frame which housed the air bag. The bottom beam also had holes cut on the bottom flange on each side of the web below each column. These holes were needed for connecting the frame to the supporting base beam which was in turn secured through the strong testing floor.

(a)

(b)

(c)

Figure 3.3 a) Steel boundary frame used for test specimens b) Fillet weld used for connecting the column to beam, c) Plasma cut holes in steel boundary frame for connections

Following the construction of steel frames, the concrete masonry infill walls were built by a certified mason to the standards of construction practice. The construction was divided into two phases. Phase 1 was completed on March 31, 2017, consisting of specimens IF-S-TG, IF-S-FS and IF-S-D1 and Phase 2 was completed on October 4, 2017, consisting of the remainder of the test specimens. Note that after the testing of Phase 1 specimens, the steel frames showed no signs of yielding, the stress (confirmed by computer modeling) was well below the yielding stress. Therefore, these steel frames were re-used for Phase 2 specimens.

During the infill wall construction, a layer of mortar was first laid on the steel beam (see **Figure 3.4 (a))** as the initial bed joint to enable a smooth surface and bond between the frame and the first course of masonry. For each masonry course, the mortar was applied on the face shells of the CMUs to form the bed joints and to their webs to form the head joint as shown in **Figure 3.4 (b)**. The thickness of the mortar between blocks was maintained at 10 *mm* using a 10 *mm* flat bar as a gauge. Each course was checked to be level and plumb after the construction. At every three courses, the head joints were troweled for a smooth finish (see **Figure 3.4 (c)**). The final course (underneath the top beam) was applied with generous amounts of mortar and delicately placed in position (see **Figure 3.4 (d)**). For specimen IF-S-TG which had a 10 *mm* top gap, each layer of mortar was reduced accordingly to achieve the gap and there was no mortar placed between the top course and the boundary frame. When the infill was constructed, it was wrapped in wet burlap to aid in the curing process (**Figure 3.4 (e)**), and then a protective plastic wrap was used to seal in the moisture (**Figure 3.4 (f)**). Alongside the test specimens, masonry prisms and mortar

cubes were built to determine the material properties in the later auxiliary tests. All specimens were moisture cured for 28 days and followed with air curing till the day of test.

Figure 3.4 Construction of concrete masonry infills

3.3 TEST SET-UP

Two test set-ups for out-of-plane loading were used and the difference in them lied in the steel bottom beam support. The out-of-plane test set-up used by Wang (2017) for specimen IF-S-C is shown in **Figure 3.5** where the steel frame was supported on two I-shaped steel members running in the perpendicular direction. These supporting members were then bolted through the strong floor. As can be seen, this set-up will leave the steel bottom beam unsupported along its length. It was felt that unlike RC frames with solid concrete sections, steel frames with W sections are more prone to bending and torsional deformations.

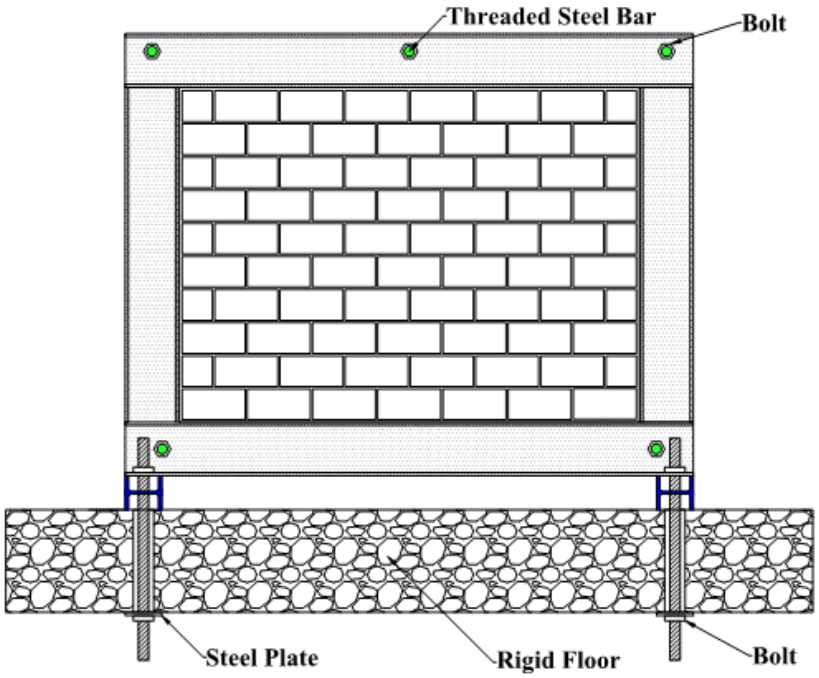

Figure 3.5 Initial out-of-plane test set-up

Therefore, in the second test set-up as seen in **Figure 3.6**, the steel frame was supported along its length on a base beam which was in turn bolted through the strong floor. Also

note that the concrete frames in first two phases of experimental work was secured directly through the strong floor (see **Figure 3.7**).

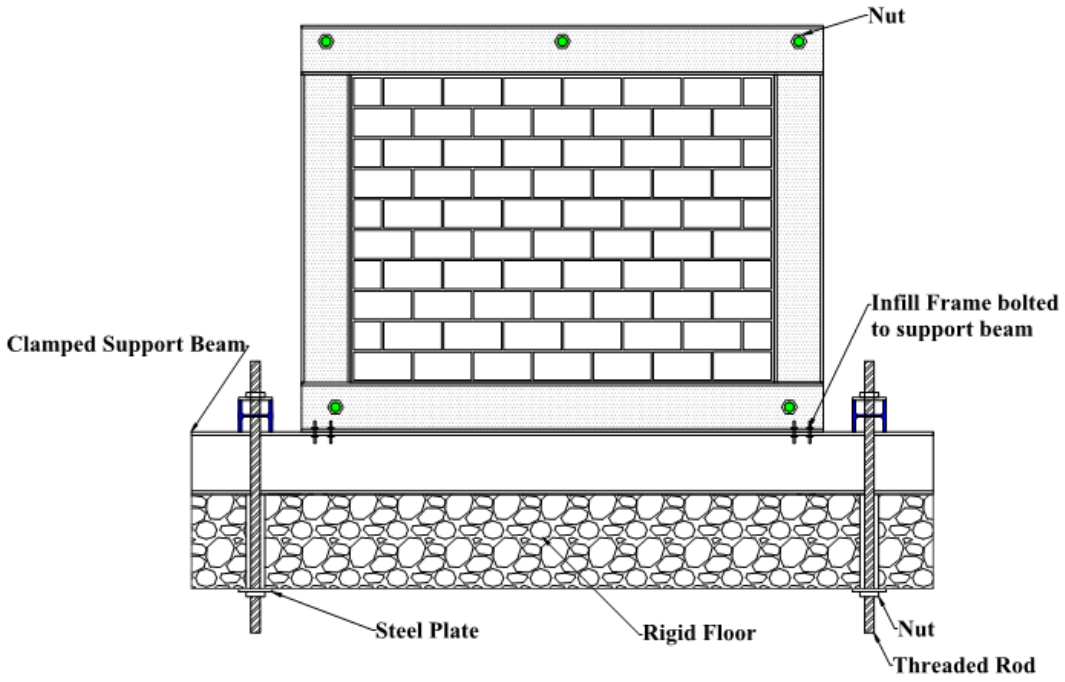

Figure 3.6 Second out-of-plane infill frame set-up

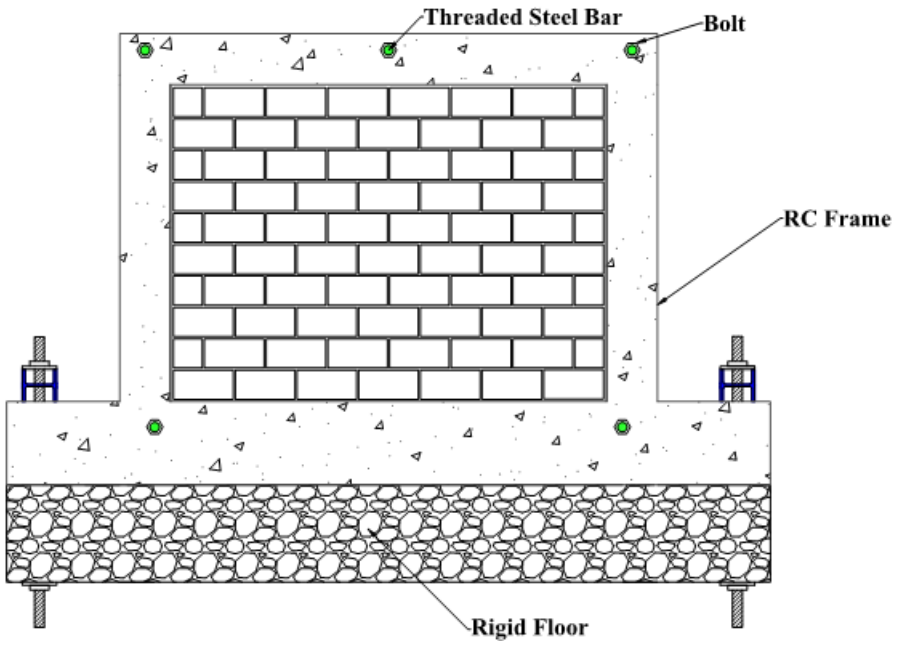

Figure 3.7 Out-of-plane RC infill frame set-up

For Specimens IF-S-SW (Stiffened Web) and IF-S-VL (Vertical Load), web stiffeners were employed on the top and bottom beams. The stiffeners, made from rectangular HSS 25x12x3.2 sections, were welded to the top and bottom flanges and the web of the steel beam as shown in **Figure 3.8**. For specimen IF-S-SW, the stiffeners were used to study the effect of stiffening beams on the arching action. The middle stiffener on the top beam was offset slightly to accommodate the reaction frame bolted connection. For specimen IF-S-VL, the stiffeners were needed at the two points of vertical load application along the top beam to avoid web buckling.

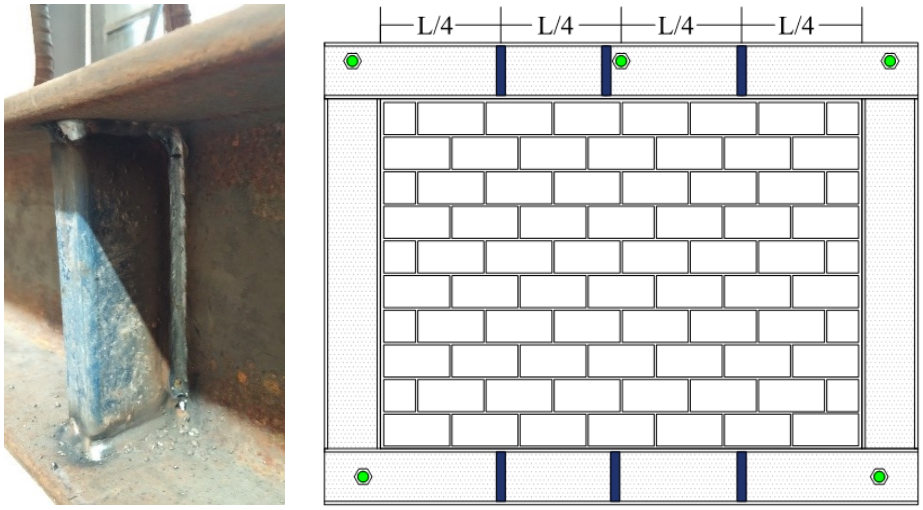

Figure 3.8 Stiffener and stiffener locations for IF-S-SW

3.3.1 Out-of-plane loading

An air bag was used to apply the out-of-plane pressure to the infill. This method of loading was also used in Phase 1 and 2 of this research. The air bag was housed in a reaction frame which was built from plywood board stiffened with HSS 114x114x4.8 steel members as

shown in **Figure 3.9 (a)**. The vertical HSS members spaced at 360 *mm*, were welded to horizontal HSS members at the top and bottom to form a rigid stiffening system. The top horizontal HSS member has holes drilled through to enable connection between the reaction frame and the steel bounding frame. Similarly, the connection between the reaction frame and the steel frame was also provided through two bolts on two channel stub members which were welded on the bottom horizontal HSS member.

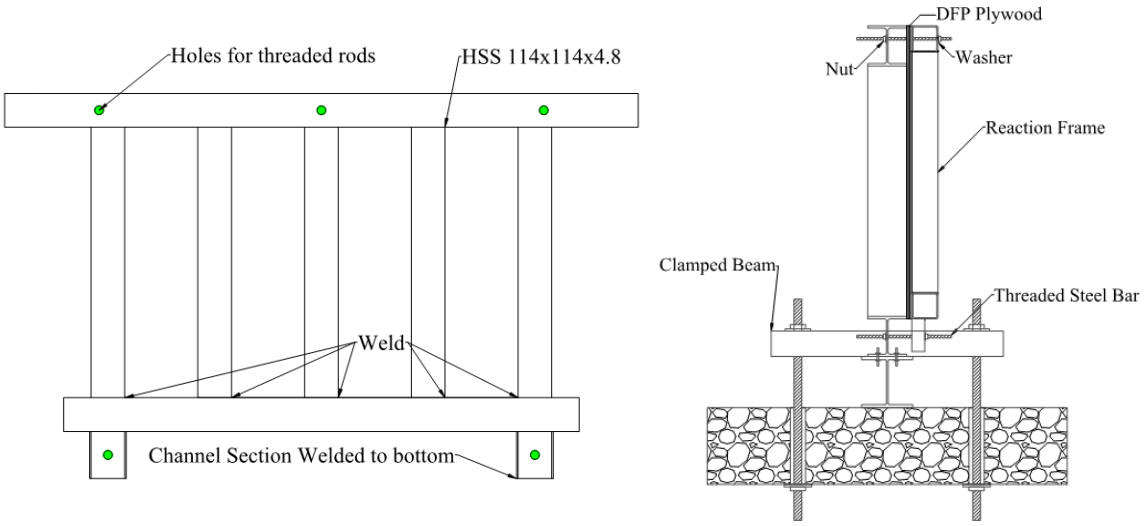

Figure 3.9 a) Steel reaction frame b) Air bag attachment system

As can be seen in **Figure 3.9 (b)**, this loading set-up resulted in a self-equilibrating system. The air bag was sandwiched between the infill and the plywood board supported by the reaction frame. The reaction frame and the infilled specimen were connected using 5 threaded rods. The airbag was connected to an air compressor through a hose. The air compressor was fitted with a pressure transducer to record pressure data as well as a pressure gauge.

For each out-of-plane test, a total of six linear variable differential transformers (LVDTs) were used to record the out-of-plane displacement of the infilled frame specimen. As seen in **Figure 3.10**, five LVDTs were mounted in the vicinity of infill center to measure the infill displacement whereas the sixth LVDT was used to measure either the deflection of the steel flange (see **Figure 3.10(b)**) or the out-of-plane displacement of the infill at the top center.

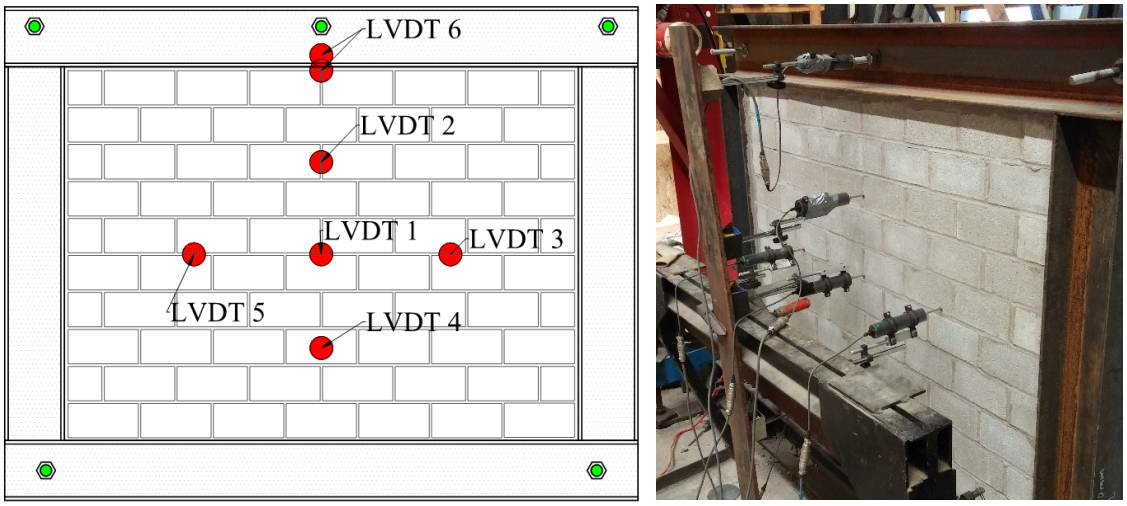

(a) (b)

Figure 3.10 a) Location of LVDTs b) Picture of test set-up

3.3.2 In-plane loading

For Specimen IF-S-D1 and IF-S-D2, in-plane loading was also required. The lateral in-plane loading set-up is shown in **Figure 3.11**. The infilled frame specimen was supported on a steel base beam which was clamped to the strong floor. The base beam was further braced against any lateral movement using hydraulic jacks which were attached to the columns of an independent reaction frame. The in-plane loading was applied using a 250 *kN* hydraulic jack which was reacted against the same independent reaction frame. At the

head of the hydraulic jack, a load cell was used to measure the in-plane force. For each in-plane test, two LVDTs were used to record the in-plane displacement, as shown in **Figure 3.11**. The difference in the two LVDT readings was calculated and used as the lateral displacement of the infilled frame.

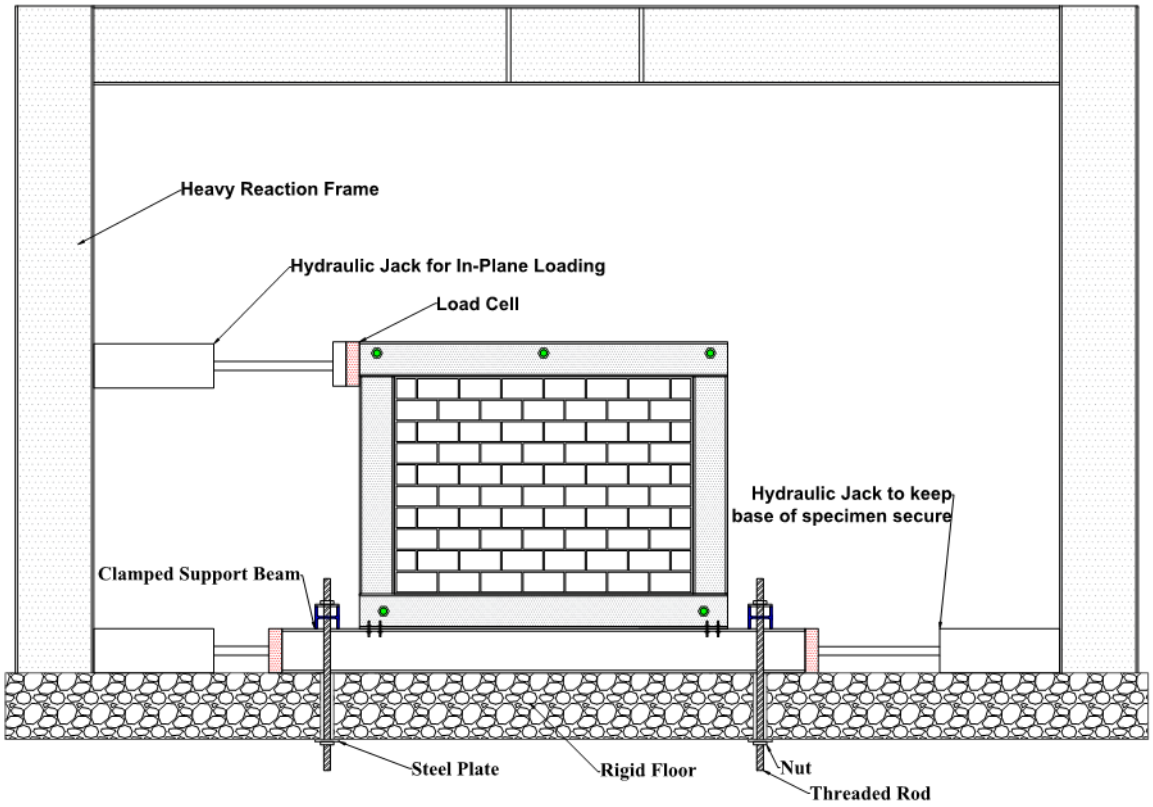

Figure 3.11 In-plane loading test set-up

3.3.3 Vertical loading

For Specimen IF-S-VL, vertical loading was applied in combination with out-of-plane loading. As shown in **Figure 3.12**, the vertical loading was applied using a hydraulic jack through a spreader beam to form a two-point loading scheme onto the specimen. The

spreader beam was made from a steel HSS 102x76x6.4 member which rested on two circular steel bars located at the third point of the infill. Underneath the two point loads, web stiffeners were provided to prevent the web of the steel frame from premature buckling. A vertical load of 100 *kN* was used for this test and it represents a fifth of the axial capacity of the infill calculated as the cross-sectional compressive capacity.

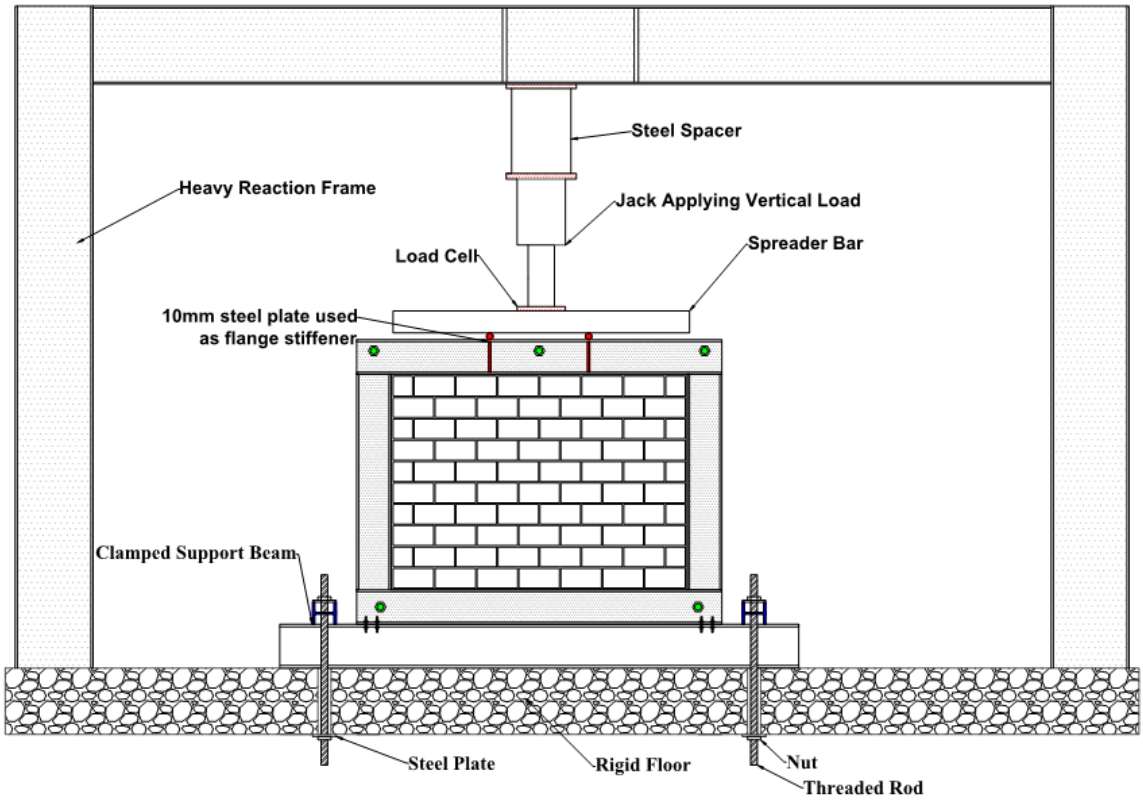

Figure 3.12 Vertical loading test set-up

3.4 TESTING PROCEEDURES

3.4.1 Out-of-plane testing

The infilled frame specimen was carefully placed on and then bolted to the support base beam. Following this, the air bag assembly (air bag and reaction frame) was attached to the

infill and connected to the infilled frame using the nuts and threaded steel rods. The LVDTs were mounted at designed locations and checked to ensure they worked properly before being zeroed at the beginning of data recording. The air bag pressure was applied at a rate of 1.5 *kPa* per minute until the failure of the specimen. Both the displacement and load were recorded at a 0.1 second interval using an electronic data acquisition system. During each test, the cracking pattern, cracking load, failure mode, and ultimate load were monitored and recorded throughout the loading history.

3.4.2 In-plane testing

During the in-plane loading, the test specimens were loaded at a rate of 6 *kN* per minute until the desired damage level was achieved. Specimen IF-S-D1 was loaded in-plane until a major diagonal crack was formed, then the load was removed, and the infill was subsequently subjected to out-of-plane loading to failure. Specimen IF-S-D2 was loaded out-of-plane until a mid-height crack was formed, after which point, the out-of-plane loading was removed, and the in-plane load was applied till the failure of the specimen. For specimen IF-S-CC, the in-plane load was applied to the same cracking load as Specimen IF-S-D1 and held constant while the wall was tested out-of-plane until failure. In all cases, the in-plane displacement and the loading were recorded at a 0.1 second interval using an electronic data acquisition system.

3.4.3 Vertical testing

Referring to **Figure 3.12**, after the specimen was positioned in place, the vertical load assembly were carefully aligned with and centered to the specimen. A 200 *kN* hydraulic jack, placed between the steel spacer and the spreader beam, was used to apply the vertical load. The rate of load application was about 20 *kN* per minute till the load of 100 *kN* was reached. This load was held constant as the infill was then subjected to out-of-plane loading to failure.

3.5 AUXILLIARY TESTS

Auxiliary tests were performed to determine the properties of materials used in the test specimens and these included masonry components (concrete masonry unit and mortar) and masonry assemblage (masonry prism), as well as steel coupons for the steel frames.

3.5.1 Concrete masonry units (CMUs)

Three CMUs were randomly selected and tested in accordance with ASTM C140/C140M (2017) Standard Test Methods for Sampling and Testing Concrete Masonry Units and Related Units. Both physical properties and compressive strength of masonry blocks were determined. The physical properties tested included the 24-hour percentage adsorption, density, and moisture content. The compressive strength was obtained in a standard compression test using an Instron universal machine and the test set-up is illustrated in **Figure 3.13**. Note that the masonry block was capped with fiberboard on two end surfaces.

Figure 3.13 Compression test for CMUs

3.5.2 Mortar

The mortar used for the infill walls was Type S, which was comprised of Portland cement, Type N mortar, and sand in volumetric proportions of 1:2:4 respectively. Two batches of mortar were used to build test specimens 2 through 4 which were built on March 29, 2017. Three batches of mortar were used for Specimens 5 through 8 which were built on October 4, 2017. For each test specimen, three 50 *mm* cubes were poured and cured in a lime solution in accordance with ASTM C270 (2014) and later used to determine the mortar strength. Compression tests on the masonry cubes were performed using the Instron universal testing machine in accordance to ASTM C109/109M (2016) and the test set-up is shown in **Figure 3.14**.

Figure 3.14 Compression test for mortar cube

3.5.3 Masonry prisms

Five-course high masonry prisms were built and later tested to determine the compressive strength of masonry, f'_m. For each infill specimen, three prisms were built using the same mortar used for the infill. The prisms incorporated both head and bed joints and had mortar placed on the face shells and the head joints, identical to the infill construction. As well, they were cured under the same conditions as the infill. The construction, curing and testing of the masonry prisms were in accordance with ASTM C1314 (2016). As illustrated in **Figure 3.15**, the compressive testing was performed using the Instron universal testing machine and the specimens were capped with fiberboards similar to the CMUs.

Figure 3.15 Compression test for masonry prisms

3.5.4 Steel tensile coupon

The yield strength, tensile strength, and modulus of elasticity of the steel frame member were determined using the steel coupon test. Five steel coupons were cut from the frame members including two from the flange and three from the web. The coupons were milled to the shape and dimension specified in accordance with ASTM Standard A370. The universal Instron testing machine was used to test the steel coupons in accordance with ASTM E8 (2008) Standard Test Methods for Tension Testing of Metallic Materials. **Figure 3.16** shows the dimensions of the cut coupon.

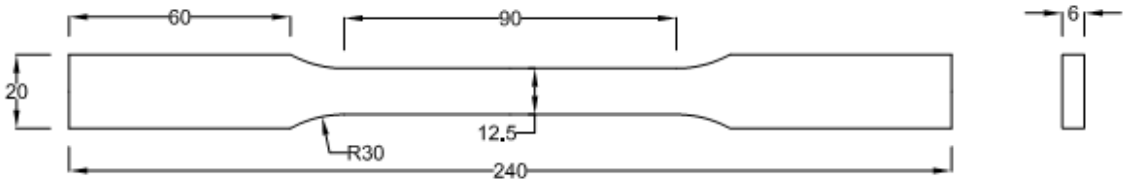

Figure 3.16 Coupon dimensions cut from steel frame ***(units in mm)***

CHAPTER 4 EXPERIMENTAL RESULTS

4.1 INTRODUCTION

This chapter presents results and discussions from the auxiliary tests and tests of infilled frame specimens. The auxiliary test results provide both the physical and mechanical properties of the CMUs, mortar and masonry prisms of the infills, and the steel section of the boundary frames. The infilled frame test results demonstrate the strength and behaviour of the infilled specimens as affected by the tested parameters.

4.2 AUXILIARY TEST RESULTS

4.2.1 CMUs

The procedure in accordance with ASTM C140/C140M was followed for obtaining the physical properties for the concrete masonry units (CMUs). Six randomly selected units were used to determine the CMU's dimensions and net area, moisture content, rate of absorption, and density. The average measured dimensions for a CMU cross-section can be found in **Figure 4.1**, resulting in a net area of 8448 mm^2. Each CMU was first weighed in its original state and then completely immersed in water for 24 hours and was measured for its immersed weight. The CMUs were then removed from the water and were surface dried before being weighed for the saturated weight. Each CMU was then dried in an oven at 100°C for 24 hours and then weighed again to produce the oven dried weight. Using these values along with the formulas specified in ASTM C140/C140M, the following

physical and material properties for the CMU were determined. The average density of CMUs was 2120.4 kg/m^3 with a COV of 1.4%; the average moisture content of CMUs was 12.6% with a COV of 10.1%; the average absorption rate of CMUs was 6.5% with a COV of 7.9%; the average absorption of CMUs was 137.4 kg/m^3 with a COV of 7.1%. Detailed results from each of the six CMUs can be found below in **Table 4.1.**

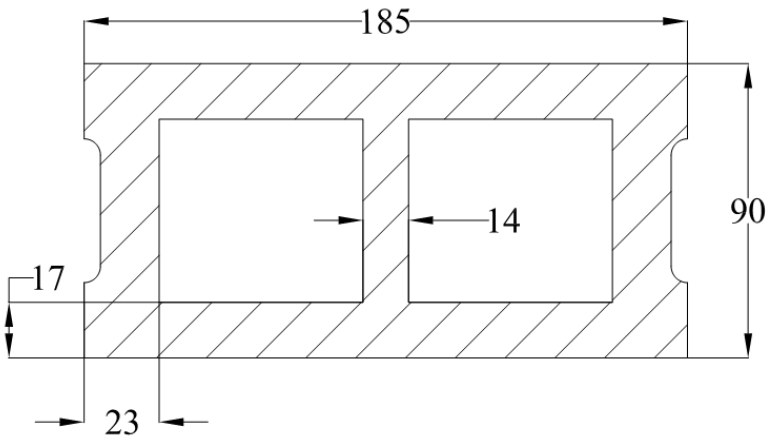

Figure 4.1 Physical dimensions for CMUs ***(units in mm)***

Table 4.1 Physical properties of CMUs

ID	Received weight (*g*)	Immersed weight (*g*)	Saturated weight (*g*)	Oven-dry weight (*g*)	Absorption		Moisture content	Density (*kg/m³*)
					kg/m³	(%)		
C1	1662.2	969.5	1749.5	1648.4	129.6	6.1	13.6	2113.3
C2	1662.5	968.3	1746.9	1648.5	126.4	6.0	14.2	2117.3
C3	1583.9	931.1	1680.3	1571.8	144.8	6.9	11.2	2098.0
C4	1589.1	936.2	1688.9	1575.4	1508	7.2	12.1	2093.0
C5	1593.4	943.8	1687.1	1581.5	142.1	6.7	11.3	2127.7
C6	1660.5	988.7	1746.9	1647.6	131.0	6.0	13.0	2173.0
				Avg.	137.4	6.5	12.6	2120.4
				COV(%)	7.1	7.9	10.1	1.4

In accordance with ASTM C140/C140M (2017), the selected CMUs were tested in compression in an Instron Universal Testing Machine. The typical observed failure mode in the CMUs was by conical shear as seen in **Figure 4.2**. The average compressive strength for the CMUs based on the net area, was 13.5 *MPa* with a COV of 7.2%. The results from each compression test can be found in **Table 4.2** below.

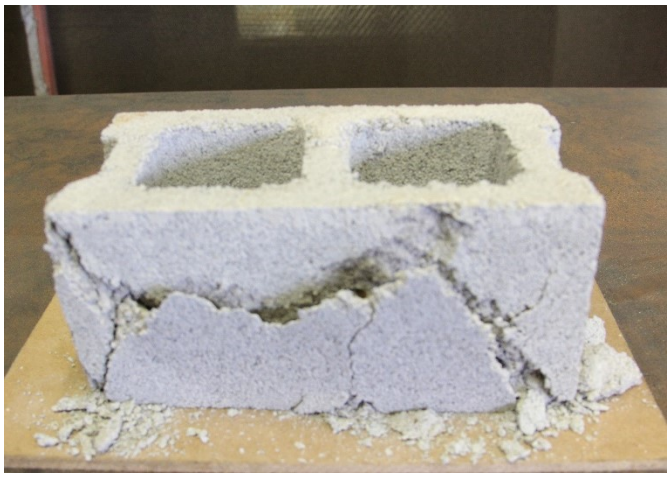

Figure 4.2 Typical failure mode - shear failure in CMUs

Table 4.2 Compressive test results of CMUs

ID	Ultimate load (*kN*)	Compressive strength (*MPa*)
1	111.2	13.2
2	114.0	13.5
3	118.6	14.0
4	105.7	12.5
5	126.8	15.0
6	105.6	12.5
	Avg. (*MPa*)	13.5
	COV (%)	7.2

4.2.2 Mortar Cubes

The mortar used to construct the masonry infill walls was mixed in five separate batches. **Table 4.3** outlines the mortar batch used for each test specimen.

Table 4.3 Mortar batches

Batch	Test specimen
A	IF-S-TG
B	IF-S-C, IF-S-D1, IF-S-FS
C	IF-S-VL
D	IF-S-CC
E	IF-S-D2, IF-S-SW

For each batch of mortar, a minimum of 3 mortar cubes were cast and tested in accordance with ASTM C109/109M using the Instron Universal Testing Machine. Additional cubes were cast for mortar batches large enough to be used for multiple specimens. The results from the compression tests and the corresponding compressive strengths can be found in **Table 4.4**. The average compressive strength for the mortar cubes ranged from 8.4 to 16.6 *MPa*. A typical conical failure mode exhibited by the mortar cubes is illustrated in **Figure 4.3.**

Figure 4.3 Mortar cube conical failure mode

Table 4.4 Mortar cube test results

Batch ID	Number of cubes	Avg. load (kN)	Avg. width (mm)	Avg. length (mm)	Average area (mm^2)	Avg. compressive strength (MPa)	COV (%)
A	6	26.4	50.0	50.6	2530.8	10.4	4.1
B	12	21.4	50.4	50.7	2557.6	8.4	4.2
C	3	37.6	49.9	50.0	2497.0	13.9	8.2
D	3	42.5	50.8	50.5	2565.5	16.6	3.0
E	6	32.6	50.1	50.2	2510.0	13.0	7.0

4.2.3 Prisms

For each batch of mortar, a minimum of three masonry prisms were built along with the construction of the infilled frame specimens. The prisms were tested in compression following the procedure specified in ASTM C1314 (2016). The typical failure mode characterized by vertical splitting through either face-shell or webs of units is illustrated in **Figure 4.4**. The masonry compressive strength had average values ranging from 10.8 to 12.4 *MPa*. The results from each test can be found in **Table 4.5**.

Table 4.5 Masonry prisms test results

Batch ID	# of prisms	Avg. ultimate load (kN)	f'_m (MPa)	COV (%)
A	3	55.8	8.8	15.6
B	9	54.9	8.8	14.9
C	1*	68.4	10.8	N/A
D	2	57.7	9.2	35.0
E	4	69.2	11.0	29.3

*Only one prism from Batch C due to damaged prisms

Figure 4.4 Typical failure mode of masonry prism test

4.2.4 Steel Coupon

A total of 5 coupons obtained at either flange or web of the steel section were tested for the material properties of the boundary frame. **Table 4.6** provides the yield strength, ultimate strength and the modulus of elasticity for each coupon test. The average yield strength was 402 *MPa* with a COV of 5.4%, and the average Modulus of Elasticity was 201,172 *MPa* with a COV of 4.0%.

Table 4.6 Steel coupon test results

Coupons ID	Location	Yield Strength (*MPa*)	Ultimate strength (*MPa*)	Modulus of elasticity (*MPa*)
S1	Flange	378	503	198684
S2	Flange	378	524	204293
S3	Web	417	530	197475
S4	Web	421	530	213306
S5	Web	415	539	192101
	Avg. (*MPa*)	402	525	201172
	COV (%)	5.4	2.6	4.0

4.3 INFILLED FRAME SPECIMEN RESULTS

The following section provides for each specimen, a description of the behaviour, ultimate strength, and failure pattern. The information is presented in the order of load vs. out-of-plane displacement curve, ultimate strength, cracking and failure mode, and vertical and horizontal displacement profile.

4.3.1 IF-S-FS

Specimen IF-S-FS was tested under out-of-plane loading and was used to study the effect of the frame beam boundary condition where the bottom beam was fully supported along its length. The pressure vs. out-of-plane displacement at LVDT 1 (center of the infill) and the cracking pattern of the leeward face of the infill prior to failure are shown in **Figure 4.5** and **Figure 4.6** respectively.

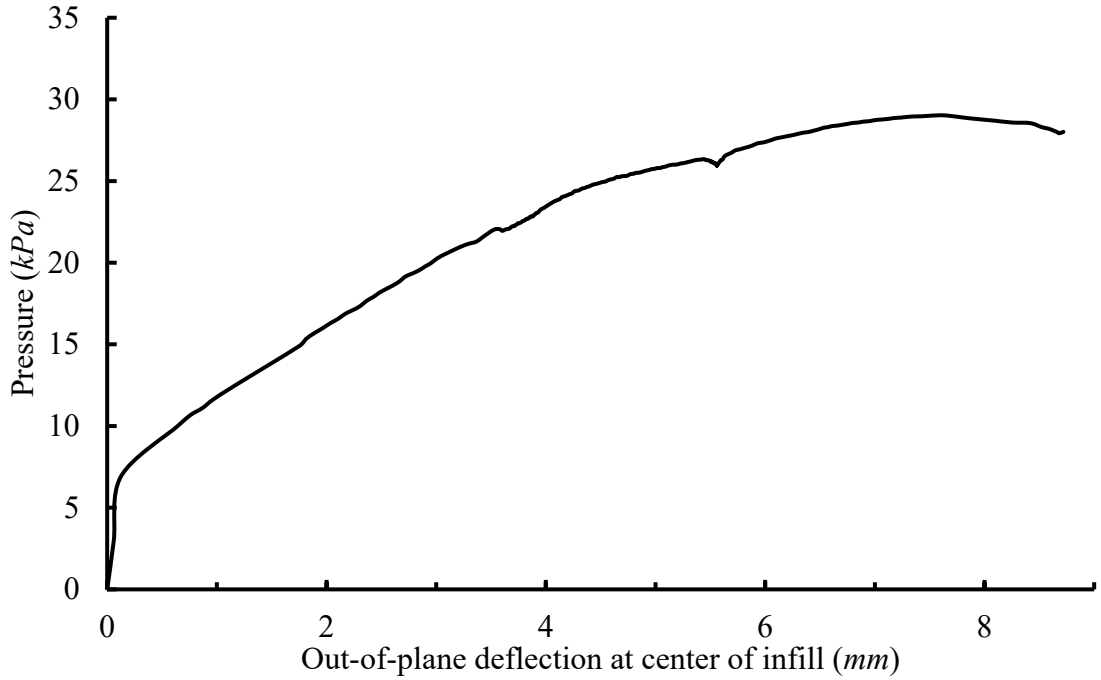

Figure 4.5 Pressure vs. displacement curve of specimen IF-S-FS

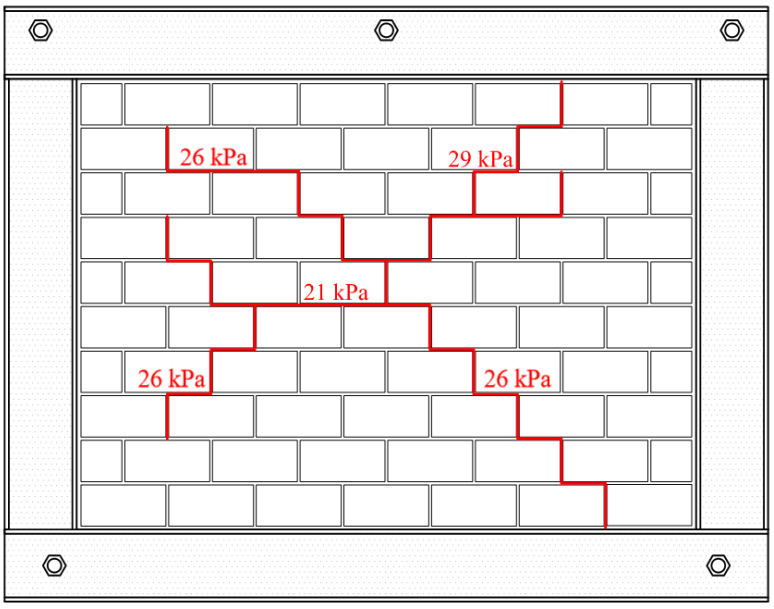

Figure 4.6 Leeward cracking pattern of IF-S-FS

When the test commenced, the infill behaved nearly linear until it reached a pressure of 6.9 *kPa* (24% of ultimate load) with a corresponding displacement of only 0.13 *mm* and showed a rather drastic softening in the response immediately after. There were no visible

cracks on the leeward face of the infill up to this load and the decrease in stiffness is believed to be attributed to the loss of the bond (slipping) between the mortar and the steel boundary frame. As the pressure increased, hairline cracks formed at the mid-point of the wall at a load of 21 *kPa* (72% of ultimate load) and began to extent outwards towards the four corners of the infill. The cracks at the mid-point of the wall began to open up at a pressure of 26 *kPa* (90% of ultimate load), and the infill reached its ultimate load at a pressure of 29 *kPa*. The infill collapsed immediately after a loading of 28 *kPa* and a corresponding displacement of 8.7 *mm*. The overall cracking pattern resembles a yield-line pattern, consistent with previous observations reported by Sepasdar (2017) and Wang (2017).

At failure, the majority of the faceshells of the infill had sheared off as shown in **Figure 4.7**. Note that this failure mode was also reported by both Sepasdar and Wang for RC framed infills. This observation shows that this failure mode also exists for steel framed infills and further confirms that web shear failure might be the governing failure mode, rather than masonry crushing as the conventional thinking suggests. Also, at the infill to boundary frame interface, all the CMUs were left in contact with the boundary frame member, indicating that although there might be some initial slipping of the infill at the early stage of loading, once the infill came to tight contact with the frame, the arching still developed, and no slip-out failure occurred.

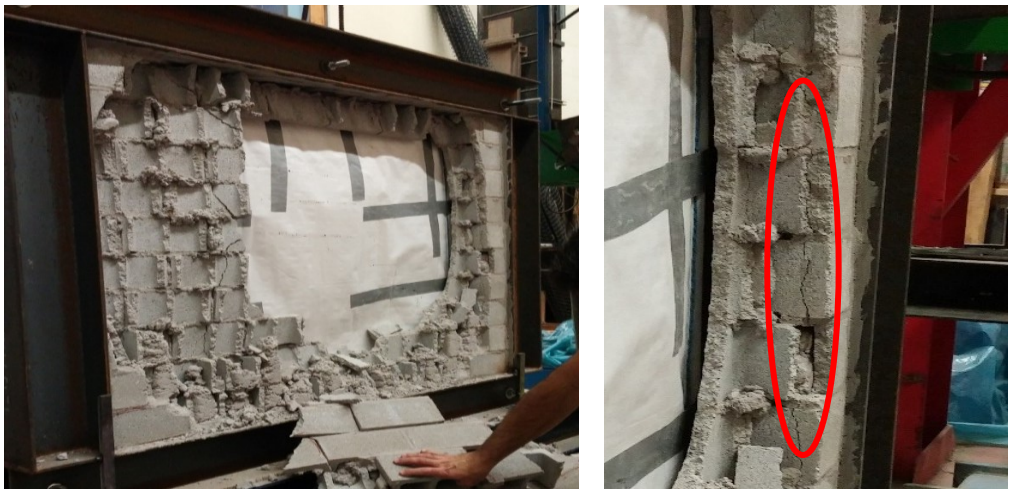

Figure 4.7 Faceshell separation due to web shear failure on specimen IF-S-FS

Figure 4.8 and **Figure 4.9** plot the out-of-plane displacement profile along the central vertical and horizontal axes, respectively. Evidently, the center of the infill at LVDT1 location experienced the maximum displacement. At the early stage of loading, the profiles in both horizontal and vertical directions were nearly symmetrical with respect to the central axis indicating that arching began to develop in both directions. After the first major crack occurred, the profile was no longer symmetrical, and the upper left side seemed to experience more displacement which is consistent with the cracking pattern figure where that region showed more cracking. Also, about 63% of the displacement occurred after visible hairline cracking, indicating a large portion of the displacement was enabled by arching action.

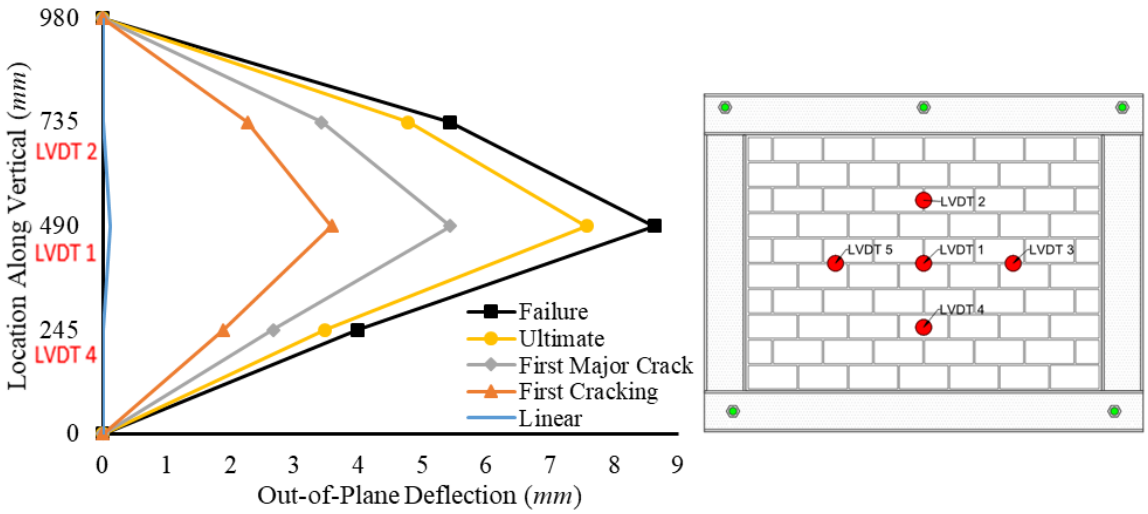

Figure 4.8 Displacement profile along the central vertical axis of IF-S-FS

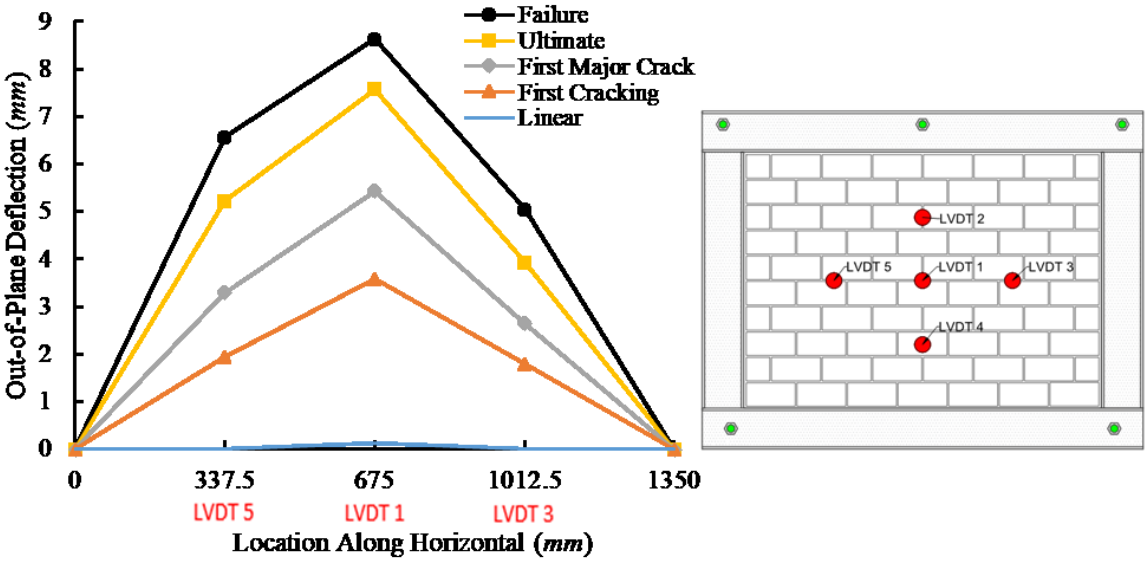

Figure 4.9 Displacement profile along the central horizontal axis of IF-S-FS

4.3.2 IF-S-SW

Specimen IF-S-SW was tested out-of-plane to determine if stiffening the frame beam by adding web stiffeners (three on the top and three on the bottom) has any effect on the arching action and thus ultimate strength of the infill. **Figure 4.10** plots the pressure vs. out-of-plane deflection at the center of the infill and **Figure 4.11** illustrates the cracking pattern of the infill at failure. The linear response lasted up to a loading of 10.4 *kPa* (35% of ultimate load) where horizontal hairline cracks began to form at mid-height of the infill. When the pressure reached a load of 24.0 *kPa* (81% of ultimate load), significant cracking was observed throughout the top half of the infill and the initial horizontal cracks began to show separation. The infill ultimately reached an out-of-plane load of 29.8 *kPa* and a corresponding displacement of 5 *mm*. When compared with Specimen IF-S-FS, a 0.8 *kPa* increase in the ultimate strength was observed. However, the cracking pattern of the former specimen showed much extensive cracking. More detailed comparison is presented in Chapter 5.

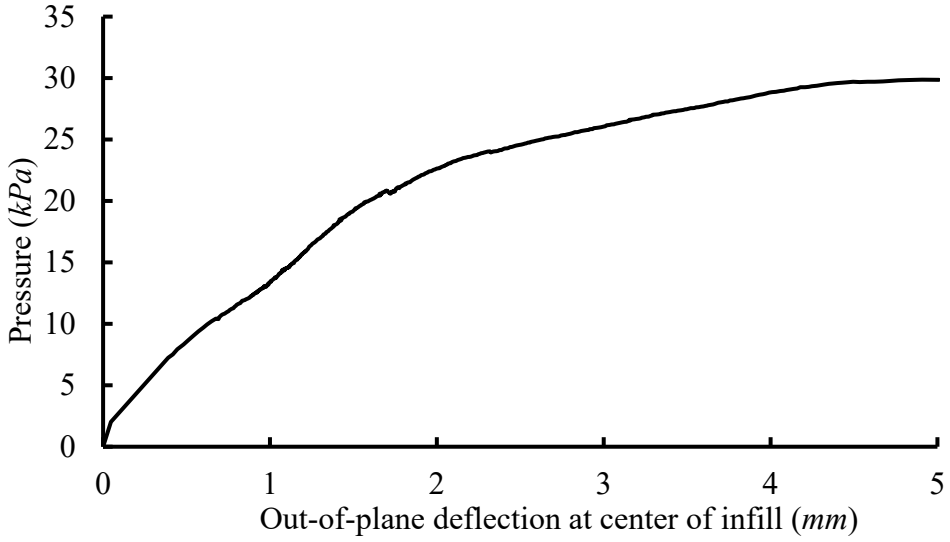

Figure 4.10 Pressure vs. displacement curve of specimen IF-S-SW

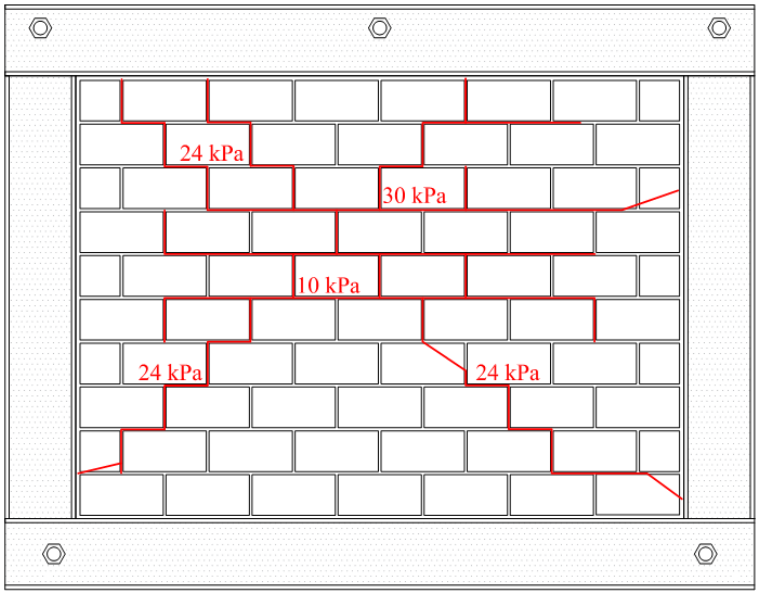

Figure 4.11 Leeward cracking pattern of IF-S-SW

Figure 4.12 shows the remainder of the specimen after failure. Similar to the previous specimen, the failure was sudden and volatile with faceshell spalling of the CMUs. A close examination also suggests web shear failure.

Figure 4.12 Faceshell separation due to web shear failure on specimen IF-S-SW

An LVDT (LVDT 6) was placed at an angle, as seen in **Figure 4.13,** on the bottom flange of the top beam to measure flange deflection. The LVDT recorded data up to a load of 22.6 *kPa* and measured a displacement of 0.38 *mm*. Due to the physical constraints of the frame, the LVDT was placed at an angle and there was minimal displacement measured on the bottom flange. When the out-of-plane load reached the pressure of 22.6 *kPa*, the incurred out-of-plane displacement of the infill caused the angled LVDT to slip out of contact and detached from the measuring device holder. The LVDT 2 (top ¼ of the infill) plunger was also slipped out of place and no longer recorded data as the load increased.

Figure 4.13 LVDT 6 measuring top beam flange deflection

Figure 4.14 and **Figure 4.15** display the displacement profiles at different loading stages along the central vertical and horizontal axes respectively. During the linear behaviour phase, the max deflection point occurred at the center of the infill and the remainder of the infill deflected symmetrically in both the vertical and horizontal directions. After the first major crack occured, the profile deviated from symmetry where the right side of the leeward face (LVDT 3) showed higher displacements than the left side (LVDT 5). This is

expected as cracking changed a continuum infill unit into one with discrete sections. As cracking is not symmetrical, the resulted discrete infill sections will experience different displacements. The overall pattern of the profiles is, however, similar to the previous specimen (IF-S-FC).

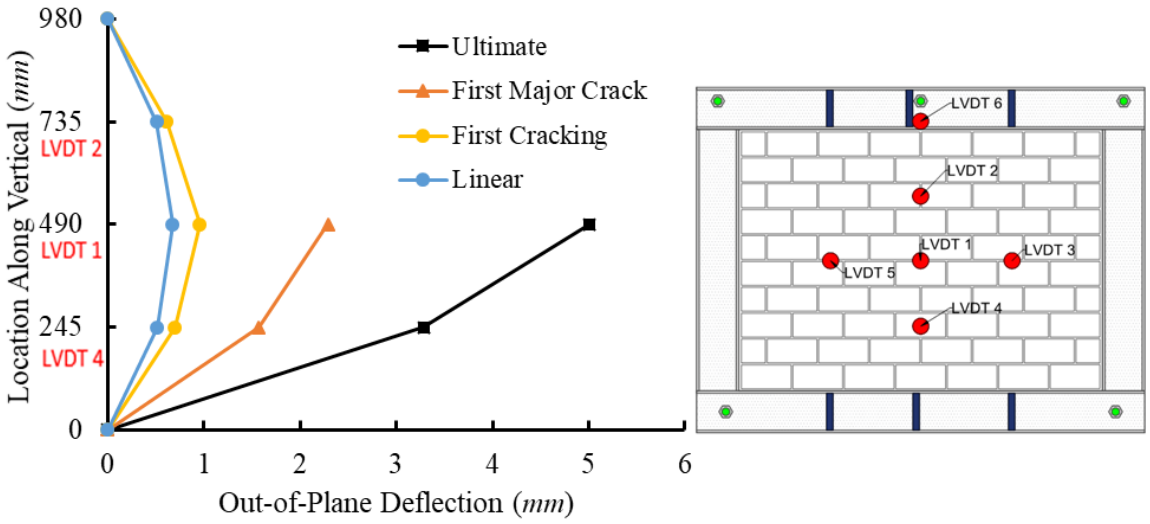

Figure 4.14 Displacement profile along the central vertical axis of IF-S-SW

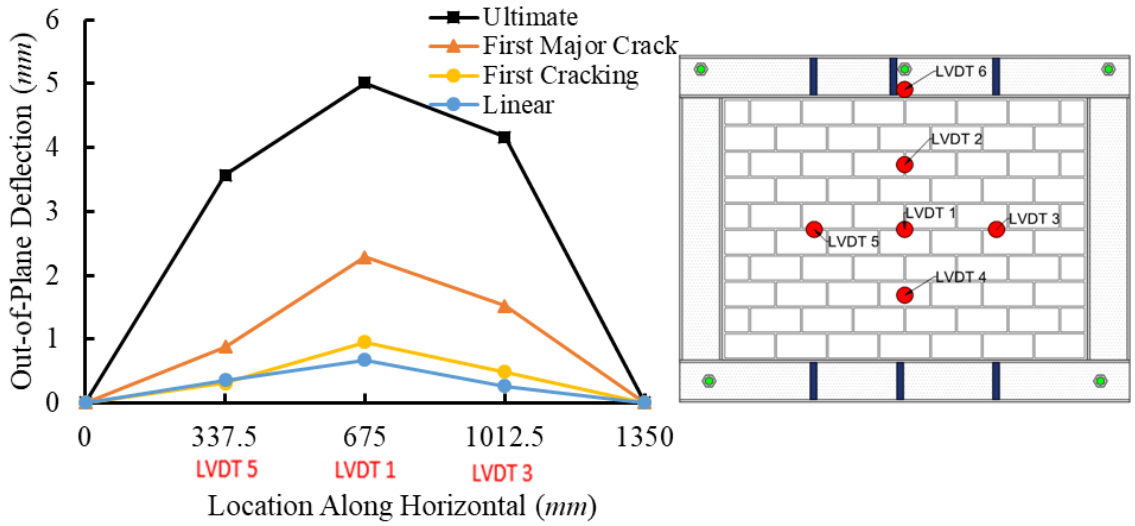

Figure 4.15 Displacement profile along the central horizontal axis of IF-S-SW

4.3.3 IF-S-TG

Specimen IF-S-TG had a 10 *mm* gap at the beam-to-infill interface. The pressure vs. out-of-plane displacement at the center of infill (LVDT1) is shown in **Figure 4.16**. As can be seen, the initial behaviour is approximately linear with a significantly lower stiffness than the control specimen. This can be attributed to the presence of the top gap, in which case, the arching action is only enabled in the horizontal direction and a small contribution from the bottom boundary condition. At a load of 10.6 *kPa* (64% of ultimate load), a visible vertical crack through the top 3 courses of the infill (**Figure 4.17)** occurred at a displacement of 1.7 *mm*. When the load increased to 13.6 *kPa* (82% of ultimate load), additional hairline cracks formed around the bottom corners of the infill and extended diagonally towards the center of the infill. When the infill reached the ultimate load (16.6 *kPa*) at a displacement of 3.3 *mm*, tension cracks formed at both sides of the initial vertical crack began to open up before the infill ultimately failed at a load of 15.2 *kPa* at a displacement of 4.9 *mm* due to a large section of the wall located at the top middle between the tension cracks suddenly dislodging from the rest of the infill. This specimen was the only one that did not suffer noticeable web shear failure. At no point during the testing, did the arching action close the gap and allow vertical arching.

Figure 4.16 Pressure vs. displacement curve for specimen IF-S-TG

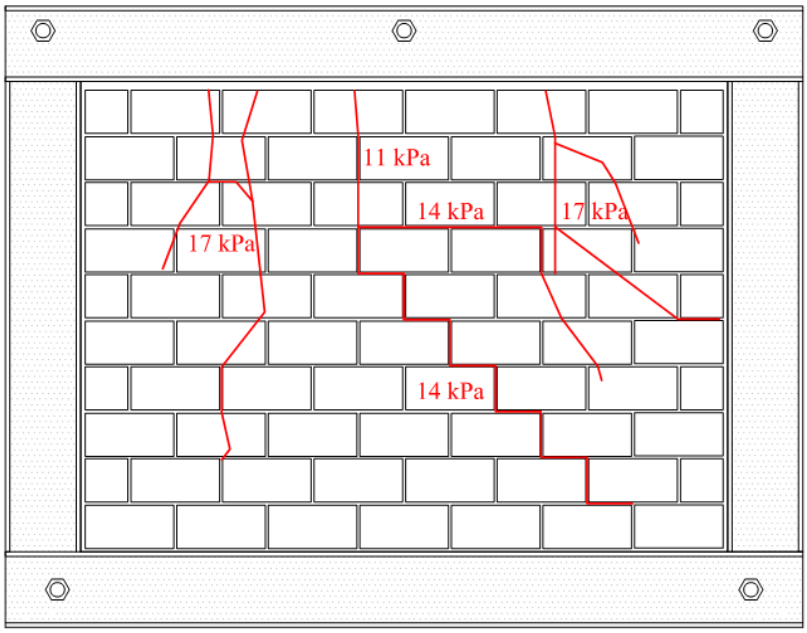

Figure 4.17 Leeward Cracking Pattern IF-S-TG

Figure 4.18 and **Figure 4.19** display the displacement profiles along the central vertical axis and horizontal axis respectively. The horizontal profile showed a symmetrical pattern

with respect to the infill center throughout the majority of the loading history, indicating arching action still developed in the horizontal span. The deformation along the vertical direction was non-symmetrical and clearly the top portion of the infill experienced greater displacement than the bottom portion. A closer examination suggested that some level of arching may still have developed as the location of max deflection shifted from LVDT 6 (top of the infill) to LVDT 2 (¾ height of the infill). However, when compared with previous specimens, the level of arching in the direction of vertical span is insignificant, conceivably due to the fact that the top beam was not engaged to provide a rigid support. As the contact between the infill and the bottom beam was maintained during the loading, the cracking pattern is similar to the yield-line pattern for a three-side supported slab. At failure, the tension crack on the left side of the infill initiates the failure as evidenced by the large increase in deflection at LVDT 5 (left ¼ of infill).

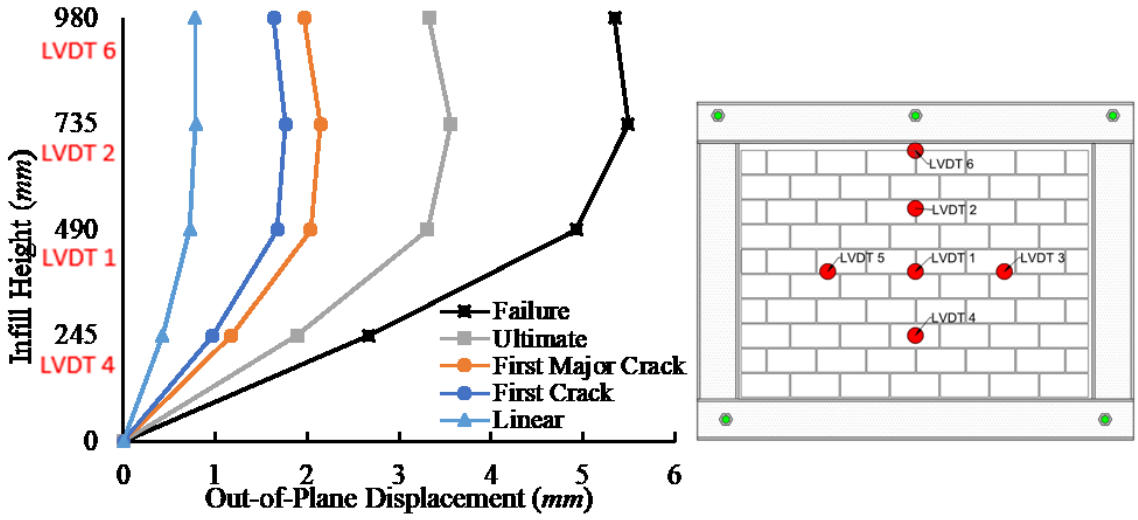

Figure 4.18 Displacement profile along the central vertical axis of IF-S-TG

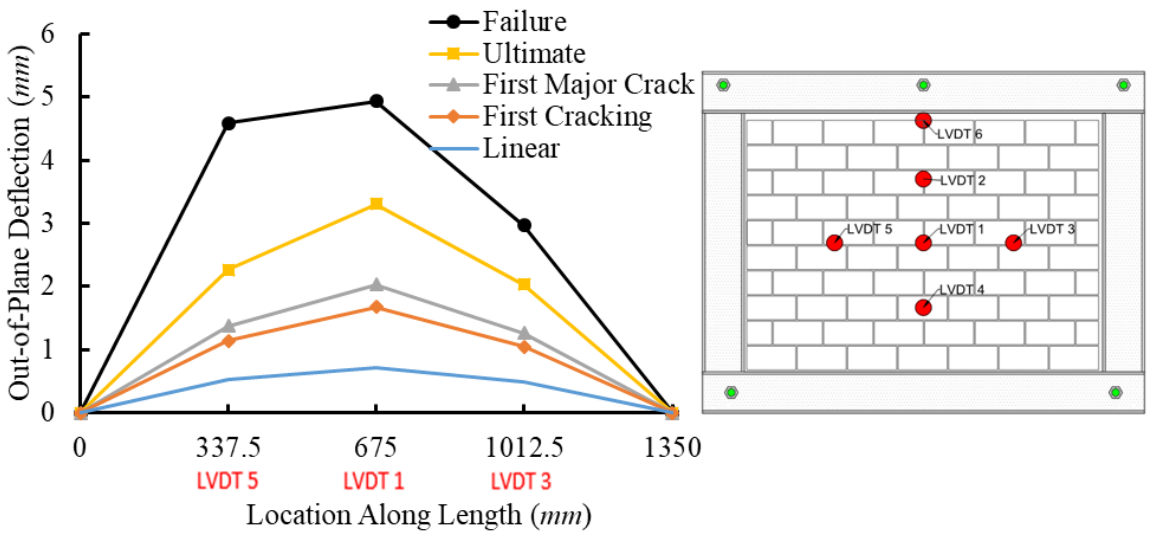

Figure 4.19 Displacement profile along the central horizontal axis of IF-S-TG

4.3.4 IF-S-D1

Specimen IF-S-D1 was designed to study the effect of prior in-plane damage on the out-of-plane capacity of an infill. The specimen was first subjected to in-plane loading till a major diagonal crack was formed. The load vs. in-plane displacement curve up to the said crack is shown in **Figure 4.20**. The behaviour remained linear up to a load of 50.5 *kN*, at which point, small hairline cracks began to form at the loaded corner. The response thereafter showed a small reduction in stiffness but remained roughly linear as cracks began to spread towards the diagonally opposite corner as the load was increased. At a load of 78.2 *kN*, a major diagonal crack (**Figure 4.23)** was observed at an in-plane deflection of 5.2 *mm*, which will henceforth be termed as F_{app} and δ_{app}. After this point, the in-plane load was removed, and the specimen was allowed to return to its original position. The specimen recovered most of the lateral displacement and the diagonal crack remained without noticeable closing. The airbag setup was then attached and the out-of-plane loading began.

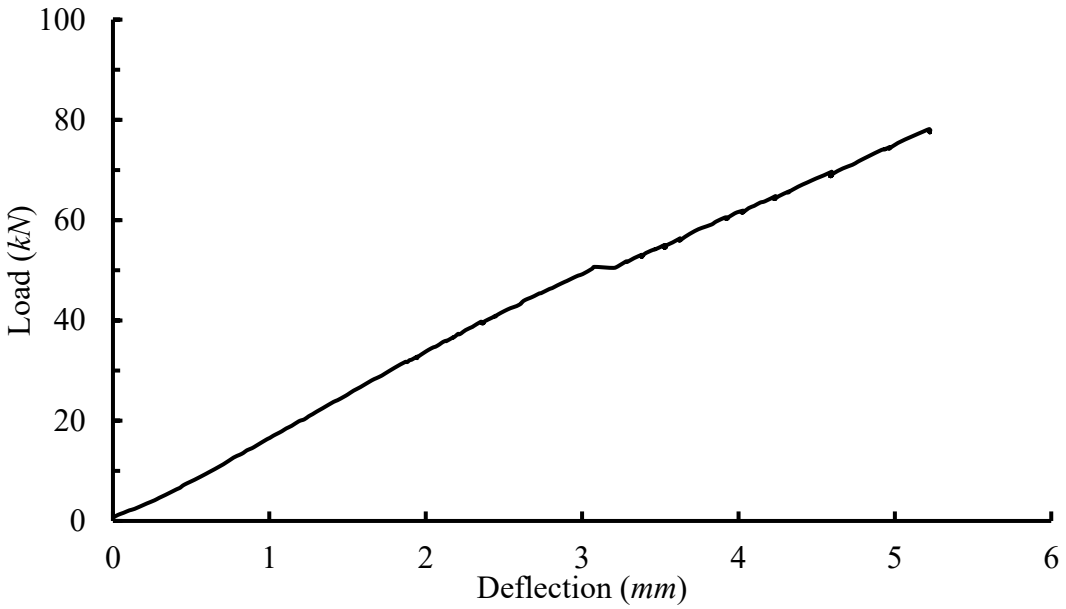

Figure 4.20 Load vs. displacement curve for the in-plane loading stage for specimen IF-S-D1

Figure 4.21 and **Figure 4.22** show the load vs. out-of-plane displacement curve and the failure mode of the specimen respectively. **Figure 4.21** shows that the specimen behaved close to linearly up to a load of 8.8 *kPa* (33% of ultimate load) and began to show marked softening with a reduced stiffness. The experimental observation confirmed that at this load, a mid-height crack began to form and connected to the diagonal crack, as shown in **Figure 4.23**. As the load increased, more cracks began to form from the center of the infill towards corners, more evidently on the top than the bottom. When the out-of-plane pressure reached 25.4 *kPa* (97% of ultimate load), the central horizontal crack widened significantly and a horizontal crack two courses up from the bottom of the infill also formed. The specimen reached an ultimate load of 26.2 *kPa* at a deflection of 4.5 *mm*. At failure, face-shell spalling was observed on the right side of the major horizontal crack at the center of the infill, and the top of the infill slipped from the top boundary beam.

Figure 4.21 Pressure vs. displacement curve for out-of-plane loading on specimen IF-S-D1

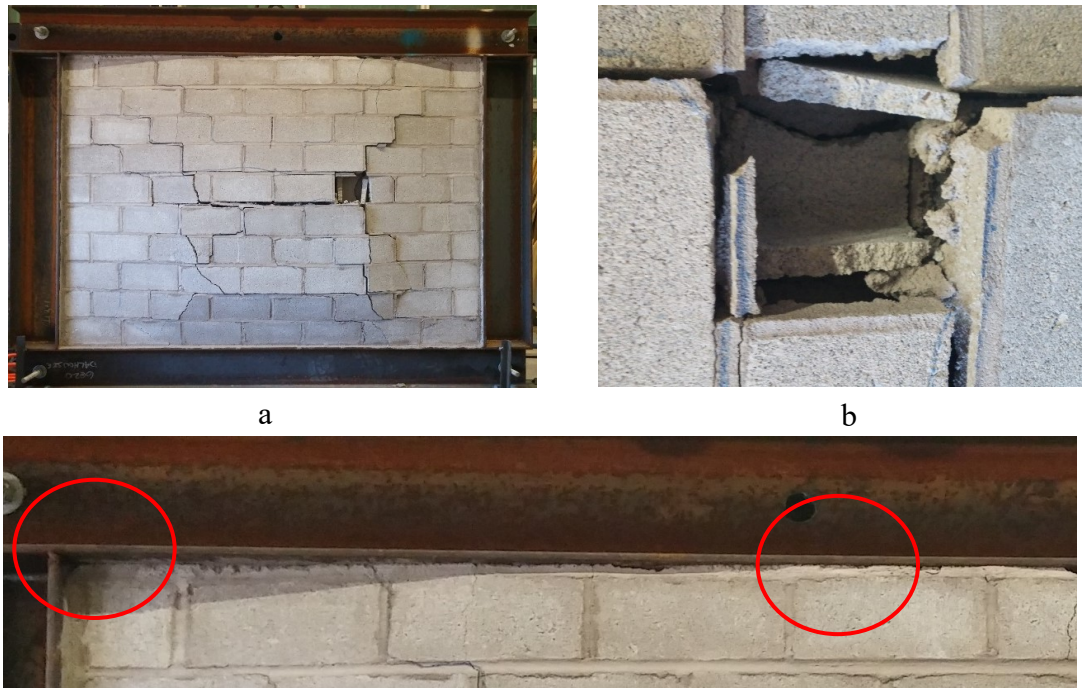

a b

c

Figure 4.22 Failure mode of IF-S-D1 a) Cracking pattern b) Face shell separation c) Slip failure along top boundary

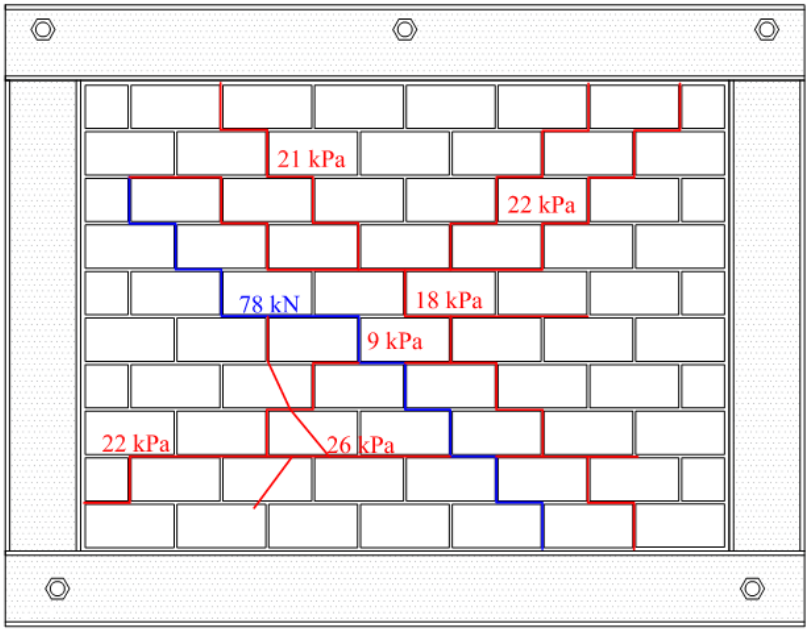

Figure 4.23 Leeward cracking pattern of specimen IF-S-D1

The vertical and horizontal displacement profiles along the centerlines of the infill are illustrated in **Figure 4.24** and **Figure 4.25** respectively. During the linear phase, the infill displaced symmetrically about the center of the infill. As load increased, LVDT 4 location (lower section of infill) deflected more rapidly than LVDT 2 location (top section of the infill) as shown in the vertical profile. This is consistent with the fact that the prior damage from the in-plane loading caused a diagonal crack that was more concentrated on the lower half of the infill. It was observed at failure that the top of the infill had marked slippage from the steel beam and thus the LVDT 6 reading was not used in the vertical profile. However, the available data points suggested arching behaviour in both the vertical and horizontal directions.

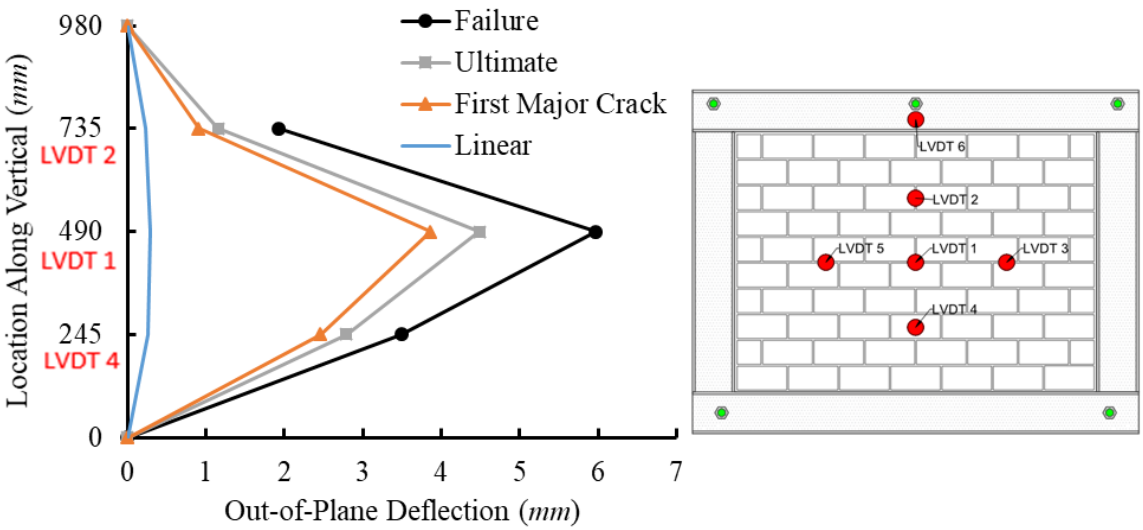

Figure 4.24 Displacement profile along the central vertical axis of IF-S-D1

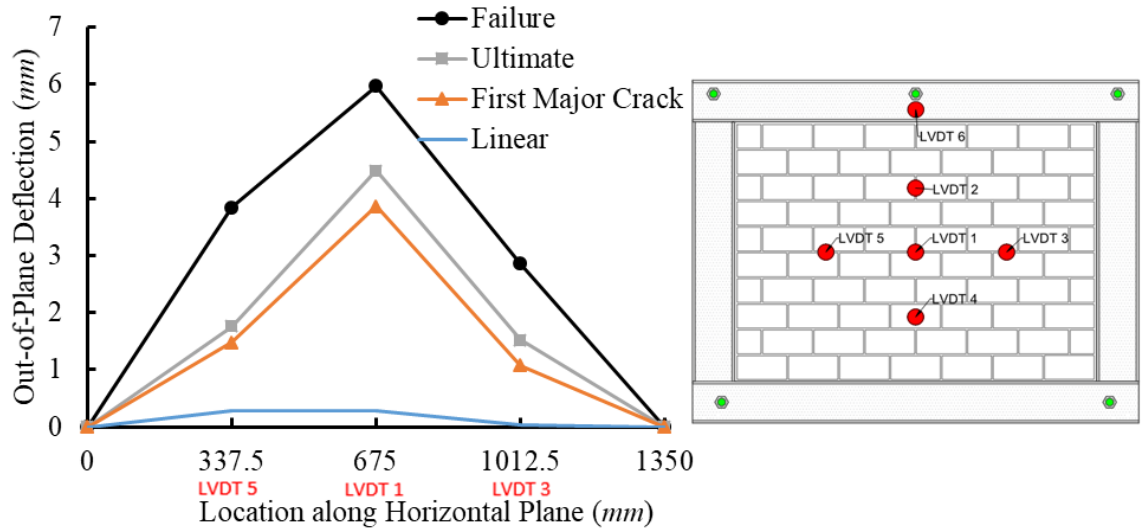

Figure 4.25 Displacement profile along the central horizontal axis of IF-S-D1

4.3.5 IF-S-D2

Specimen IF-S-D2 was used to investigate the in-plane strength of infills which have sustained prior out-of-plane damage. **Figure 4.26** plots the pressure vs. displacement at the center of the infill for the out-of-plane loading stage. The behaviour of IF-S-D2 was linear up to a loading of 10.1 *kPa* where hairline cracks began to form along the bed joints at mid-height of the infill. The loading was continued to generate more significant cracks. When

the load reached at 27.2 *kPa*, the main horizontal crack began to widen and diagonal cracks extending to the four corners formed from the initial horizontal cracks. The loading was discontinued at this point and the cracking pattern is illustrated in **Figure 4.30** as the red lines. A comparison with specimen IF-S-FS indicates that the loading applied to IF-S-D2 was about 93.7% of the out-of-plane strength of IF-S-FS which was an identical specimen but loaded to failure under out-of-plane loading.

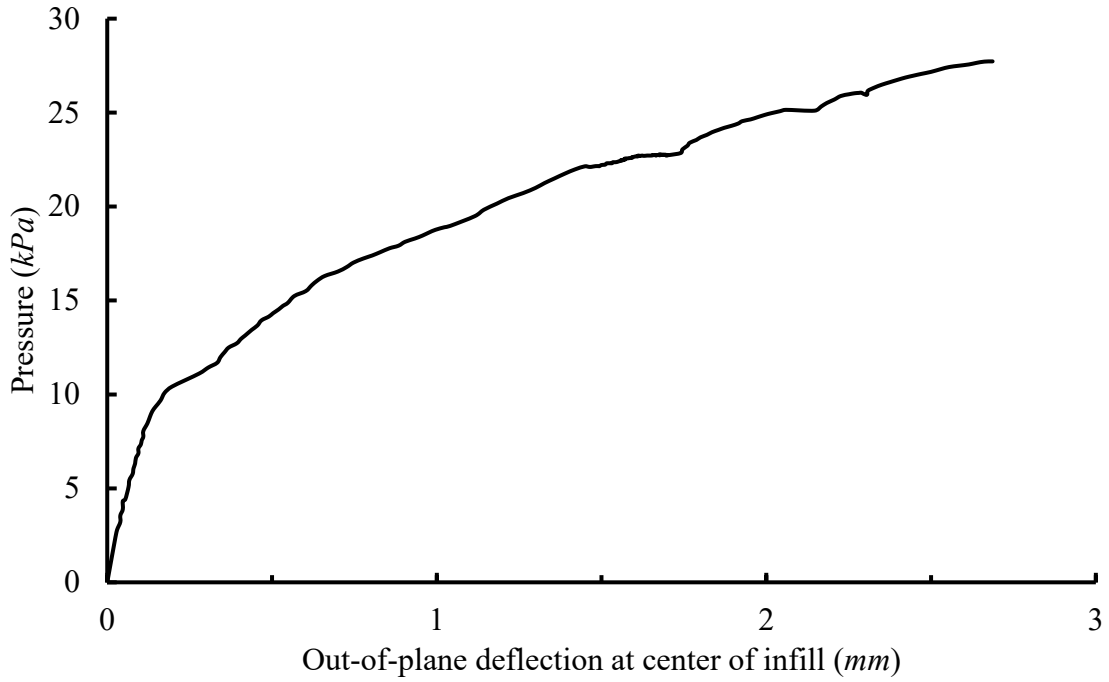

Figure 4.26 Pressure vs. displacement curve for initial out-of-plane loading stage for specimen IF-S-D2

Figure 4.27 and **Figure 4.28** plot the out-of-plane displacement profile along central vertical and horizontal axes respectively for this loading stage. Both profiles are relatively symmetrical, and arching is observed in both the vertical graph and horizontal graph at the final loading.

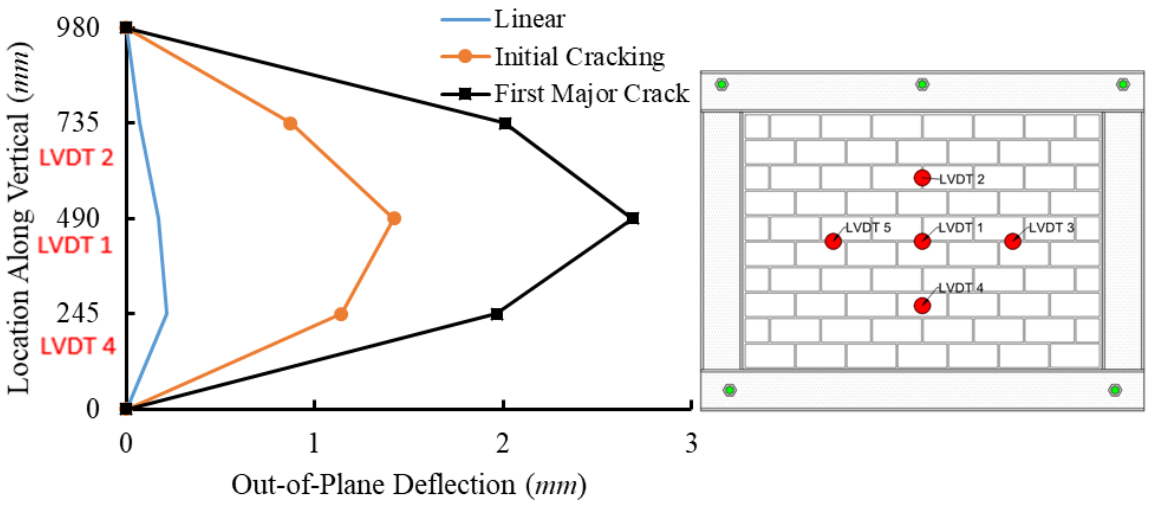

Figure 4.27 Displacement profile along the central vertical axis for cracking load on IF-S-D2

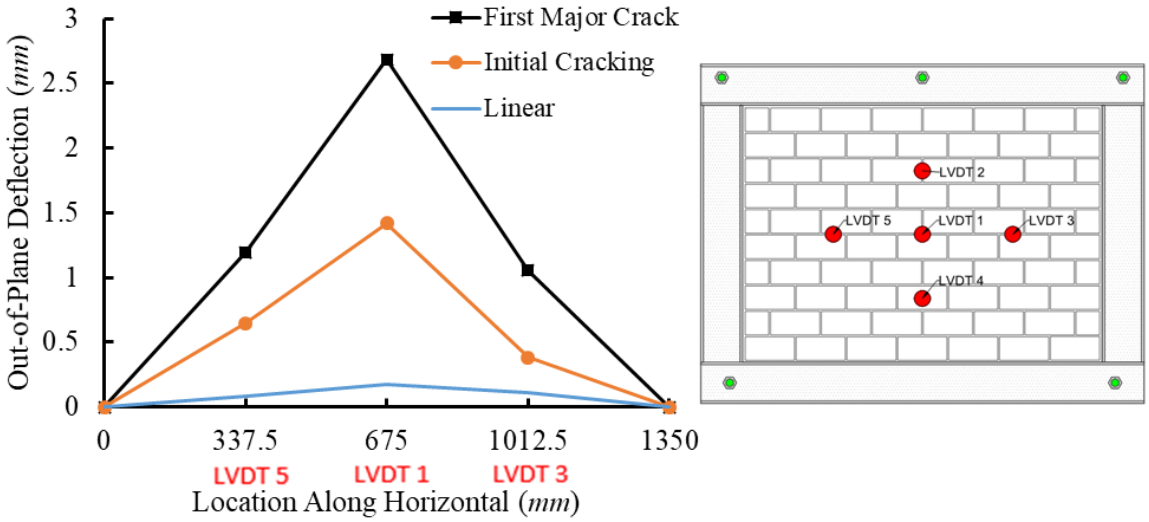

Figure 4.28 Displacement profile along the central horizontal axis for cracking load on IF-S-D2

When the out-of-plane loading phase was completed, the airbag assembly was removed with an overhead crane. The infill was then loaded in-plane thereafter. **Figure 4.29** plots the load vs displacement curve for the in-plane loading. The in-plane behaviour was linear up to approximately a loading of 72 *kN* when additional diagonal cracks connecting loaded corners began to form in the infill. As loading continued, more cracks formed in the general

diagonal directions but in different regions of the infill panel. At a load of 145 *kN*, the infill reached its in-plane capacity as the mortar crushing occurred in the corners of the infill and the load began to level off. **Figure 4.30** displays the cracking patterns from both the prior out-of-plane damage as well as the in-plane damage after ultimate was reached. The red cracks signify the prior out-of-plane loading and the blue cracks signify the in-plane damage.

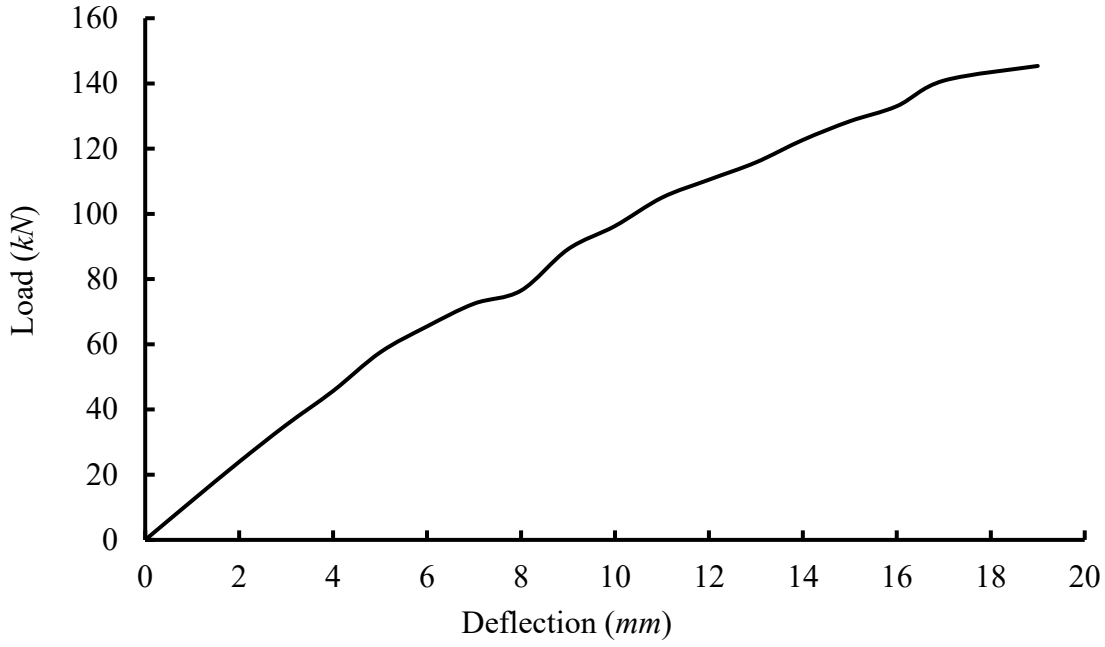

Figure 4.29 Load vs. displacement curve for ultimate in-plane loading stage of specimen IF-S-D2

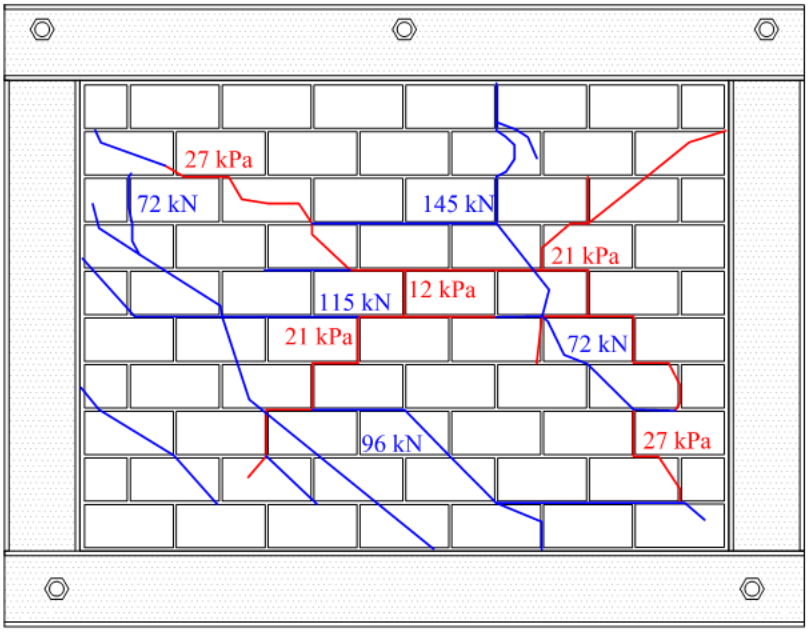

Figure 4.30 Leeward cracking pattern after ultimate in-plane loading on specimen IF-S-D2

Following the infill reaching its ultimate in-plane capacity, the load was removed, and it was decided to test the infill again under out-of-plane loading to determine whether there was any residual strength remaining. **Figure 4.31** displays the curve of pressure vs. out-of-plane deflection of LVDT 1 (center of the infill). The specimen experienced a brief linear stage up until a loading of 4.5 *kPa* (27% of ultimate loading). At a loading of 14.5 *kPa* (87% of ultimate load), the existing horizontal cracks at mid-height of the infill widened and web shear failure began to occur in some CMUs. Faceshell separation failure occurred suddenly at the ultimate load of 16.6 *kPa*. **Figure 4.32** displays the failed test specimen. The failure of the infill was more localized in regions above the bottom two courses of the infill. The specimen did not suffer from a top boundary slip out, and ultimately failed due to face shell separation cause by prior damage and web shear failure. Note that this specimen which has been loaded to its in-plane ultimate capacity still has approximately 60% of its out-of-plane strength remained when compared to specimen IF-S-FS.

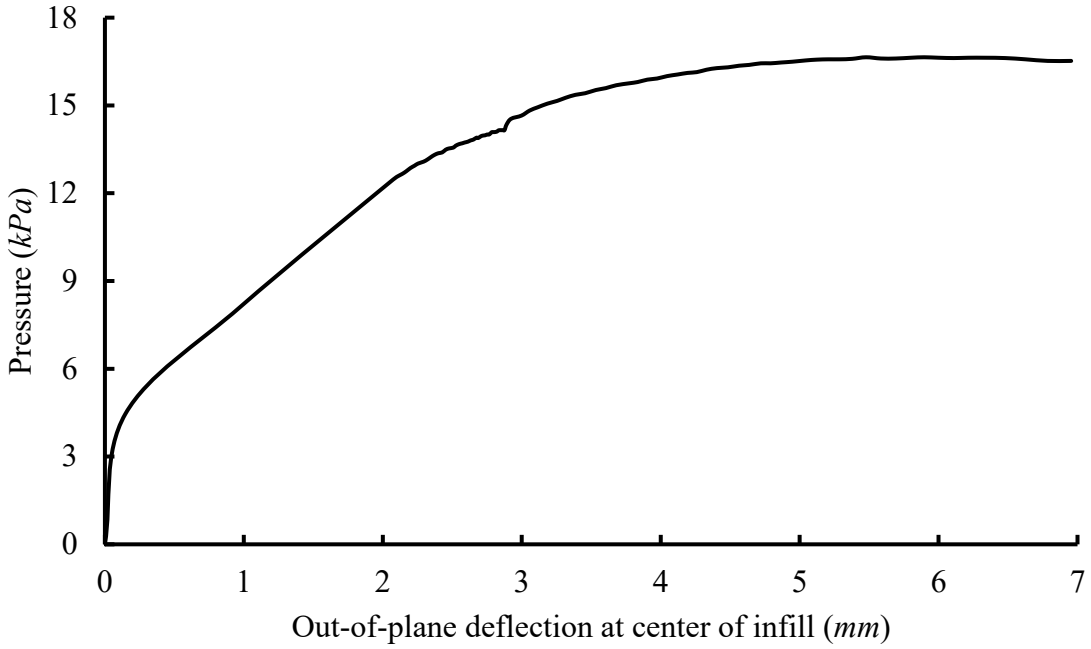

Figure 4.31 Pressure vs. displacement curve for residual out-of-plane loading stage for specimen IF-S-D2

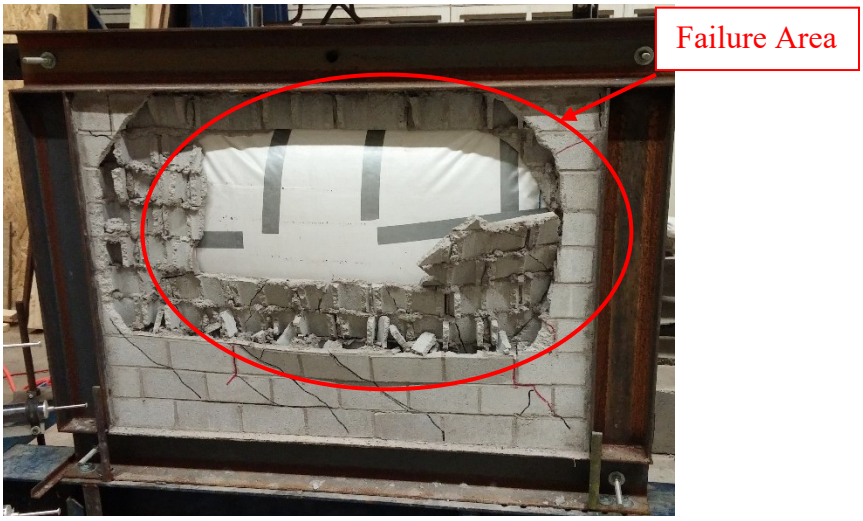

Figure 4.32 Out-of-plane failure mode for specimen IF-S-D2

Figure 4.33 and **Figure 4.34** displays the out-of-plane displacement profiles along vertical and horizontal axes respectively for the second time of out-of-plane loading. Note that LVDT 2, at the first major crack loading stage was caught in a crack and therefore is not displayed in **Figure 4.33**. While vertical arching was more or less symmetric about the

center of the infill at the failure load, LVDT 4 (bottom ¼ of infill) consistently read a higher out-of-plane deflection than LVDT 2 (top ¼ of the infill) throughout the test. This was also consistent with the final failure pictured in **Figure 4.32**. For horizontal arching, LVDT 3 (right side of the leeward face) showed a consistently higher out-of-plane displacement than LVDT 5 (left side of leeward face). This non-symmetry in displacements about the center of the infill is expected due to the extensive damage the infill had sustained but what is of note is that both vertical and horizontal arching did occur.

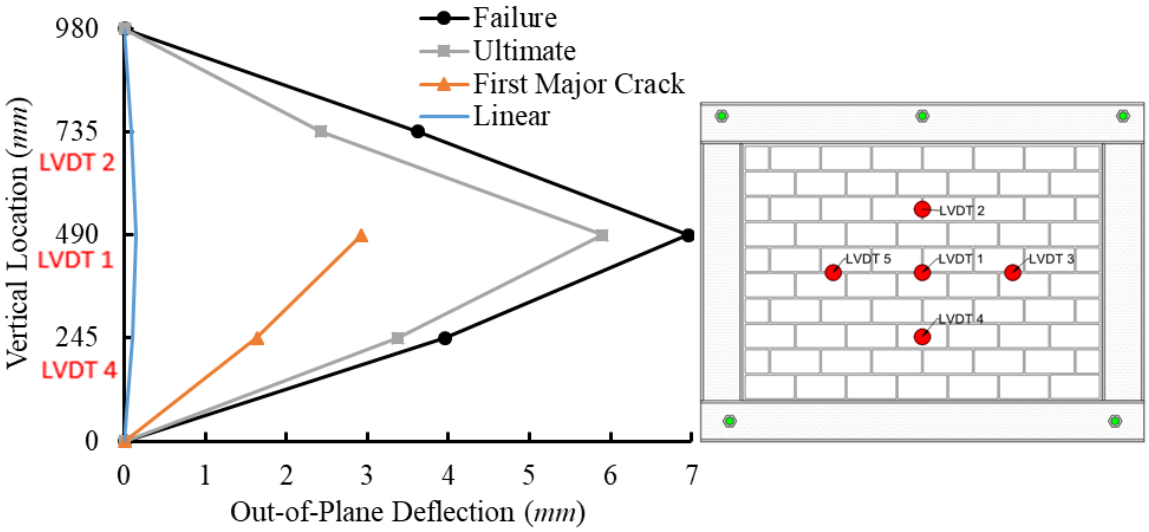

Figure 4.33 Displacement profile along the central vertical axis for final loading for IF-S-D2

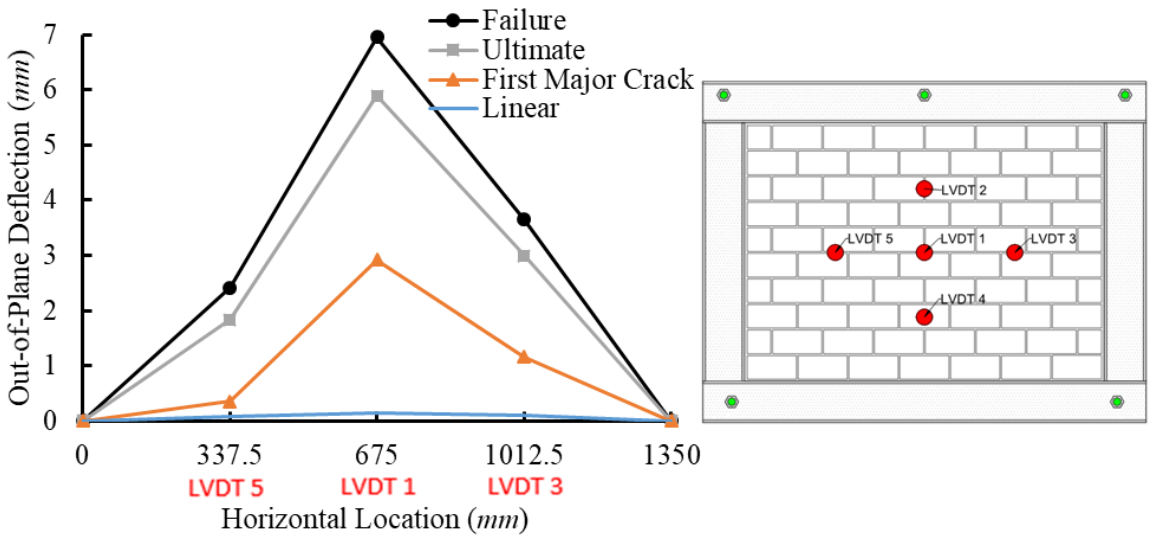

Figure 4.34 Displacement profile along the central horizontal axis for final loading for IF-S-D2

4.3.6 IF-S-CC

Similar to Specimen IF-S-D1, Specimen IF-S-CC was also designed to investigate the out-of-plane strength of infills that were damaged due to previous in-plane loading and the difference from the former was that the in-plane loading generating the damage was held constant in the process of out-of-plane loading. **Figure 4.35** shows the load vs. displacement graphs for both IF-S-D1 and IF-S-CC during the in-plane loading stage. Both specimens were loaded to 78 *kN*, but specimen IF-S-CC showed a higher stiffness and deflected 1 *mm* less than IF-S-D1 overall. This additional stiffness is believed to be attributed to the fact that for Specimen IF-S-CC, the airbag assembly was attached to the specimen frame for the in-plane loading to facilitate the setup for out-of-plane loading immediately thereafter. **Figure 4.37** illustrates the diagonal cracking (blue lines) of the leeward face of IF-S-CC after the in-plane load was reached at 78 *kN*.

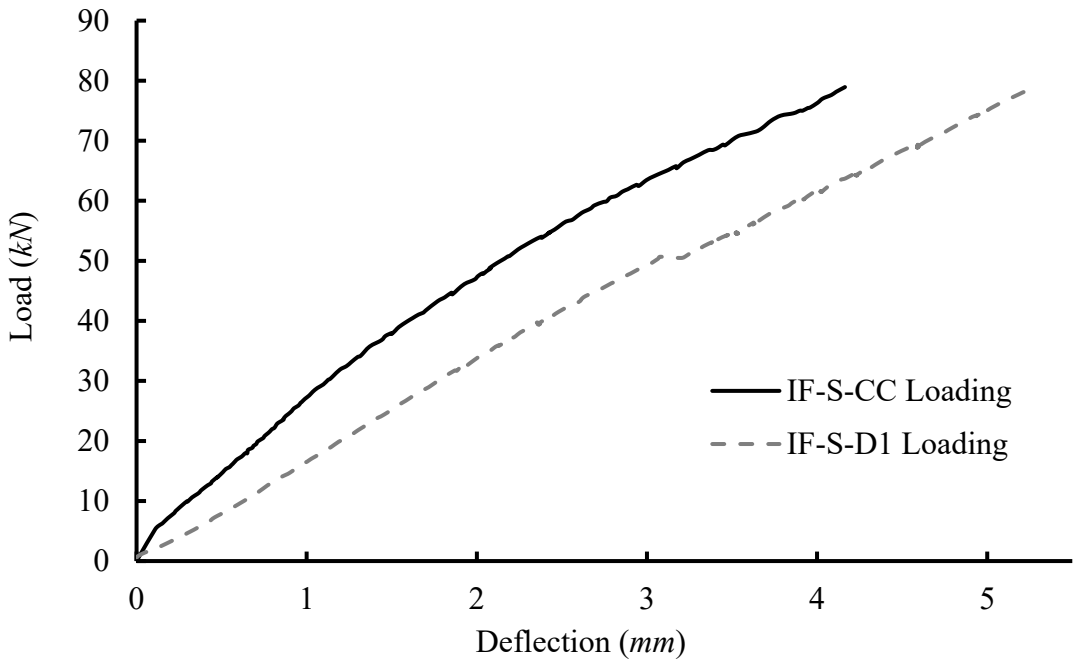

Figure 4.35 Load vs. deflection for in-plane loading of specimen IF-S-CC

The out-of-plane loading vs deflection of LVDT 1 (center of infill) curve is plotted in **Figure 4.36.** A linear portion of response up to a loading of 8.0 *kPa* is observed. At this point, additional horizontal cracks began to extend from the in-plane diagonal cracking at mid-height of the infill. When the out-of-plane pressure reached 16.7 *kPa*, cracks were observed to spread towards the two previously un-damaged corners and the horizontal cracks at mid-height began to show visible separation. The infill ultimately reached a pressure of 18.4 *kPa* before a sudden failure occurred. The cracking pattern before failure is illustrated in **Figure 4.37**. The sudden failure of the infill happened due to face shell spalling of the CMUs and can be seen in **Figure 4.38.**

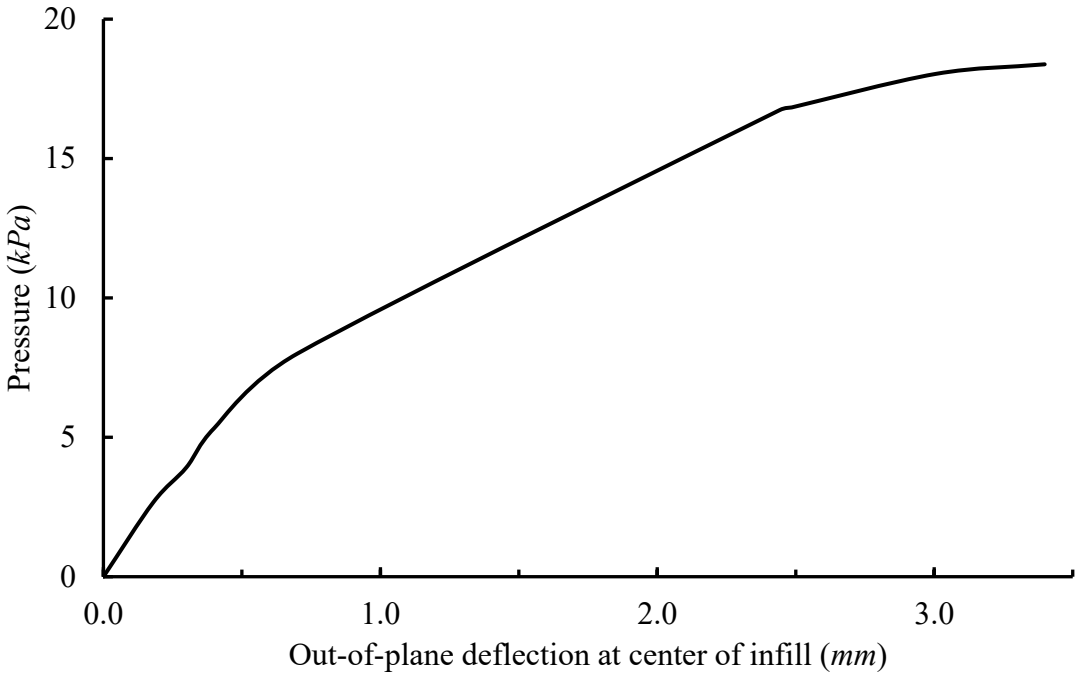

Figure 4.36 Pressure vs. displacement curve for the out-of-plane loading on specimen IF-S-CC

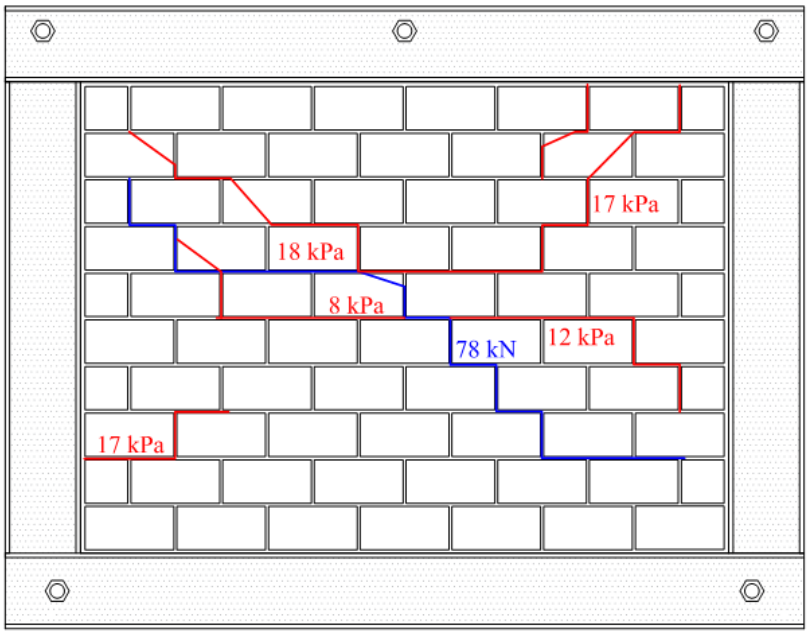

Figure 4.37 Cracking pattern on the leeward face after out-of-plane loading on specimen IF-S-CC

Figure 4.38 Out-of-plane failure mode for specimen IF-S-CC

The horizontal displacement profile and the vertical displacement profile of the top half of the infill for out-of-plane loading stage are shown in **Figure 4.39** and **Figure 4.40** respectively. The horizontal profile shows symmetry about the center right from the beginning of the test until the ultimate loading indicating horizontal arching occurred. The vertical profile is not complete because LVDT4 was used to measure the in-plane displacement and no other LVDTs were available at the test. However, comparing with vertical displacement profile obtained for IF-S-D1, the trend for the top portion is similar and it may be deduced that the overall vertical profile is also similar. This suggests in both tests, horizontal and vertical arching developed.

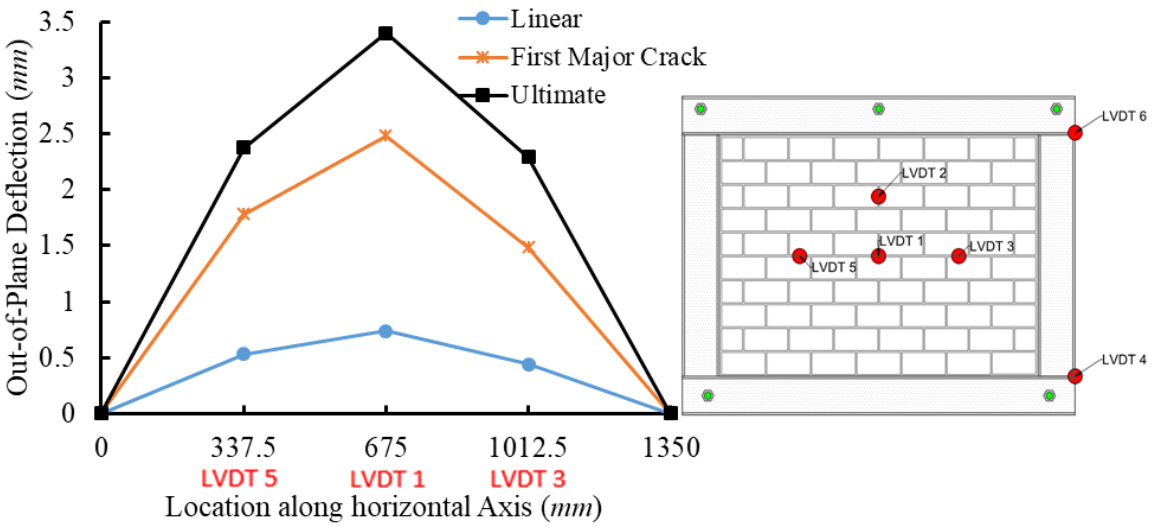

Figure 4.39 Displacement profile along the central horizontal axis of IF-S-CC

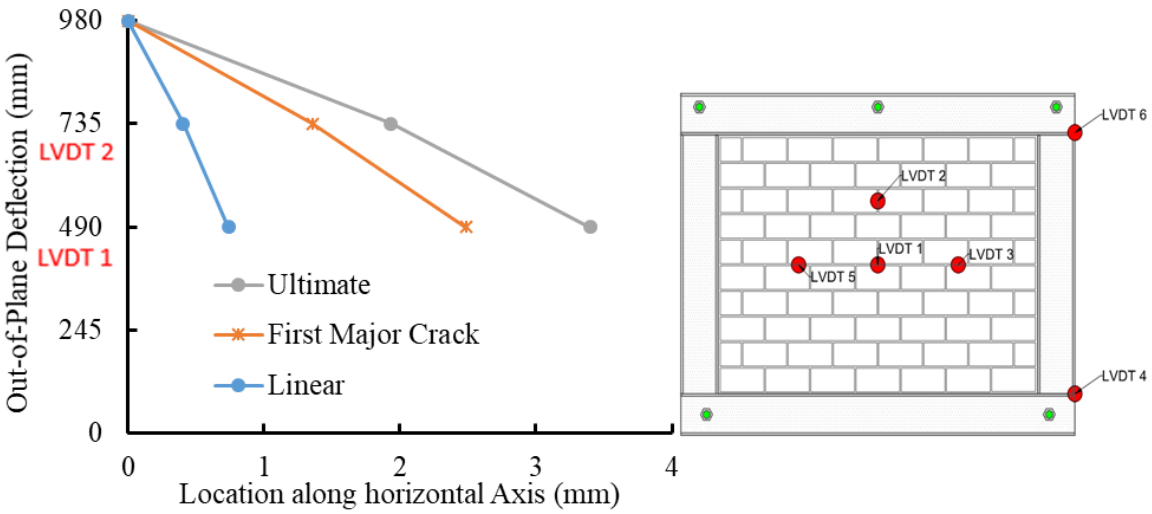

Figure 4.40 Displacement profile along the central vertical axis of IF-S-CC

4.3.7 IF-S-VL

Specimen IF-S-VL was used to determine the effect of vertical loading applied on the top frame beam on the out-of-plane strength of the infill. A vertical load of 100 *kN* was applied to the top beam and held constant while the infill was tested out-of-plane. The pressure vs. out-of-plane displacement curve at the center of the infill is plotted in **Figure 4.41**. The infill response remained quite linear up to a higher load (11.4 *kPa*, 63% of ultimate pressure) when compared with previous specimens. This may be attributed to the fact that the presence of vertical load acting in-plane delayed the cracking caused by out-of-plane loading. The first major crack occurred in the infill at a loading of 16.8 *kPa* (94% of ultimate pressure). The infill ultimately reached a load of 18.0 *kPa* which was lower than its counterpart specimen without vertical load. This is surprising as it was thought that the vertical load would increase the frame beam's stiffness by restraining its upward deformation and thus increase the capacity of the infill.

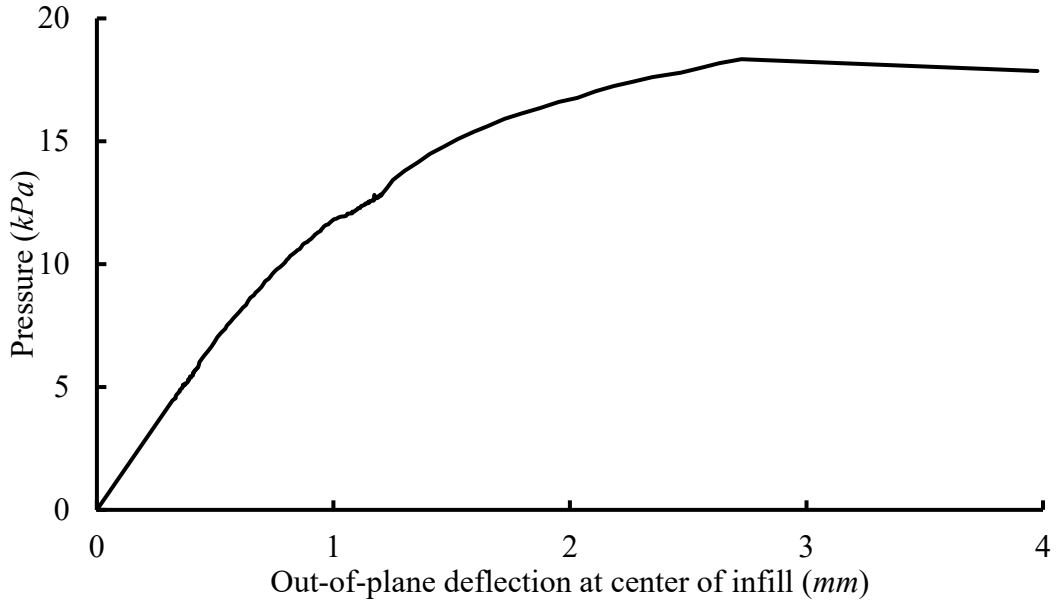

Figure 4.41 Pressure vs. displacement curve for specimen IF-S-VL

A close examination of failure mode revealed that prior to failure, the top of infill slipped out from under the top frame beam. It was also observed that the mortar layer between the top of infill and the underside of the frame beam was crushed as the vertical load was increased and beam showed evident signs of bending deformation accompanied with some level of twisting. The breaking of the bond and beam deformation facilitated slipping of the top infill. The loss of top support reduced a two-way arching to one-way arching in the horizontal direction. With the loss of vertical arching, two major vertical cracks quickly formed under the points of concentrated vertical load as seen in **Figure 4.42**.

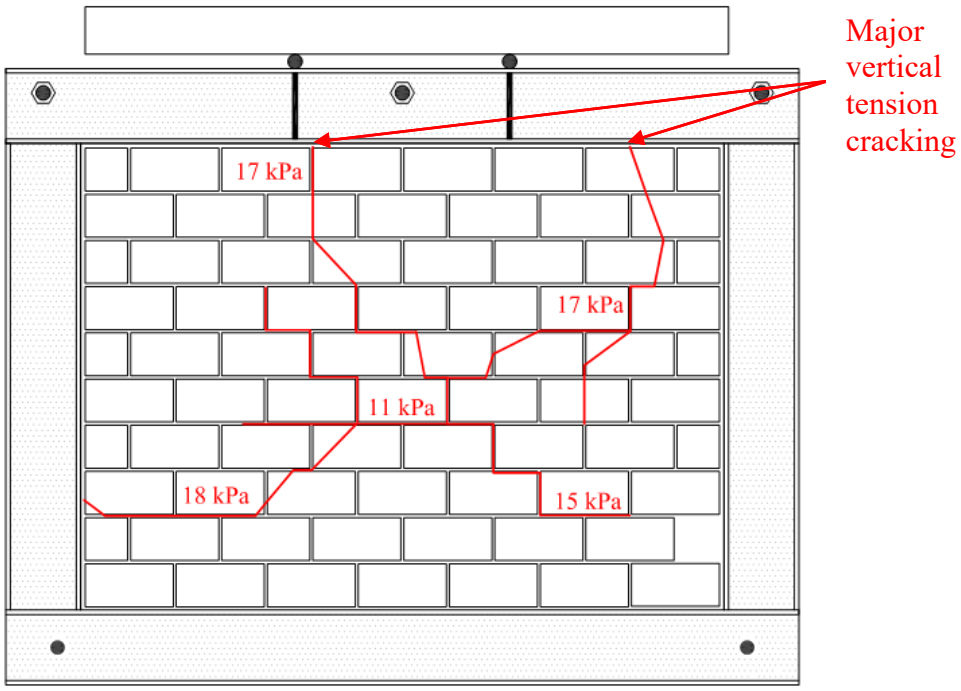

Figure 4.42 Cracking on leeward face for specimen IF-S-VL

Figure 4.43 shows that the failure of the infill was instigated by the top boundary interface with full delamination between the mortar and the steel frame. At failure, the webs of the masonry units have all failed due to horizontal shear causing face shell separation.

Figure 4.43 Specimen IF-S-VL failure pattern after out-of-plane loading

The out-of-plane deflection along a vertical plane and a horizontal plane are displayed in **Figure 4.44** and **Figure 4.45** respectively. Along the vertical plane, the deflection at LVDT 1 (center of the infill) was never greater than the deflection at LVDT 2 (top ¼ of the infill). At the ultimate load and failure, it can be seen that the top of the infill had slipped out from the boundary frame and completely removed all vertical arching. Along the horizontal plane, the infill deflected symmetrically about the infill center and arching can be seen throughout all loading stages

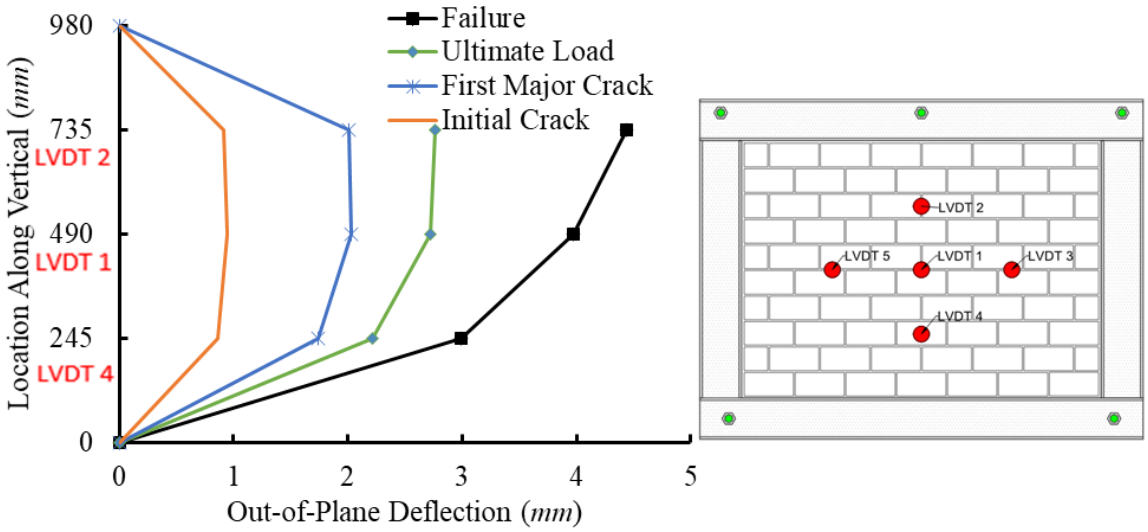

Figure 4.44 Displacement profile along the central vertical axis of IF-S-VL

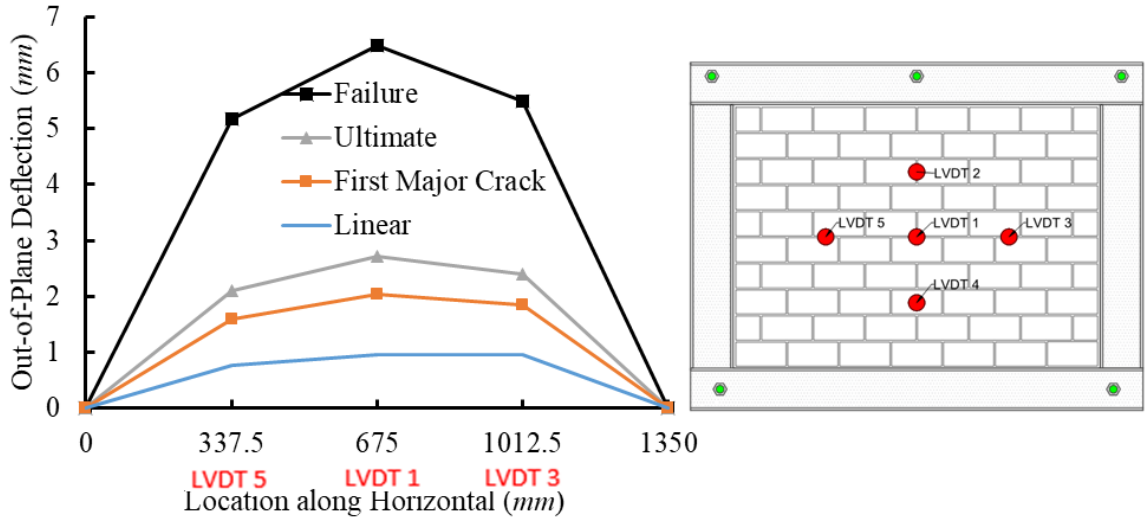

Figure 4.45 Displacement profile along the central horizontal axis of IF-S-VL

4.4 SUMMARY OF RESULTS

The test results of all the specimens are presented in **Table 4.7**. The displayed results include the load at the first cracking (P_i), the load at the first major crack (P_{cr}), the ultimate loading (P_{ult}) and the load at final failure (P_{res}) as well as the corresponding out-of-plane displacements at the mid-point of the infills. **Table 4.7** also presents the stiffness of the

infill for the initial crack (k_i), at the occurrence of the first major crack (k_{cr}), and ultimate load (k_{ult}). Also listed in the table are the results from the in-plane tests where the in-plane loading (P_{app}) and the corresponding in-plane displacement (δ_{app}) are provided.

The definition of the above terms is illustrated in **Figure 4.46.** The slope of the initial linear portion of the load over the displacement is defined by the initial stiffness (k_i). The load at which the first crack occurs is denoted as P_i and the corresponding out-of-plane displacement as Δ_i. After this point, the response curve shows a stiffness reduction. The cracked stiffness (k_{cr}) is defined by the slope of the line connecting the origin and the load at which the first major crack occurs causing the response curve to have a second marked stiffness reduction. The point in time in which the first major crack occurs is an experimental visual observation of significant crack formation that was checked against the load vs displacement graph to determine that there is a difference in the infill behaviour. The load and displacement at this point are defined by P_{cr} and Δ_{cr}. The ultimate stiffness (k_{ult}) is defined by the slope of the line connecting the origin and the point of ultimate strength, and the ultimate load and displacement are denoted as P_{ult} and Δ_{ult} respectively. The load at the final failure and the corresponding displacement are termed as P_{res} and Δ_{res}, respectively.

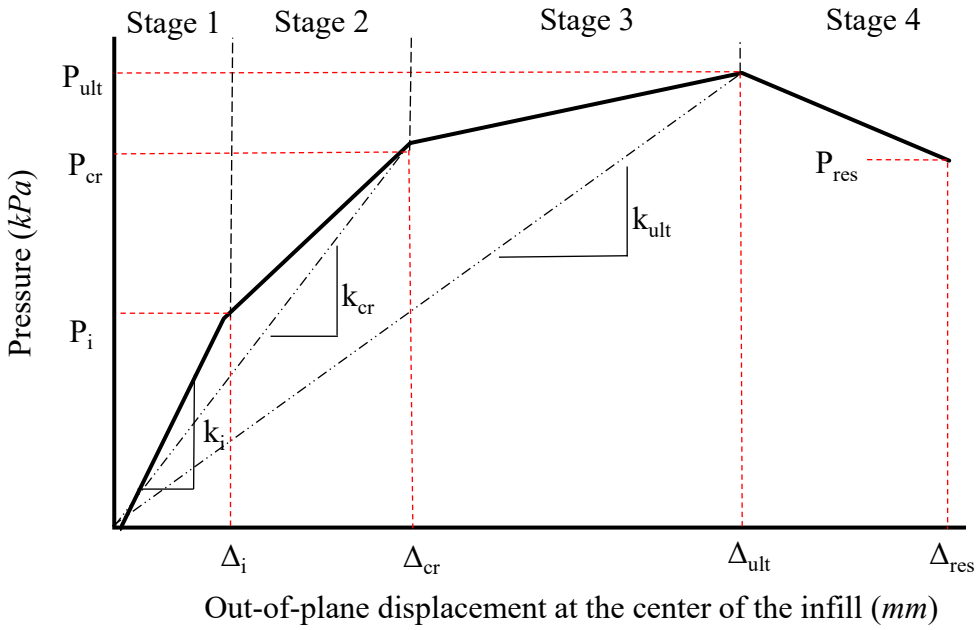

Figure 4.46 Definition of terms for load, displacement and stiffness

Table 4.7 Summary of steel framed infill results

	Result	C	FS	SW	TG	D1	CC	D2	VL
Out-of-plane	P_i (*kPa*)	7.2	6.9	10.4	6.5	8.8	8.0	4.5	11.4
	P_{cr} (*kPa*)	24.4	26.3	24.0	13.6	25.4	16.7	14.5	16.8
	P_{ult} (*kPa*)	30.6	29.0	29.9	16.6	26.2	18.4	16.7	18.3
	P_{res} (*kPa*)	30.1	28.1	*	15.1	24.3	*	*	17.9
	Δ_i (*mm*)	0.1	0.13	0.7	1.7	0.3	0.7	0.2	1.0
	Δ_{cr} (*mm*)	4.0	5.4	2.3	2.4	3.9	2.4	2.9	2.0
	Δ_{ult} (*mm*)	6.8	7.6	5.0	3.3	4.5	3.4	5.9	2.7
	Δ_{res} (*mm*)	8.5	8.6	*	4.9	6.0	*	*	4.0
	k_i (*kPa/mm*)	79.6	53.2	15.3	6.3	31.5	10.8	29.7	12.0
	k_{cr} (*kPa/mm*)	6.1	4.9	10.5	5.7	6.6	6.9	5.0	8.3
	k_{ult} (*kPa/mm*)	4.5	3.8	6.0	5.0	5.8	5.4	2.8	6.7
In-plane	P_{app} (*kN*)					77.5	77.5	145.4	
	δ_{app} (*mm*)					5.2	4.2	19.1	

*Some specimens underwent a sudden failure at ultimate and didn't have data after ultimate

CHAPTER 5 ASSESSMENT OF STUDIED PARAMETERS AND ANALYTICAL MODELS

5.1 INTRODUCTION

This chapter focuses on presentation and discussion of effect of the studied parameters through a comparison study using test results of this study presented in Chapter 4. Further, the comparison study also extends to include results from experimental studies conducted in Phase 1 (Sepasdar 2017) and 2 (Wang 2017) of the research framework to hopefully shed some light on the behaviour characteristics of RC frames vs. steel frames on masonry infills. This chapter also examines efficacy of the current analytical methods through a comparison analysis with the experimental results.

5.2 EFFECT OF STUDIED PARAMETERS

5.2.1 Additional strength from arching action

Using the flexural strength calculations found in APPENDIX A Out-of-plane flexural strength Calculations A, the Yield Line Analysis calculated an out-of-plane strength of 8.3 *kPa* for the "regular" specimens. The "regular" specimens reached an ultimate out-of-plane strength of 30 *kPa*. Arching Action caused the infill to reach a strength 3.6 times greater than the predicted flexural strength.

5.2.2 Effect of boundary frame (RC frame vs. steel frame)

A control specimen of concrete masonry infills bounded by a RC frame was tested in Phase 1 of the research project (Sepasdar 2017). This specimen, having the same infill geometries and CMUs, is considered the counterpart of Specimen IF-S-FS. **Figure 5.1** compares the pressure vs. out-of-plane displacement obtained at the center of the infills for both the RC framed and steel framed specimens. The RC frame specimen began with a high rigidity and behaved linearly till a loading of 26.8 *kPa*, which is a 74% increase compared to the pressure the infill with a steel frame reached in the linear phase. The RC framed specimen reached a pressure that was 28.5 *kPa* higher than the steel framed specimen before the first major crack occurred. The RC framed infill attained an ultimate capacity at 66.3 kPa which is approximately 2.3 times the steel framed specimen failed at 29 kPa.

Table 5.1 summarizes the pressure, displacement and stiffness of both infills at both the first major crack as well as at the point of ultimate load.

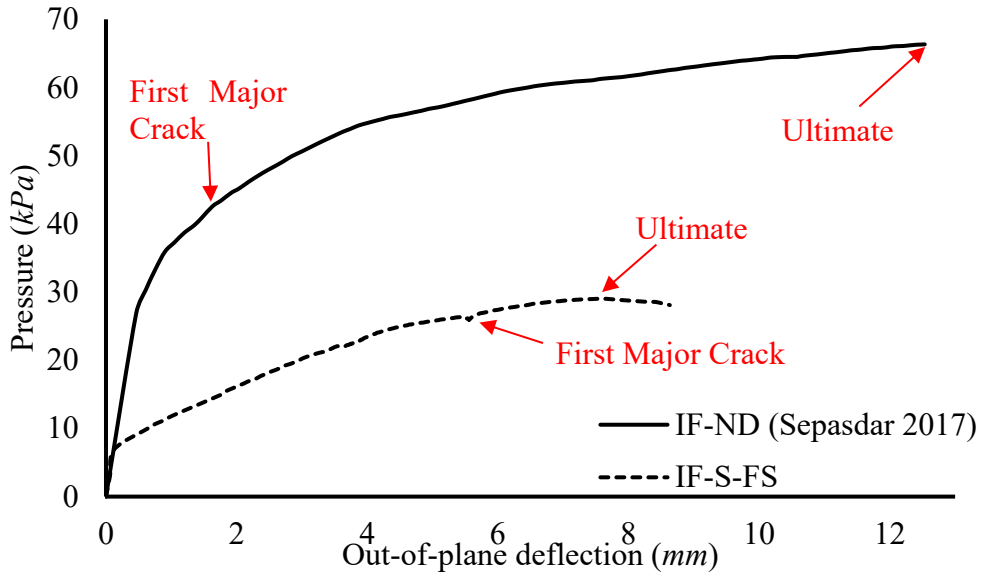

Figure 5.1 Comparison of pressure vs. displacement curves for RC framed and steel framed specimens

Table 5.1 Results from control specimens for both steel and RC framed infills

Test	P_{cr} (kPa)	P_{ult} (kPa)	Δ_{cr} (mm)	Δ_{ult} (mm)	k_{cr} (kPa/mm)	k_{ult} (kPa/mm)
IF-ND	45.2	66.3	2.0	12.5	22.6	5.3
IF-S-FS	26.3	29.0	5.4	7.6	4.9	3.8

Figure 5.2 displays the cracking pattern for the steel framed control specimen on the left and the RC framed control specimen on the right. Both infills had initial horizontal cracking at the mid-height of the infill. As the pressure increased, both infills began to crack towards the four corners resembling a yield line pattern. The RC framed infill had a more symmetrical cracking pattern than the steel framed infill, but general patterns remained relatively similar. Following the cracking pattern, the RC framed specimen underwent a significantly greater degree of arching action which in turn resulted in a significantly higher strength. At failure, both infills had the majority of faceshells sheared off. Web shear failure was the governing failure mode for both infills.

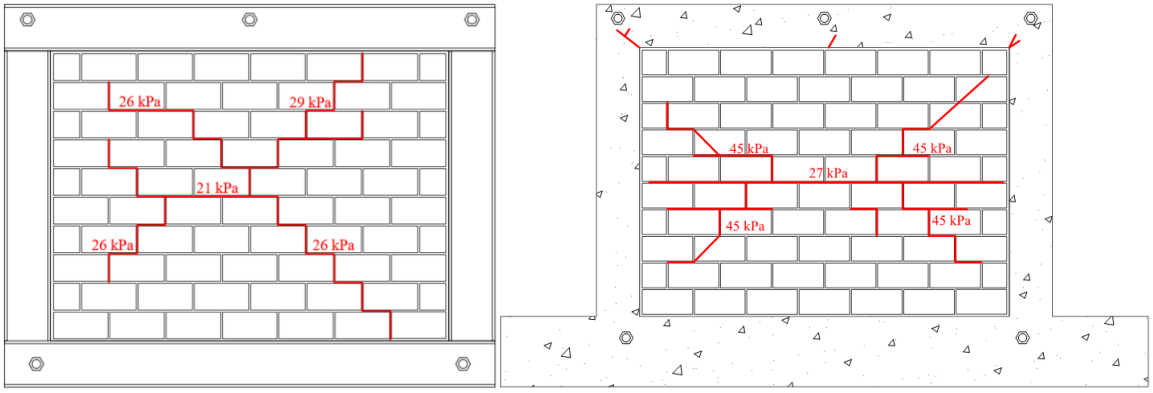

IF-S-FS IF-ND

Figure 5.2 Comparison of failure pattern between RC framed and steel framed control specimens

5.2.3 Effect of boundary frame support condition

Specimens IF-S-C, IF-S-FS, and IF-S-SW investigated the influence of boundary support conditions on the infill out-of-plane behaviour. The IF-S-C (Wang 2017) was tested with the bottom base beam not fully supported along its length; IF-S-FS provided a fully supported base beam; and IF-S-SW further provided stiffeners to the top and bottom boundary beams to increase the stiffness and torsional strength of the boundary beams. **Figure 5.3** compares the pressure vs. out-of-plane displacement for IF-S-C, IF-S-FS and IF-S-SW and **Table 5.2** summarizes the pressure, deflection and stiffness of the three infills at the first major crack and the ultimate stage. It is interesting to note that the three specimens attained similar strength and the minor differences may be attributed to material variation or inherent uncertainty in an experimental test. On the other hand, the behaviour of the three specimens showed more noticeable difference. While IF-S-C and IF-S-FS displayed similar stiffness and overall behaviour throughout the loading history, IF-S-SW exhibited an overall higher stiffness and deflected much less at the ultimate load.

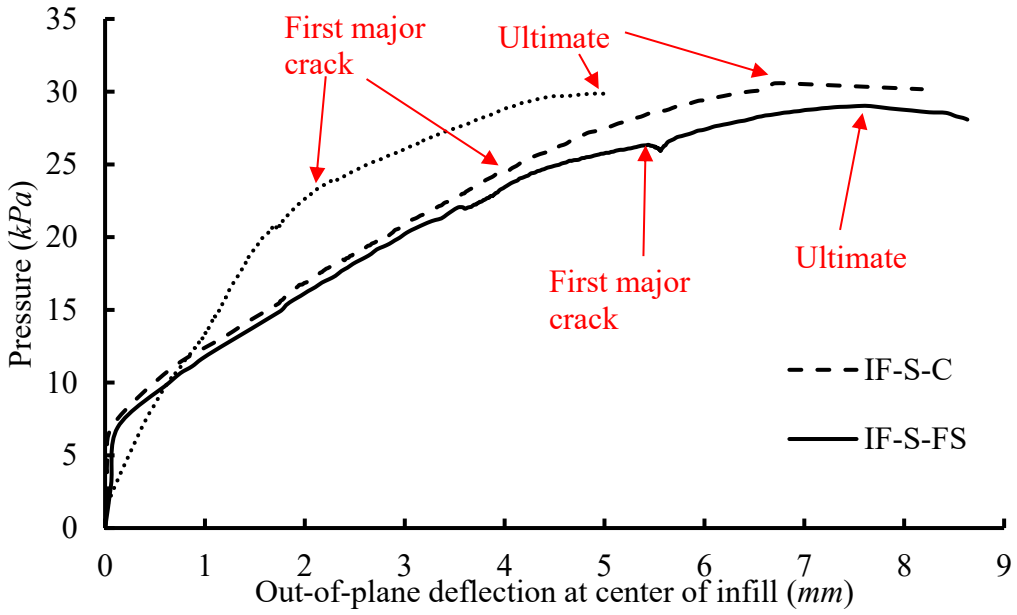

Figure 5.3 Comparison of pressure vs. displacement curves for boundary support condition study

Table 5.2 Results for the effect of boundary support condition

Test	P_{cr} (kPa)	P_{ult} (kPa)	Δ_{cr} (mm)	Δ_{ult} (mm)	k_{cr} (kPa/mm)	k_{ult} (kPa/mm)
IF-S-C	24.4	30.6	4.0	6.8	6.1	4.5
IF-S-FS	26.3	29.0	5.4	7.6	4.9	3.8
IF-S-SW	24.0	29.9	2.3	5.0	10.5	6.0

Figure 5.4 displays the cracking pattern for the three specimens. They showed a more or less similar cracking pattern and the noted difference is that IF-S-SW sustained more extensive cracking than the other two test specimens. All three infills had the same failure mechanism of web shear failure due to face shell separation. It was thought that the web stiffeners would increase the stiffness of the boundary beam which would in turn lead to higher strength. The test results did not support the initial hypothesis. While more test results are needed to make a definitive conclusion, the results seem to suggest that the base beam support as investigated herein does not add significant benefit to out-of-plane strength of the infill. It needs to be cautioned that since only intermittent stiffeners were used to stiffen the beam, the results may also suggest that this type of stiffening technique is not sufficient to cause a significant beam stiffness increase.

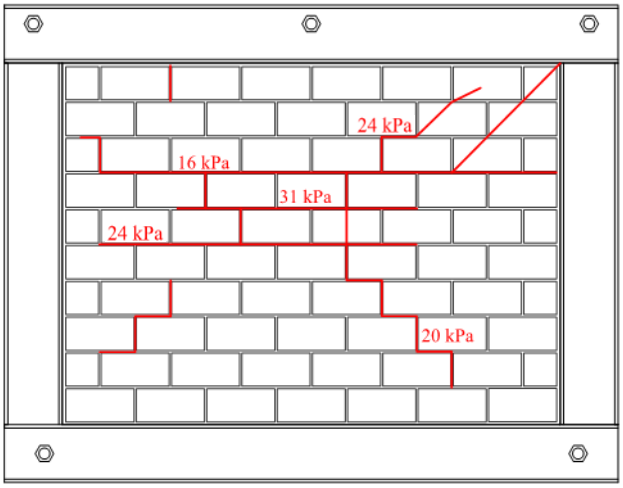

IF-S-C

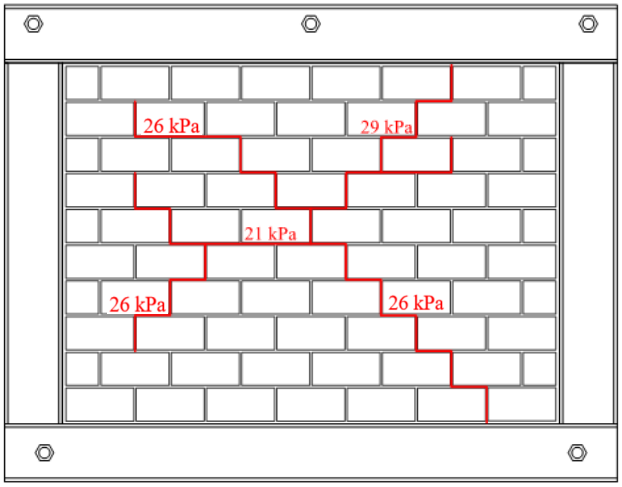

IF-S-FS

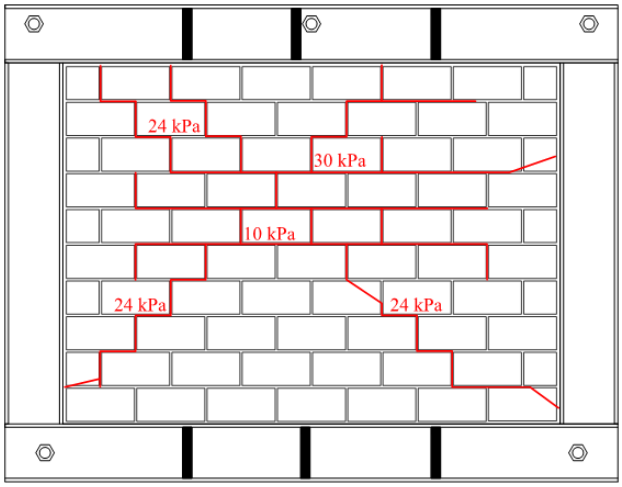

IF-S-SW

Figure 5.4 Comparison of cracking pattern of steel framed infills with different support conditions

5.2.4 Effect of top gap

The effect of gap between the frame top beam and the infill is illustrated by comparing specimens IF-S-TG and IF-S-FS. **Figure 5.5** shows the pressure vs. out-of-plane displacement curves whereas **Table 5.3** summarizes the pressure, displacement and stiffness at the first major crack and ultimate stages of these two specimens. The difference in both behaviour and strength is distinctive. The presence of a top gap caused the infill to have a lower initial stiffness, earlier onset of cracking, and lower ultimate strength with reduced ductility. A 10 mm top gap resulted in more than 40% reduction in both the cracking and ultimate strength and about 56% less displacement at failure.

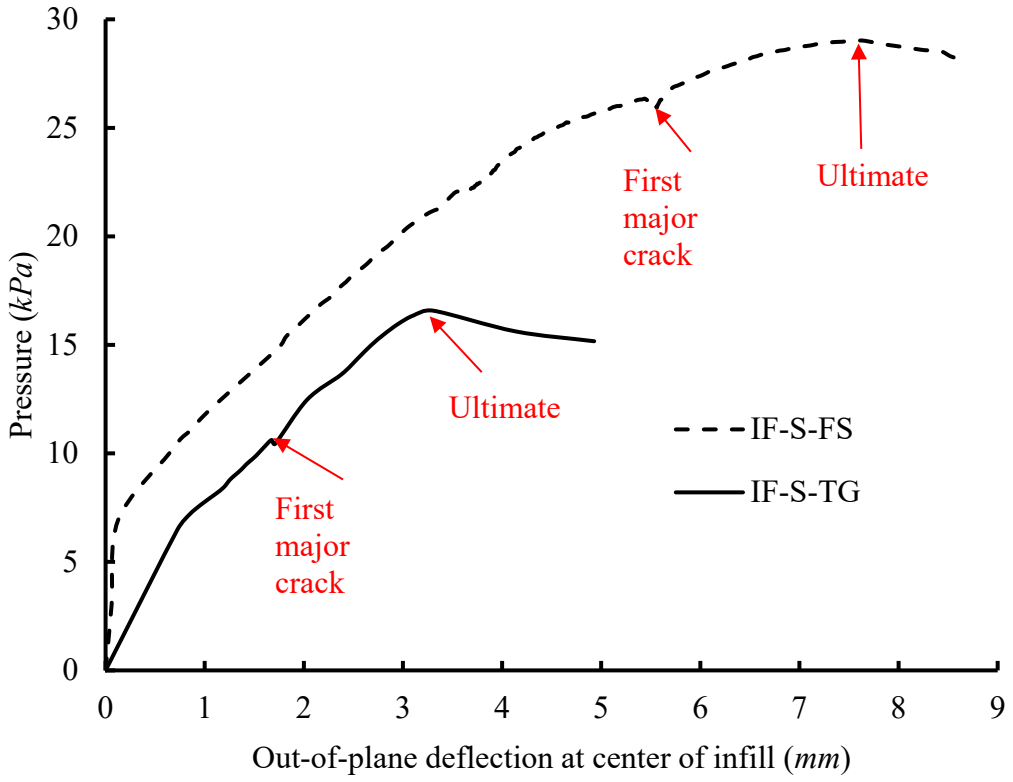

Figure 5.5 Comparison of pressure vs. displacement curves for top gap study – steel frames

Table 5.3 Results for top gap study- a 10 *mm* top gap and steel frame

Test	P_{cr} (kPa)	P_{ult} (kPa)	Δ_{cr} (mm)	Δ_{ult} (mm)	k_{cr} (kPa/mm)	k_{ult} (kPa/mm)
IF-S-FS	26.3	29.0	5.4	7.6	4.9	3.8
IF-S-TG	13.6	16.6	2.4	3.3	5.7	5.0
Effect of top gap	-48.2%	-42.9%	-56.2%	-56.4%	18.1%	31.1%

The cracking pattern for the two specimens are further compared in **Figure 5.6**. The control specimen, IF-S-FS, displayed a cracking pattern consistent with a yield line pattern of an infill with four boundary supports, specimen IF-S-TG, on the other hand, showed a pattern resembling more to a cracking pattern for a panel with only three side supported indicated by pronounced vertical cracking. As discussed previously, it is believed that arching in the vertical direction did not fully develop which resulted in lower strength and different failure mode.

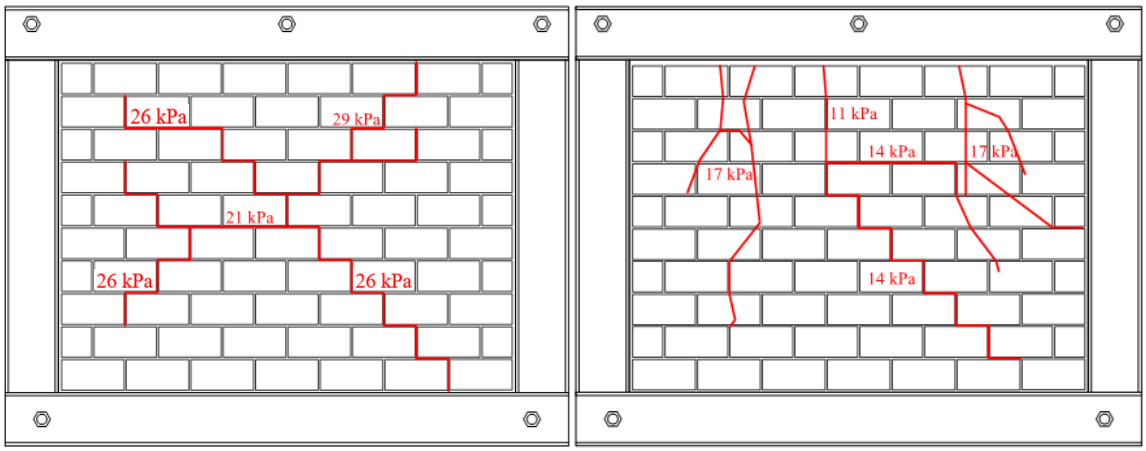

Figure 5.6 Comparison of cracking pattern for steel framed control specimen and specimen with a top gap

In Phase 2 of this research project, Wang (2017) tested a RC framed infill with a 10 *mm* gap at the frame top beam and infill interface. **Figure 5.7** then compares the pressure vs. out-of-plane displacement curves for the gapped and control specimens with RC frames.

Table 5.4 summarizes the pressure, displacement and stiffness at the first major crack and ultimate stages and **Figure 5.8** compares the cracking patterns for the two specimens. It can be seen that the effect of top gap for a RC framed infill in terms of reducing initial stiffness, overall ductility, cracking pattern and ultimate strength is comparable to a steel framed infill. When the exact magnitude is concerned, the presence of the top gap of same size (10 mm) seems to have a greater effect on RC framed infills where a decrease of 72% in ultimate strength was observed.

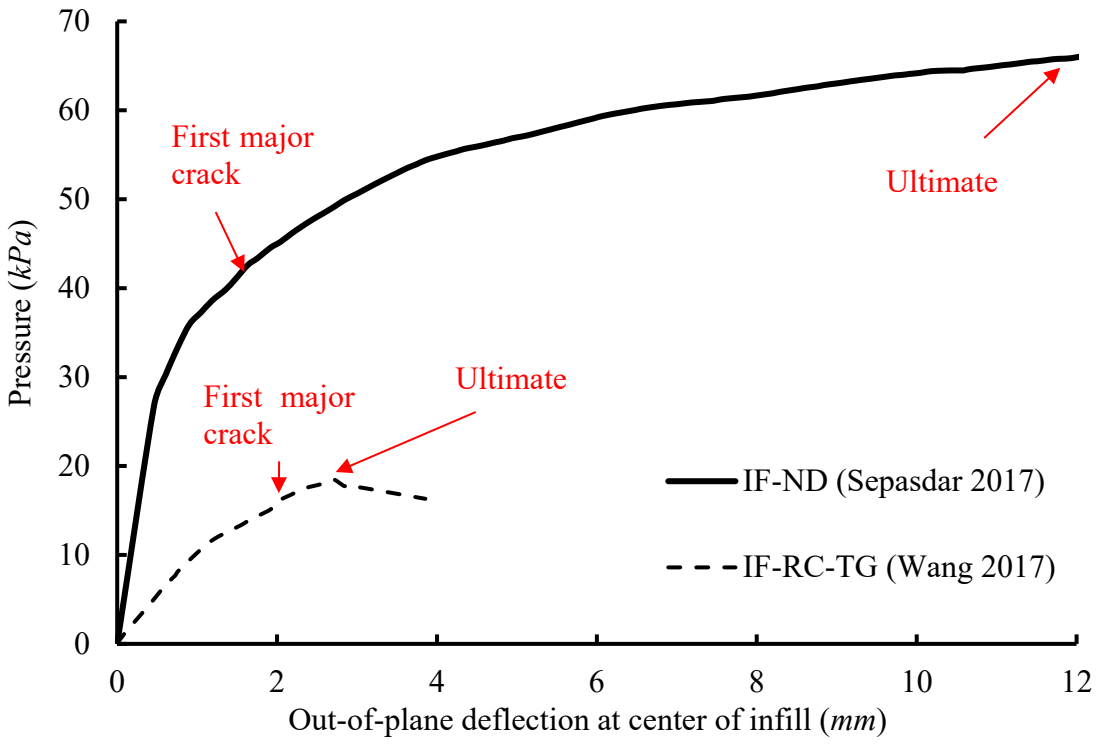

Figure 5.7 Comparison of pressure vs. displacement curves for top gap study - RC frames

Table 5.4 Results for top gap study- a 10 *mm* top gap and RC frame

Test	P_{cr} (kPa)	P_{ult} (kPa)	Δ_{cr} (mm)	Δ_{ult} (mm)	k_{cr} (kPa/mm)	k_{ult} (kPa/mm)
IF-ND	45.2	66.3	2.0	12.5	22.6	5.3
IF-RC-TG	16.1	18.5	2.0	2.7	8.1	6.9
Effect of top gap	-64.4%	-72.1%	0.0%	-78.4%	-64.2%	30.2%

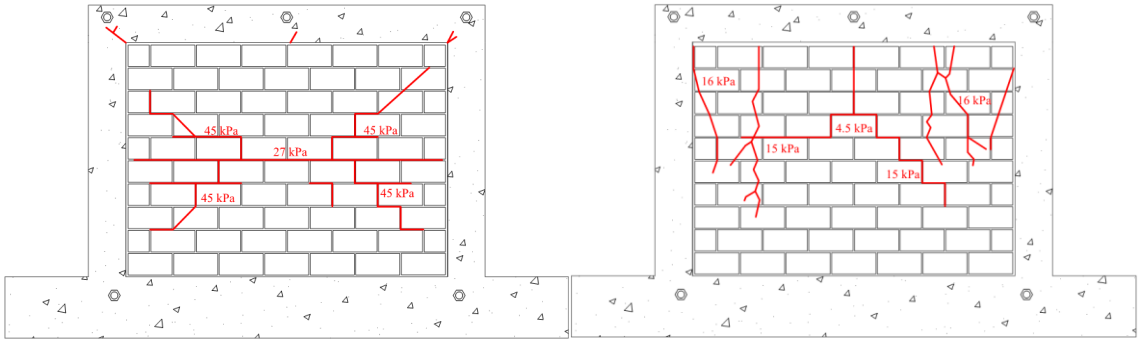

IF-RC IF-RC-TG

Figure 5.8 Comparison of cracking pattern for RC framed control specimen and specimen with a top gap

Figure 5.9 compares the pressure vs. out-of-plane displacement curves for steel and RC framed infill specimens which had the 10 *mm* top gap. The behaviour of both infills began linearly, the steel framed infill underwent initial cracking much earlier than the RC framed counterpart (45% reduction). The steel framed specimen underwent its first major crack at a reduced pressure (15.5%). The steel framed specimen had a 10% reduction in ultimate pressure but displayed a slightly greater ductility. It shows that overall, the gapped RC framed infill still attained higher ultimate strength than the gapped steel framed infill, but the strength difference is much less than that between the control specimens. A potential reasoning is provided in the following. First, a control RC framed infill sustained much greater strength (128% greater) than a control steel framed infill (Section 5.2.1). This is believed to be due to 1) higher torsional stiffness of the RC frame members ($GJ=1.09x10^{12}$

$N{\cdot}mm^2$) than the steel frame members (GJ=7.81x10^9 $N{\cdot}mm^2$); and 2) better bond between the mortar and the RC boundary frame than the steel boundary frame. The higher torsional stiffness of boundary frame members will enable better development of arching action by providing a more rigid boundary for the infill, which leads to higher ultimate strength of an infill. A better mortar bond would provide a higher initial stiffness as well as an increased friction force for increased arching action. Removing a top boundary support as in the case of the top gap essentially eliminates the beneficial effects of the stiffness of the top beam and bond at top beam location, the two main contributor to a higher strength of a RC framed infill. Thus, it has more adversary effect on a RC framed infill than a steel framed infill.

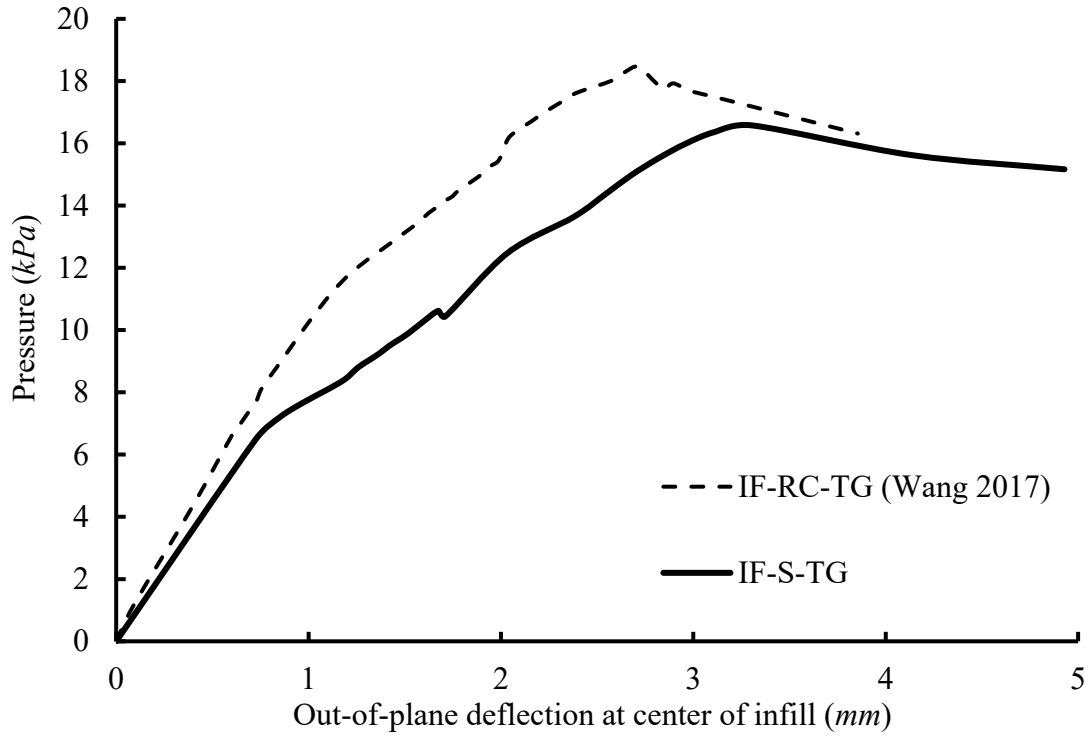

Figure 5.9 Comparison of pressure vs. displacement curves for specimens with a 10 *mm* top gap and different boundary frame materials

5.2.5 Effect of in-plane damage on the out-of-plane strength

In this experimental study, specimens IF-S-D1 and IF-S-D2 were tested to study the effect of in-plane damage on the out-of-plane strength. The former was loaded to the occurence of a visible diagonal crack at 77.5 *kN* and a resulting in-plane displacment of 5.2 *mm*. The latter was first loaded out-of-plane, than loaded in-plane to its ultimate in-plane capacity at a load of 145 *kN* and the resulted displacement of 19 *mm*. The specimen was then loaded again out-of-plane to determine its residual out-of-plane capacity. **Figure 5.10** displays the pressure vs. displacement curves for specimens IF-S-D1 and IF-S-D2 (2^{nd} out-of-plane loading) along with the control specimen, IF-S-FS. **Table 5.5** provides a summary of the results from out-of-plane loading on infills with prior in-plane damage. When comparing damaged specimens with the control specimen, it is found that in-plane damage resulted in reduction in the out-of-plane strength of the infill and degree of the reduction is related to the level of damage. Qualitatively, the more the damage, the more the reduction. Further, specimen IF-S-D2 showed much softer load-displacement response while specimen IF-S-D1 exhibited similar or slightly higher stiffness than the control specimen. **Figure 5.11** displays the cracking patterns on the leeward face for IF-S-FS, IF-S-D1, and IF-S-D2. The cracks in red represent the out-of-plane damage whereas the cracks in blue represent in-plane damage. The out-of-plane damage displayed for specimen IF-S-D2 is from the initial loading. The much softer response for IF-S-D2 is then attricuted to more extensive in-plane cracking and it may be observed that in-plane damage in the form of a single diagonal crack did not result in a significant change in infill stiffness.

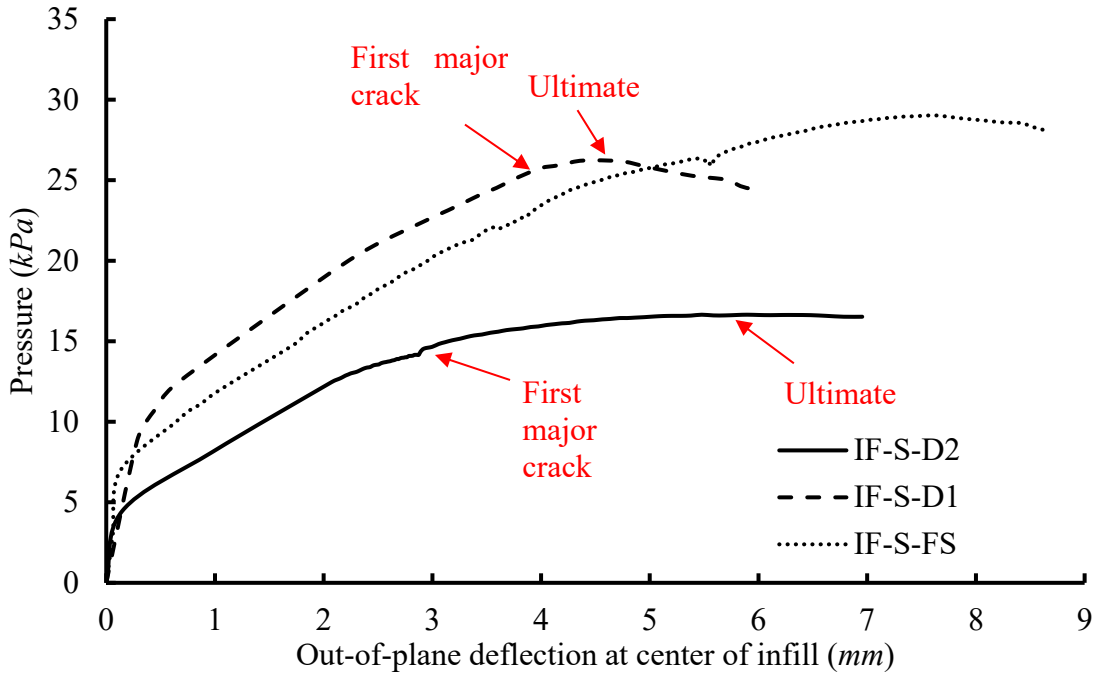

Figure 5.10 Comparison of pressure vs. displacement curves for prior in-plane damage study

Table 5.5 Summary of results for prior in-plane damage study

Test	P_{cr} (*kPa*)	P_{ult} (*kPa*)	Δ_{cr} (*mm*)	Δ_{ult} (*mm*)	k_{cr} (*kPa/mm*)	k_{ult} (*kPa/mm*)
IF-S-FS	26.3	29.0	5.4	7.6	4.9	3.8
IF-S-D1	25.4	26.2	3.9	4.5	6.5	5.8
IF-S-D2	14.5	16.7	2.9	5.9	5.0	2.8

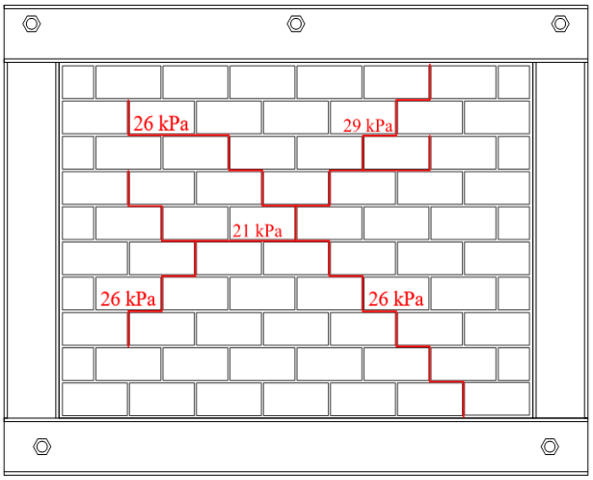

IF-S-FS

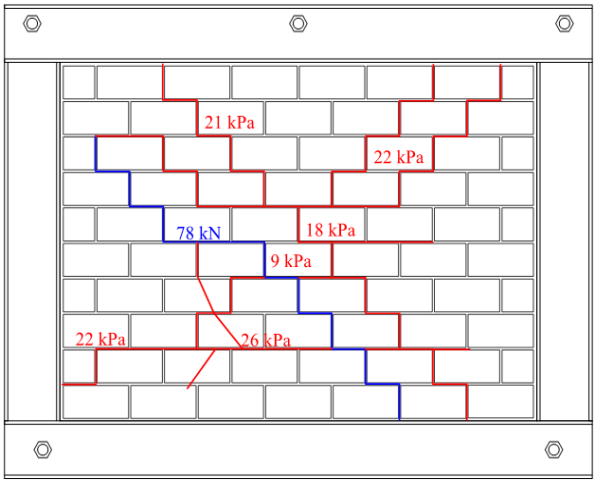

IF-S-D1

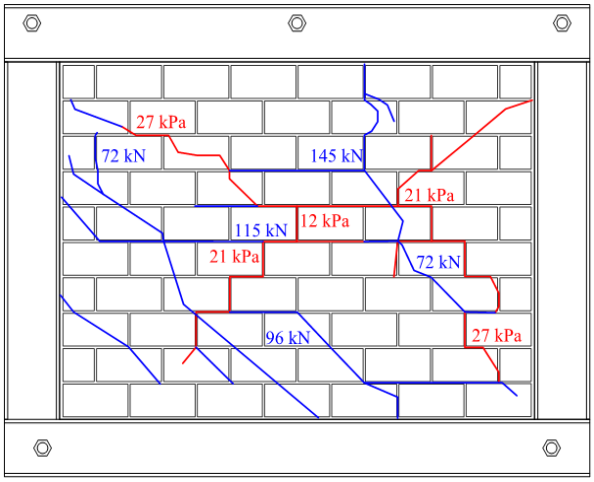

IF-S-D2

Figure 5.11 Comparison of cracking patterns for steel framed infills with and without prior damage

In addition to these two tests, three tests were conducted with prior in-plane damage in the Phase I and II of this research framework but on RC framed infills.

Table 5.6 summarizes the results from both sets of tests with calculated reductions with respect to control specimens of each set. The prior in-plane damage level is defined as the ratio of applied in-plane displacement to the displacement at the ultimate in-plane strength, $\delta_{app}/\delta_{ult}$. The value of δ_{ult} was found to be 19 *mm* for steel framed specimens from the loading on IF-S-D2 and 17 *mm* for RC framed specimens from test IF-RC-D2 conducted by Sepasdar (2017).

Table 5.6 Results from specimens with prior in-plane damage on RC framed infills

Research	Test	$\delta_{app}/\delta_{ult}$	Ultimate Strength (*kPa*)	Reduced Capacity (%)
Sepasdar (2017)	IF-ND	-	66.3	-
	IF-RC-D1	0.38	44.7	33.1
	IF-RC-D2	1.56	26.4	60.0
Wang (2017)	IF-RC-ID	0.80	37.5	43.4
Smith (2018)	IF-S-FS	-	29.0	-
	IF-S-D1	0.27	26.2	9.7
	IF-S-D2	1	16.6	42.6

Figure 5.12 illustrates the trend for both steel and RC framed infills of reduction in ultimate capacity based on the degree of in-plane damage as described above. For RC framed infills the trend is more or less linear for the data obtained. More data points on different damage levels are in need to provide a definable correlation for steel framed infills. The general observation can be made that if a linear trend is also assumed for $\delta_{app}/\delta_{ult}$ less than 0.4 for RC framed infills, it suggests that the steel framed infill showed less reductions in the out-

of-plane strength for a given damage level either at cracking or reaching prior in-plane ultimate level.

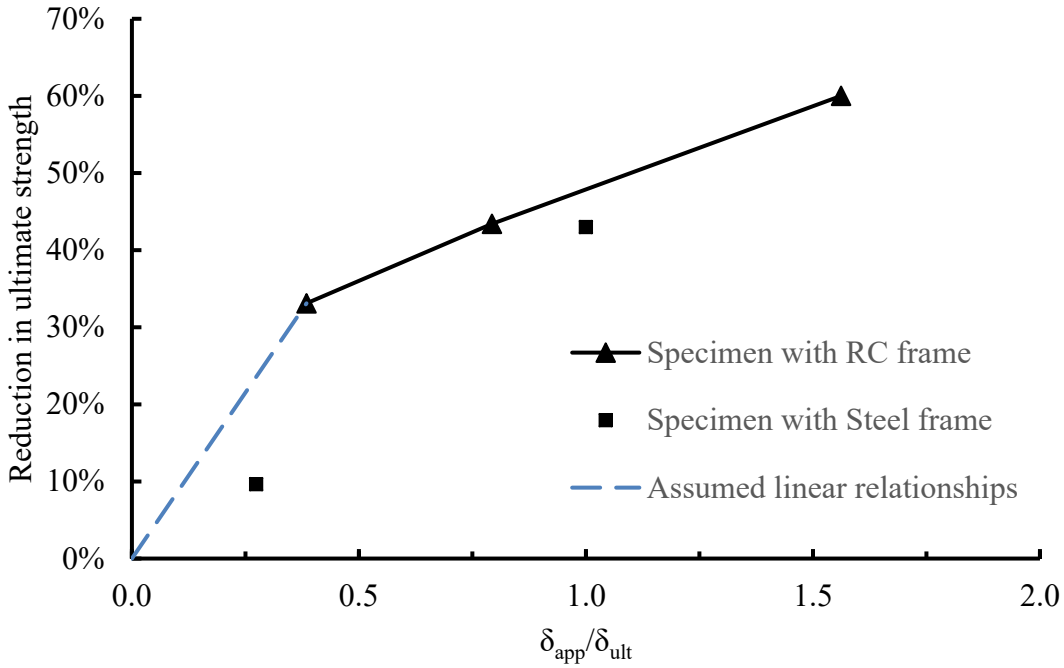

Figure 5.12 Reduction in out-of-plane strength vs degree of in-plane damage on masonry infills

5.2.6 Effect of in-plane damage and loading on the out-of-plane strength

Specimen IF-S-CC sustained the same in-plane load of 77.5 *kN* that caused a visible diagonal crack as in specimen IF-S-D1. This loading however, was kept constant while the out-of-plane loading was applied. **Figure 5.13** compares the pressure vs. displacement curves for specimens IF-S-CC, IF-S-D1 and IF-S-FS. It shows that the presence of prior damage as well as prior loading had a more pronounced effect than the presence of prior damage alone. With the combined prior damage and loading, the reductions in the ultimate strength was 36.6% and in the out-of-plane displacement at ultiamte was 55.1%, significant increases from respective 9.7% and 40.7% for prior damage alone. The combined prior

damge and loading resulted in a much softer response at the onset of loading and much reduced ductility at the ultimate.

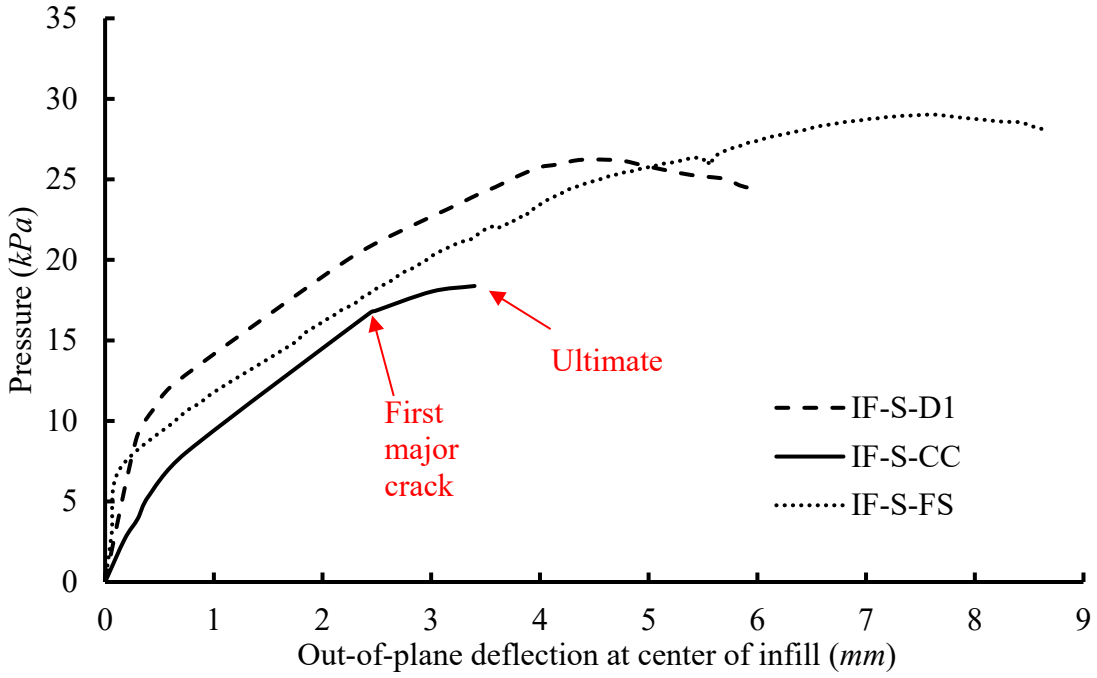

Figure 5.13 Comparison of pressure vs. displacement curves for influence of concurrent loading

Figure 5.14 illustrates the cracking patterns for IF-S-D1 and IF-S-CC. It can be observed that when the in-plane load was removed, the infill was able to undergo more arching as indicated by more extensive cracking. The in-plane crack pattern is similar in both cases and the failure mode for both specimens was by web shear failure of CMUs. It is conceivable that the presence of in-plane as well as out-of-plane loading may weaken the CMUs and accelerate the web cracking.

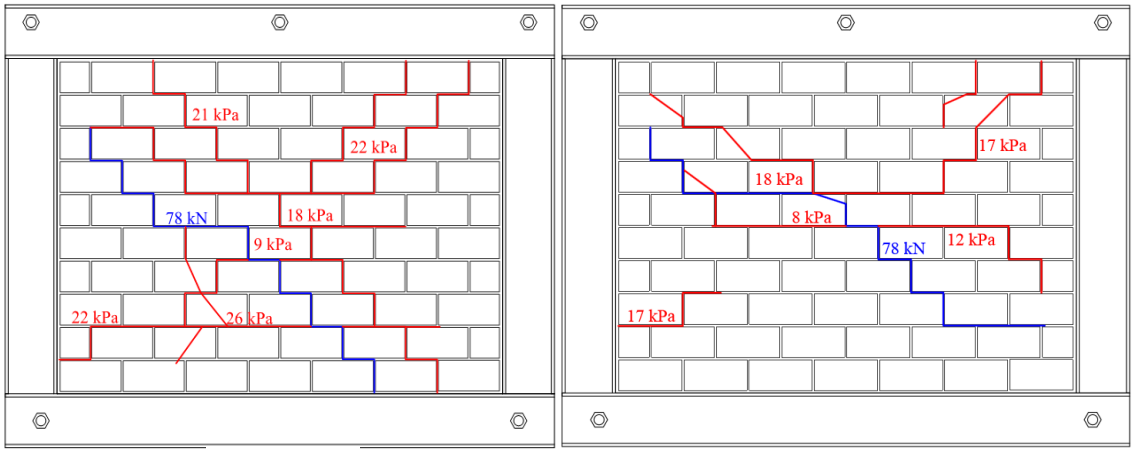

IF-S-D1 IF-S-CC

Figure 5.14 Comparison of cracking patterns for infills with prior damage and concurrent loading

5.2.7 Effect of out-of-plane damage on the in-plane strength

Specimen IF-S-D2 was loaded out-of-plane first to a cracking load (occurrence of a mid-height horizontal crack) before the infill was tested in-plane. The load vs. displacement curves for the in-loading stage for IF-S-D2 as well as the in-plane loading response for IF-S-D1 are together shown in **Figure 5.15**. The lower initial stiffness (36% lower) from IF-S-D2 is believed to be attributed to the prior out-of-plane damage. In order to determine whether the prior out-of-plane damage has any effect on the infill in-plane strength, a control specimen subjected to in-plane loading to its ultimate capacity is needed for comparison. Although this specimen was not included in this testing program, the following comparison on tested RC framed infills may provide some qualilative observations. Specimens IF-RC-D1 and IF-RC-D2 tested by Sepasdar (2017) had same design parameters as IF-S-D1 and IF-S-D2 in terms of prior loading damage. **Figure 5.16** displays the load vs. displacement curves for specimen IF-RC-D2 during the in-plane loading stage (after sustain out-fo-plane damage in the form of a horizontal mid-height

crack) as well as the prior in-plane loading stage for IF-RC-D1. The RC framed specimens displayed similar initial stiffnesses, indicating the prior out-of-plane damage had negligible effect on a RC frame. Specimen IF-RC-D2 was loaded to its ultimate in-plane capacity showing an approximately 140 kN in this case. Since the in-plane strength of an infilled frame is largely dependent on its infill property and geometry, it is reasonable to deduce that the ultimate in-plane strength of the steel framed infill is similar to the RC framed infill with the same infill gemetry and material properties. Hence, specimen IF-S-D2 in-plane strength can be reasonably assumed to be around 140 kN. As IF-S-D2 was loaded till 140 kN (then close to its ultimate strength), it can be concluded that the prior out-of-plane damage had little effect on the in-plane strength of the infilled frame.A similar conclusion was also made with RC framed infills.

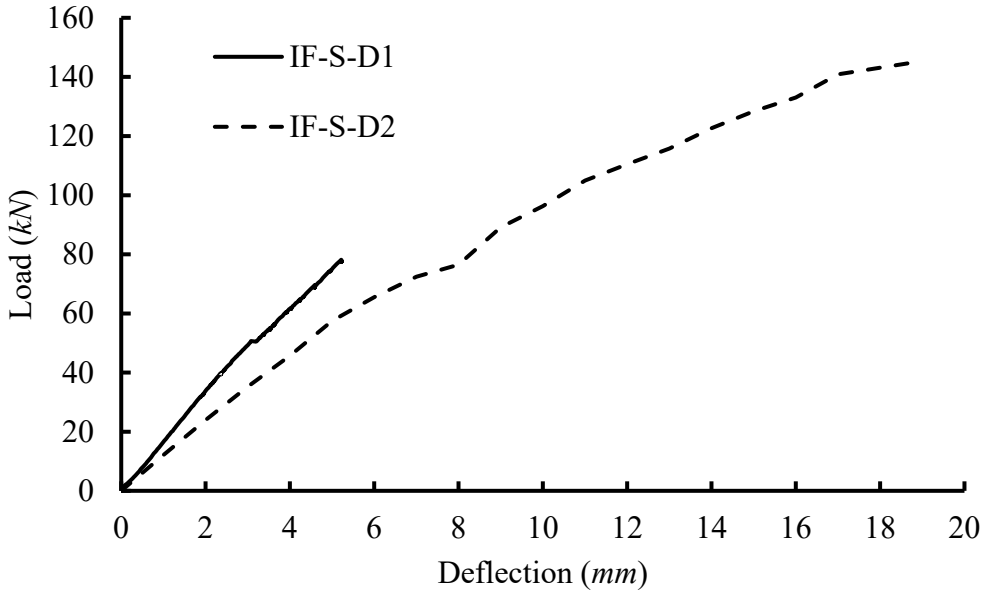

Figure 5.15 Comparison of load vs. deflection curves for in-plane loadings on steel framed infills

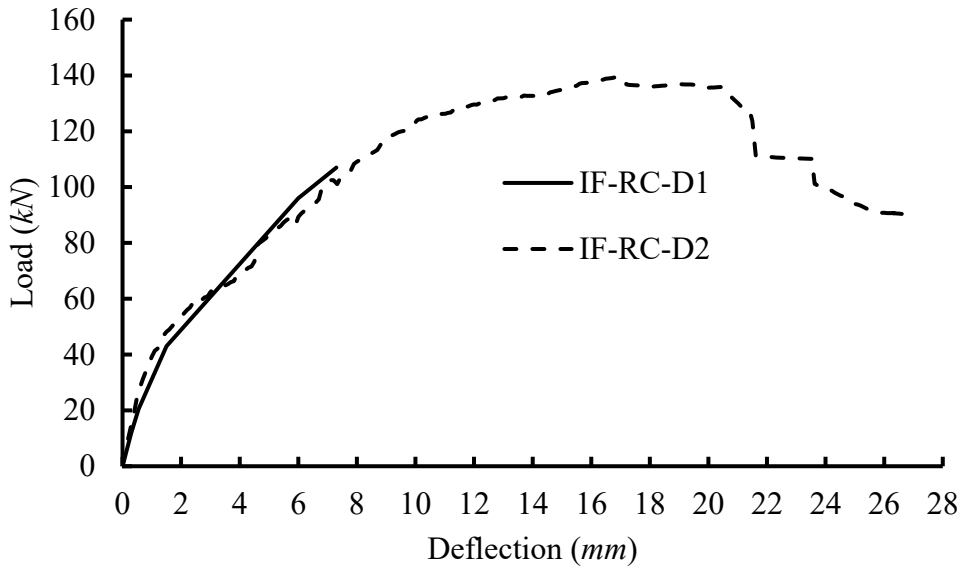

Figure 5.16 Comparison of load vs. deflection curves for in-plane loadings on RC framed infills

5.2.8 Effect of vertical load

The effect of vertical load on the out-of-plane behaviour is illustrated in **Figure 5.17** where pressure vs. out-of-plane displacement curves of specimens IF-S-VL and IF-S-FS are compared. **Table 5.7** summarizes the results of the two tests. As soon as the test began, the infill with the vertical load displayed a reduced initial stiffness and the first major crack occurred at much earlier loading stage. The vertical load caused the infill to reach its ultimate capacity at a pressure 36.8% less than the control specimen. The addition of the vertical load also caused a severe reduction in ductility as the infill had deflected only 2.7 *mm* out-of-plane before reaching the ultimate load, compared to 7.6 *mm* for the control specimen (63.9% less). While the reduction of ductility is reasonable, the reduction in strength is somewhat unexpected as it was thought that the presence of vertical load would increase the stiffness of the bounding beam and therefore increase the strength. A

comparison of the cracking patterns of the two specimens as shown in **Figure 5.18** may suggest an explanation.

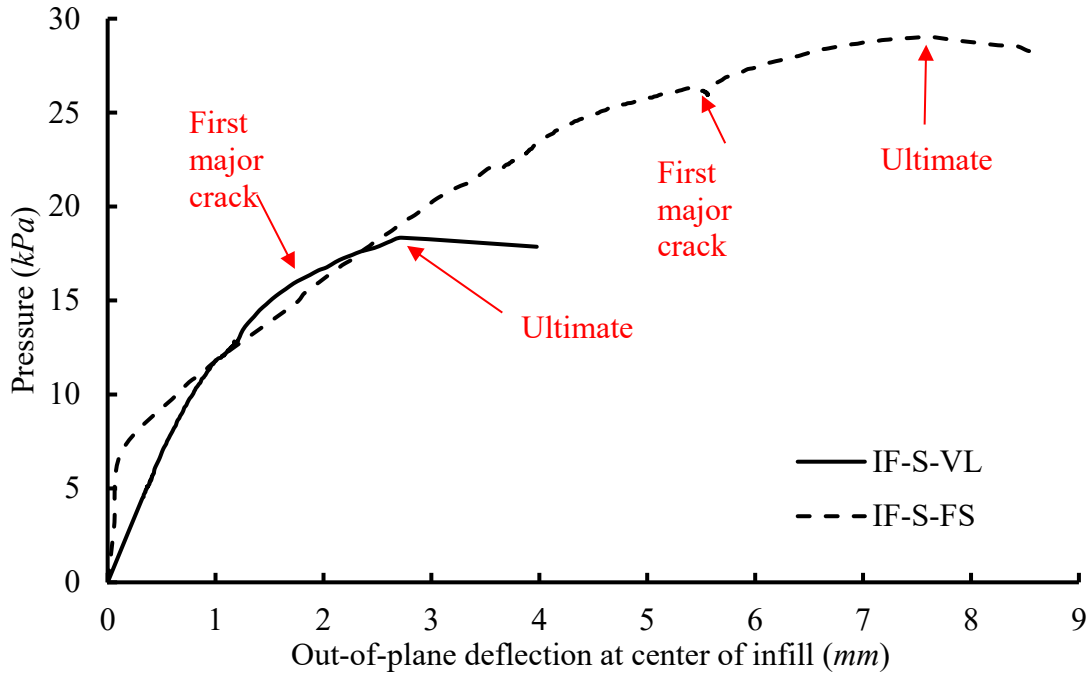

Figure 5.17 Comparison of pressure vs. displacement curves for the vertical loading study

Table 5.7 Results for vertical load study

Test	P_{cr} (kPa)	P_{ult} (kPa)	Δ_{cr} (mm)	Δ_{ult} (mm)	k_{cr}	k_{ult}
IF-S-FS	26.3	29.0	5.4	7.6	4.9	3.8
IF-S-VL	16.8	18.3	2.0	2.7	8.3	6.7
Effect of vertical load	-36.3%	-36.8%	-62.6%	-63.9%	70.3%	75.5%

In addition to expected yield line like cracks, the presence of the vertical load caused the marked vertical cracks first to occur one course below the mid-height of the infill and then two vertical tensile cracks roughly below the applied vertical load. This cracking pattern at failure is similar to the cracking pattern for IF-S-TG which had the 10 *mm* top gap. The cause of failure for IF-S-VL was due to the vertical tensile cracking as opposed to the

faceshell separation caused by web shear failure displayed in the control specimen. The introduction of predominant vertical cracks may have interfered with the development of effective arching. It is premature to draw conclusions on whether the vertical load can be beneficial or detrimental to the out-of-plane strength of infills. This specimen revealed that however, application methods are important and if the application is such that it leads to localized vertical cracks, the out-of-plane strength may be reduced.

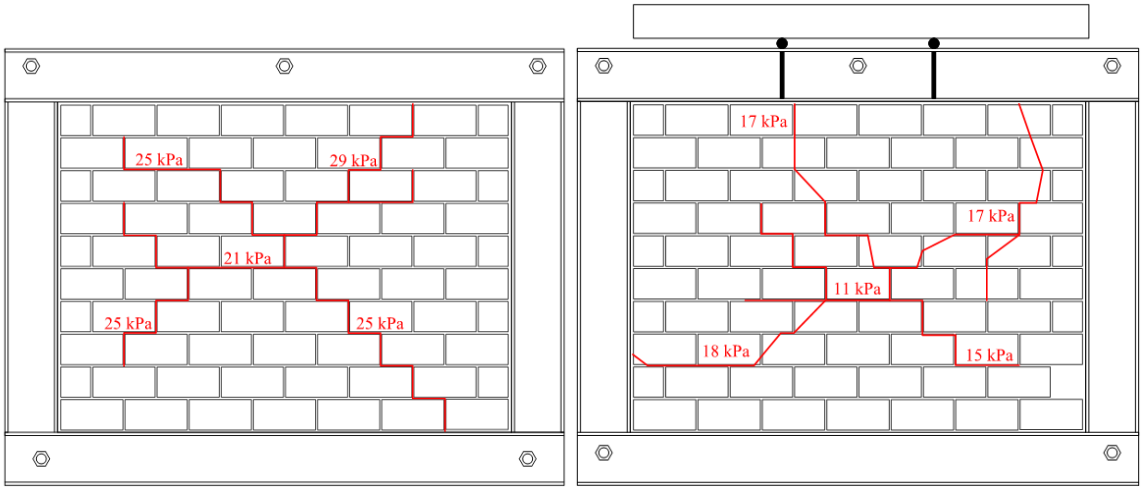

IF-S-FS IF-S-VL

Figure 5.18 Comparison of cracking patterns between steel framed control specimen and specimen with vertical loading

5.3 VALIDATION OF ANALYTICAL MODELS USING EXPERIMENTAL RESULTS

This section evaluates the validity of existing analytical models for determining the out-of-plane strength and displacement of masonry infills using the experimental results from this study, as well as from Phase 1 and Phase 2 studies by Sepasdar (2017) and Wang (2017) respectively. The material and geometric properties for each test specimen, which are used

in the evaluation of the analytical models, are summarized in **Table 5.8**, **Table 5.9**, and **Table 5.10.**

For additional results comparison, **Table 5.11** and **Table 5.12** contain the material and geometric properties of research conducted by previous researchers on "regular" masonry infills with steel framed and RC frames specimens respectively.

Table 5.8 Material and geometric properties of specimens from Sepasdar (2017)

ID	IF-ND	IF-D1	IF-D2
t (*mm*)	90	90	90
h (*mm*)	980	980	980
l (*mm*)	1350	1350	1350
f'_m (*MPa*)	9.4	9.7	9.7
E_m (*MPa*)	7990	8245	8245
f'_j (*MPa*)	20.4	21.6	21.6
$E_b=E_c$ (*MPa*)	16911	16911	20357
$I_b=I_c$ ($x10^6$ mm^4)	104.7	104.7	104.7
EI ($N{\cdot}mm^2$)	$1.77x10^{12}$	$1.77x10^{12}$	$2.13x10^{12}$
$G_b=G_c$ (*MPa*)	7352.6	7352.6	8850.9
$J_b=J_c$ ($x10^6$ mm^4)	147.9	147.6	147.6
GJ ($N{\cdot}mm^2$)	$1.09x10^{12}$	$1.09x10^{12}$	$1.31x10^{12}$

Table 5.9 Material and geometric properties of specimens from Wang (2017)

ID	IF-RC-DO	IF-RC-ID	IF-RC-TG	IF-S-C
t (*mm*)	90	90	90	90
h (*mm*)	980	980	980	980
l (*mm*)	1350	1350	1350	1350
f'_m (*MPa*)	8.1	9.4	8.2	8.8
E_m (*MPa*)	6885	7990	6970	7480
f'_j (*MPa*)	10.4	10.4	7.6	8.4
$E_b=E_c$ (*MPa*)	16911	16911	16911	201172
$I_b=I_c$ ($x10^6$ mm^4)	104.7	104.7	104.7	17.2
EI ($N{\cdot}mm^2$)	$1.77x10^{12}$	$1.77x10^{12}$	$1.77x10^{12}$	$3.46x10^{12}$
$G_b=G_c$ (*MPa*)	7352.6	7352.6	7352.6	77374
$J_b=J_c$ ($x10^6$ mm^4)	147.9	147.6	147.6	0.101
GJ ($N{\cdot}mm^2$)	$1.09x10^{12}$	$1.09x10^{12}$	$1.09x10^{12}$	$7.81x10^{9}$

Table 5.10 Material and geometric properties from specimens from this study

ID	IF-S-FS	IF-S-SW	IF-S-TG	IF-S-D1	IF-S-D2	IF-S-CC	IF-S-VL
t (*mm*)	90	90	90	90	90	90	90
h (*mm*)	980	980	980	980	980	980	980
l (*mm*)	1350	1350	1350	1350	1350	1350	1350
f'_m (*MPa*)	8.8	11.0	8.8	8.8	11.0	9.2	10.8
E_m (*MPa*)	7480	7820	7480	7480	9350	7820	9180
f'_j (*MPa*)	8.4	13.0	10.4	8.4	13.0	16.6	13.9
E_b=E_c (*MPa*)	201172	201172	201172	201172	201172	201172	201172
I_b=I_c (x10^6 mm^4)	17.2	17.2	17.2	17.2	17.2	17.2	17.2
EI ($N{\cdot}mm^2$)	3.46x10^{12}	3.46x10^{12}	3.46x10^{12}	3.46x10^{12}	3.46x10^{12}	3.46x10^{12}	3.46x10^{12}
G_b=G_c (*MPa*)	77374	77374	77374	77374	77374	77374	77374
J_b=J_c (x10^6 mm^4)	0.101	0.101	0.101	0.101	0.101	0.101	0.101
GJ ($N{\cdot}mm^2$)	7.81x10^9	7.81x10^9	7.81x10^9	7.81x10^9	7.81x10^9	7.81x10^9	7.81x10^9

Table 5.11 Material and geometric properties with experimental results from experimental programs consisting of steel framed masonry infills subjected to out-of-plane loading

Research	Dawe and Seah (1989)				Flanagan and Bennett (1999)		
ID	WE2	WE4	WE8	WE5	#22	#18	#25
t (*mm*)	190	140	140	90	330	195	93
h (*mm*)	2800	2800	2800	2800	2250	2250	2250
l (*mm*)	3600	3600	3600	3600	2250	2250	2250
f'_m (*MPa*)	28.1	22.7	27.4	20.2	5.6	5.6	5.6
E_m (*MPa*)	23000	13800	16200	15600	5300	5300	5300
E_b=E_c (*MPa*)	200000	200000	200000	200000	200000	200000	200000
I_b (x10^6 mm^4)	45.4	45.4	45.4	45.4	556	119	120
I_c (x10^6 mm^4)	87.3	87.3	87.3	87.3	216	71.1	71.1
P_{ult} (*kPa*)	19.2	11.2	13.4	7.8	39.5	26.6	8.1
Δ_{ult} (*mm*)	50	90	60	80	49.5	11.5	25.3

Table 5.12 Material and geometric properties with experimental results from experimental programs consisting of RC framed masonry infills subjected to out-of-plane loading

Research	Angel (1994)	Furtado et al. (2016)
ID	Test 1	Inf_02
t (*mm*)	46	150
h (*mm*)	1560	2300
l (*mm*)	2330	4200
f'_m (*MPa*)	11.5	0.5
E_m (*MPa*)	7800	1400
E_b=E_c (*MPa*)	33500	24700
I_b (x10^6 mm^4)	963	3125
I_c (x10^6 mm^4)	721	675
P_{ult} (*kPa*)	8.2	7.0
Δ_{ult} (mm)	16.0	15.0

5.3.1 Analytical models for "Regular" infills

Table 5.13 summarizes the analytical models for predicting the out-of-plane strength of "regular" masonry infills. The detailed descriptions of each analytical model can be found in Chapter 2. The model from BS 5628 is essentially the one-way arching model based on the principle of mechanics. For application of this model, the out-of-plane deflection of the infill is needed. In this case, two methods were used to determine the out-of-plane displacement. The first method is to relate the out-of-plane displacement with the axial shortening of the infill using geometry as described in Chapter 2; and the second method is to use the measured out-of-plane deflection from the experimental results. The compressive stress is taken as the lower of 0.85 f'_m and the compressive strength of the

mortar f'$_j$, as recommended by BS 5628 (2005). Example calculations of each model using test IF-S-FS can be found in Appendix A.

Table 5.13 Analytical models for the out-of-plane strength of "regular" masonry infills

Method	Out-of-Plane Strength	Notes
BS 5628 (2005)	$w_{fv} = \frac{8C}{h^2}(\gamma t - \Delta_o)$	$C = \phi_m f_{cv}(1-\gamma)t$ $\Delta_o = \frac{(\Delta_{exp}\ or\ \Delta_{axial})h}{4\gamma t}$ $\gamma = 0.9$
MSJC 2013	$q_{ult} = 729(f'_m)^{0.75}t^2\left\{\frac{\alpha}{l^{2.5}} + \frac{\beta}{h^{2.5}}\right\}$	$\alpha_s = \frac{1}{h}(EI_c h^2)^{0.25} \le 50$ $\beta_s = \frac{1}{l}(EI_b l^2)^{0.25} \le 50$
FEMA 273	$q_{ult} = \frac{0.7f'_m\lambda_2}{h/t} \times 144$	h/t: 5 — 10 — 15 — 25 λ_2: 0.129 — 0.060 — 0.034 — 0.013
Dawe and Seah (1989)	$q_{ult} = 800(f'_m)^{0.75}t^2\left\{\frac{\alpha}{l^{2.5}} + \frac{\beta}{h^{2.5}}\right\}$	$\alpha_s = \frac{1}{h}(EI_c h^2 + GJ_c th)^{0.25} \le 50$ $\beta_s = \frac{1}{l}(EI_b h^2 + GJ_b tl)^{0.25} \le 50$
Klinger et al. (1996)	$q = \frac{8}{h^2 l}\left\{M_{yv}[(l-h) + h\ln(2)] + M_{yh}\left(\frac{x_{yv}}{x_{yh}}\right)\ln\left(\frac{l}{l-h/2}\right)l\right\}$	$x_{yv} = \frac{tf'_m}{E\left[1 - \frac{h}{2\sqrt{\left(h/2\right)^2 + t^2}}\right]}$ $M_{yv} = \frac{0.85f'_m}{4}\left(t - x_{yv}\right)^2$
Angel (1994)	$q = \frac{2f'_m}{h/t}R_1R_2\lambda$	$R_1 = 1$ $R_2 = 0.357 + 7.14\times10^{-8}EI \le 1$ $\lambda = 0.154e^{-0.0985\frac{h}{t}}$
Moghaddam and Goudarzi (2010)	$q_r = min\{q_{cr}, q_{max}\}$ $q_{cr} = \left[0.85 - \left(0.12 + \frac{0.045}{\alpha}\right)\frac{f'_m}{E_m}\lambda^2\right]\frac{f'_m}{\lambda^2}$ $q_{max} = \frac{0.18E_m}{\left(0.12 + \frac{0.045}{\alpha}\right)\lambda^4}$	$K = \frac{384E_f I_b}{l^3}$ $\alpha = \frac{K}{\left(\frac{E_m tl}{h}\right)}$ $\lambda = \frac{h}{t}$

Table 5.14 presents the ratio of analytical to experimental ultimate strength (P_{ana}/P_{exp}) for the tests with "regular" infills. Ideally for design, the analytical model "should" give results that are lower than the test results to have a margin of safety for design. **Table 5.14** shows that for the three "regular" steel framed infills, all analytical models over-estimated their strength. FEMA 356 and and the model by Angel (1994) provided the closest estimate to the test results. On the contrary, for the RC framed infill (specimen IF-ND), all models under-estimated the strength of the infills except for the model by Klinger et al. (1996). The model by Moghaddam and Goudarzi (2010) was the most accurate with a P_{ana}/P_{exp} ratio of 0.99 which was followed by the models from BS 5628. Most models (except for Dawe and Seah's method) only relate the infill strength to frame flexural stiffness. From stiffness standpoint, the flexural stiffness (EI) of steel frame members is higher (2 times) than that of RC frame members (3.46×10^{12} vs. 1.77×10^{12} $N \cdot mm^2$) whereas the torsional stiffness (GJ) of steel frame members is significantly (140 times) lower than that of RC frame members (1.09×10^{12} vs. 7.81×10^{9} $N \cdot mm^2$). Therefore, the analytical strengths for steel framed infills would be even greater than for RC framed infills, which is clearly contradictory to the trend observed in the tests.

Table 5.14 Validation of existing analytical models for "regular" infills using experimental results

Test	Test Results P_{exp} (kPa)	P_{ana}/P_{exp}							
		BS 5628 (2005) $\Delta_o = \Delta_{as}$	BS 5628 (2005) $\Delta_o = \Delta_{exp}$	MSJC (2013)	FEMA 356	Dawe and Seah (1989)	Angel (1994)	Klingner et al. (1996)	Moghaddam and Goudarzi (2010)
C	30.6	1.83	2.05	1.86	1.02	2.04	1.23	3.51	2.02
FS	29	1.93	2.17	1.96	1.08	2.15	1.30	3.70	2.13
SW	29.9	2.33	2.62	2.25	1.31	2.46	1.58	4.49	2.58
Avg.		2.03	2.28	2.02	1.17	2.22	1.37	3.90	2.24
IF-ND	66.3	0.9	0.95	0.76	0.51	0.85	0.55	1.73	0.99

Table 5.15 presents the ratio of analytical to experimental ultimate strength (P_{ana}/P_{exp}) for the tests with "regular" infills conducted by other researchers. The table is separated into steel framed infills at the top and RC framed infills at the bottom. The same trend observed in this research is also supported by the previous results as well. The predicted strengths for steel framed infills are greater than the experimental strength whereas they are lower than the experimental results for RC framed infills.

Based on above, it is found that no methods perform universally well for both types of bounding frames, which is an indication that all methods were developed by calibrating against a specific data set and thus cannot cover all frame materials.

Table 5.15 Validation of existing analytical models for "regular" infills using experimental results from previous research

Test	Test Results P_{exp} (kPa)	P_{ana}/P_{exp}							
		BS 5628 (2005) $\Delta_o = \Delta_{as}$	BS 5628 (2005) $\Delta_o = \Delta_{exp}$	MSJC (2013)	FEMA 356	Dawe and Seah (1989)	Angel (1994)	Klingner et al. (1996)	Moghaddam and Goudarzi (2010)
WE2	19.2	5.25	4.68	2.00	2.46	2.19	5.67	83.32	1.31
WE4	11.2	3.50	1.42	1.58	1.67	1.74	3.44	59.22	0.86
WE8	13.4	3.52	2.63	1.53	1.68	1.67	3.48	59.58	0.73
WE5	7.8	1.50	0.03	0.86	0.76	0.95	0.95	28.89	0.32
#22	39.5	3.68	3.12	3.05	1.51	3.34	4.69	24.90	2.57
#18	26.6	1.87	1.82	1.38	0.66	1.52	1.28	12.54	1.32
#25	8.1	1.22	1.00	1.03	0.29	1.13	0.58	8.34	0.91
Avg.		2.93	2.10	1.63	1.29	1.79	2.87	39.54	1.15
Test 1	8.2	0.50	0.53	0.83	0.38	0.91	0.43	2.19	0.78
Inf_02	7.0	0.20	0.22	0.30	0.11	0.33	0.25	2.61	0.26
Avg.		0.35	0.38	0.57	0.25	0.62	0.34	2.37	0.52

Based on experimental observation, the marked lower strength of steel framed infills may be attributed to the following factors. First, the top of steel framed infill tended to slip out from the frame at some point of loading which prevented effective arching in the vertical direction. This was not observed in the RC framed infill test. The bond between concrete and mortar is better in comparison with steel and mortar and unless the bond can be ensured at the steel and mortar interface, full arching strength cannot be relied upon for steel framed infills. Second, the steel frame member is more prone to torsional deformation than RC frame members. It is conceivable that compressive force caused by arching acting on the flange of the steel, if not through the center of the web, may cause twisting of the steel frame, which in turn may enable the slipping out of the infill. It can be concluded that to improve the analytical method, one needs to either include the interfacial bond as a factor or ensure the bond is maintained throughout the loading.

5.3.2 Analytical models for infills with prior in-plane damage

The only analytical model available for evaluating out-of-plane strength of masonry infills with prior in-plane damage is the model proposed by Angel (1994). The model includes a strength reduction factor (R_1) for prior in-plane damage consideration and is expressed below:

$$R_1 = \left[1.08 - 0.015\left(\frac{h}{t}\right) - 0.00049\left(\frac{h}{t}\right)^2 + 0.000013\left(\frac{h}{t}\right)^3\right]^{\frac{\delta}{2\delta_{cr}}} \qquad [5.1]$$

The ratio ($\delta/2\delta_{cr}$) is defined as the applied in-plane deflection before the out-of-plane loading, δ, to the in-plane deflection at the cracking load δ_{cr}. The cracking load for steel framed infills was found to be 77.5 *kN* from the in-plane loading on specimen IF-S-D1 and the resulting deflection was 5.2 *mm.* For the RC framed infills, specimens IF-RC-D1, IF-RC-ID, and IF-RC-D2 had observed cracking at in-plane deflections of 6.5, 7.2, and 8.7 *mm* respectively. **Table 5.16** compares the experimental and analytical (Angel 1994) strength reduction for the infills with prior in-plane loading.

Table 5.16 Validation of strength reduction factor for infills with prior in-plane loading

Test	$\delta/2\delta_{cr}$	Prior In-Plane Damage Strength Reduction Factor (R_1)	
		Test Result	Angel (1994)
IF-S-D1	0.5	0.90	0.94
IF-S-D2	1.84	0.58	0.78
IF-RC-D1	0.5	0.67	0.94
IF-RC-ID	0.93	0.57	0.88
IF-D2	1.53	0.40	0.82

It is found that the model by Angel (1994) under-predicted the reduction in strength for all specimens. In other words, the model overestimates the out-of-plane capacity of an infill

which has sustained prior in-plane damage. The higher the degree of damage in the specimen, the greater the discrepancy between the actual and predicted strengths. Specimen IF-S-D1 with the lowest degree of damage had the closest result. In the case of specimens IF-S-D2 and IF-RC-D2 with prior in-plane loading to the in-plane capacity of the infill, a larger discrepancy between the test and the model results was observed.

5.3.3 Validation of analytical models for infills with a top gap

For the treatment of gap effect, three existing analytical models adopt two different approaches as seen in **Table 5.17**. Dawe and Seah (1989) and MSJC (2013) simply reduce the standard two-way arching equation to one-way in the direction where boundary supports are available. However, neither considers the gap size. On the other hand, BS 5628 (2005) method specifies a gap size limit (eqn. [2.5]) below which arching action hs the potential to develop, albeit at a lesser degree. This is to recognize that the rigid body rotation of the infill segment after cracking may still be able to close the gap and make the contact with the boundary frame. For the method proposed by BS 5628, the maximum gap that can exist and still allow arching to possibly develop is first calculated and was determined to be 26.8 mm for top gaps. The gap size for specimens IF-RC-TG was 10 mm which met the specified limit and the arching action had the potential to be developed in the vertical direction. During testing however, at no point did the arching of the infill overcome the top gap and allow vertical arching. Using Eqn. [2.4], the required out-of-plane deflection to overcome a 10 mm top gap was 30.2 *mm*. For all tested specimens with a 10 *mm* top gap, the maximum out-of-plane displacement was well below 10 *mm.* This scenario can lead to engineers over-estimating the strength of infills with a top gap by

assuming vertical arching can still occur. Maximum allowable gap equation for arching to still occur is therefore only a theoretical maximum gap size when the maximum gap is a function of the out-of-plane deflection. Additional research is required to formulate an analytical formula for the maximum allowable gap size for arching to occur.

Table 5.17 Analytical models for the out-of-plane strength of masonry infills with a top gap

Method	Out-of-Plane Strength	Notes
BS 5628 (2005) *horizontal only	$w_{fv} = \frac{8C}{h^2}(\gamma t - \Delta_o)$	$C = \phi_m f_{cv}(1-\gamma)t$ $\Delta_o = \frac{(\Delta_{exp}\ or\ \Delta_{axial})h}{4\gamma t}$ $\gamma = 0.9$
MSJC 2013	$q_{ult} = 729(f'_m)^{0.75}t^2\left\{\frac{\alpha}{l^{2.5}}\right\}$	$\alpha_s = \frac{1}{h}(EI_c h^2)^{0.25} \leq 50$
Dawe and Seah (1989)	$q_{ult} = 800(f'_m)^{0.75}t^2\left\{\frac{\alpha}{l^{2.5}}\right\}$	$\alpha_s = \frac{1}{h}(EI_c h^2 + GJ_c th)^{0.25} \leq 75$

Table 5.18 presents the comparison between the experimental and analytical results of the infills with a 10 *mm* top gap. Sample calculations can be found in Appendix B.

Table 5.18 Valididtidy of analytical models for infills with a top gap

ID	Test Result	P_{ana}/P_{exp}			
		BS 5628 (2005)		Dawe and Seah (1989)	MSJC (2013)
	P_{exp} (kPa)	Horizontal Arching Strength	Horizontal Arching with $\Delta_o = \Delta_{exp}$		
IF-S-TG	16.6	1.35	1.38	1.30	1.18
IF-RC-TG	18.5	1.20	1.23	0.98	0.90

As seen in the table, BS 5628 (2005) provides an over-estimate for both the steel framed and RC framed specimens. The models by Dawe and Seah (1989) and MSJC (2013) over-predict the strength for the steel framed specimens while under-predicting results for the RC framed specimen but with a smaller margin of difference. It is concerning that these

models over-predicted the strength of the infills, they are only considering arching in one-direction and are not considering the additional strength from the third boundary (bottom boundary). However, more data is needed to make further assessment on whether this level of accuracy can be maintained for different gap sizes and gap locations.

CHAPTER 6 SUMMARY AND CONCLUSION

This study was part of an on-going research on the out-of-plane strength and behaviour of masonry infills bounded by steel/RC frames. Built on previous studies on RC framed infills, the objective of this study was focused on behaviour and strength of steel framed masonry infills as affected by several influential parameters including boundary conditions, interfacial gaps, prior in-plane damage and vertical loading presence. This study consisted of seven steel framed concrete masonry infills tested under out-of-plane loading applied through an air bag. All the test specimens were built with the same geometry as used in the previous phases of this research study and the infills were constructed using half-scale standard 200 *mm* concrete masonry units. The experimental results were presented and discussed in terms of pressure vs. displacement curves, cracking pattern, failure mode, and the vertical and horizontal displacement profiles along the centerline axis at different loading stages. The effects of the above-mentioned parameters were assessed and described using the experimental results. The validity of several analytical methods for out-of-plane strength was evaluated using the experimental results.

6.1 CONCLUSIONS

The following conclusions were drawn from this study:

Effect of boundary frame material:

- A steel framed infill attained less ultimate load than a RC framed counterpart. For "regular" infills, when bounded by a steel frame, there was reductions in both cracking load (>50%) and ultimate capacity (>50%) when compared with a RC framed infill.

- Some of the steel framed specimens showed a top beam interface slip out due to weak bond between steel and mortar surfaces. This is believed to be a main contributor of lower strength of steel framed infills than RC framed infills.

Effect of boundary frame condition:

- Providing a fully supported bottom beam of the bounding frame did not have any significant effect on the strength of the infill
- The inclusion of web stiffeners on the steel boundary beams did not result in an increase in strength or ductility, the observed cracking pattern showed an increase in arching action, but the infill still failed due to web shear failure at the same strength.

Effect of top gap:

- Experimental observation showed that the infill was not able to close the 10 *mm* top gap to allow the arching action to develop in the vertical direction.
- The top gap changed the failure mode from web shear failure through two-way arching action to vertical tension cracks running parallel to the boundary columns, which is more comparable to a yield line pattern of a three-side supported panel.
- The decrease in ultimate load for steel boundary frame and RC frame specimens were 43% and 72% respectively.
- Accompanying the large decrease in strength was a severely reduced ductility, the ultimate out-of-plane displacement was reduced by 56% and 78% for the steel and RC framed specimens respectively.

Effect of prior in-plane damage:

- For both RC framed and steel framed infills, the strength reduction from in-plane damage is a function of the degree of in-plane damage sustained.
- Looking at the results from the RC framed specimens, it seems to indicate a bi-linear correlation, the steel framed infills showed less reduction for a similar damage level, but more data is required to establish the correlation.

Effect of combined in-plane damage and loading:

When the in-plane load which has resulted in in-plane damage on the infill is kept in place while the out-of-plane loading is being applied, the out-of-plane strength and ductility of the infill experiences further reduction, from 9.7% to 36.6% and 40.7% to 55.1% respectively, when compared with the case where the in-plane load cauing in-plane damage was removed during the out-of-lane loading

Effect of vertical loading:

- The presence of vertical load, applied through the top boundary beam, was found to result in significant reductions in cracking load, ultimate load and the ductility of the infill.
- The observed failure was initiated by the top infill slip out and formation of vertical cracks underneath the loading points. It is believed that the bending deformation caused by the vertical load on the beam has actually reduced the contact between the beam and infill.

- It is cautioned that when considering vertical load effect, the application method needs to be taken into account.

Evaluation of analytical models:

- In general, the analytical models for "regular infills" under-predicts the strength of RC framed infills while over-estimating the strength of the steel framed infills. None of them can provide close estimates for both steel and RC frames infills.
- The analytical model for prior in-plane damage underestimates the reduction in the out-of-plane strength of infills.
- Current design equations for maximum allowable top gap for arching to still occur are inadequate.
- The analytical models for gap effect performed reasonably well while it is noted that more test data is needed to confirm. The fact that the gapped infills essentially behave more or less in one-way arching seems to suggest that analytical models are better developed for one-way arching consideration.

6.2 RECOMMENDATIONS FOR FUTURE WORK

While a general behavioral trend of steel framed infills vs. RC framed infills is presented and discussed, more experimental results are in need to quantify the effect of various parameters on the infill strength and how they differ for steel and RC bounding frames. In that context, the following future work is recommended.

- More specimens are required to understand the bonding effect between infill and its bounding frames of either steel or RC material. Specimens with steel frames but with slipping prevented should be tested to be compared with specimens of this study.
- More specimens are required to investigate the frame boundary conditions, in particular, whether the low torsional stiffness of steel member has any marked effect on the strength difference between steel and RC framed infills.
- More specimens with a steel boundary frame subjected to different degrees of prior in-plane damage are needed to develop correlations between damage and strength.
- More testing is required to produce an equation for maximum allowable gap for arching to occur. Maximum gap is a function of both geometry and out-of-plane deflection.
- More testing is needed to evaluate the effect of vertical load including application methods and magnitudes on the out-of-plane strength of steel/RC framed infills.

REFERENCES

Anderson, C. (1984). Arching action in transverse laterally loaded masonry wall panels. *The Structural Engineer*, *62*(1), 12.

Angel, R., Abrams, D. P., Shapiro, D., Uzarski, J., & Webster, M. (1994). *Behavior of reinforced concrete frames with masonry infill walls. Engineering, Civil.* University of Illinois at Urbana-Champaign.

ANSI 41.1: *Building code requirements for masonry.* (1953). Washington: American National Stadards Association.

ASTM:C1314. *Standard Test Method for Compressive Strength of Masonry Prisms*, ASTM International (2015). https://doi.org/10.1520/C1314-14.2

ASTM. *Standard Test Methods for Sampling and Testing Concrete Masonry Units and Related Unit*, Annual Book of ASTM Standards (2016).

ASTM C270. (2007). *Standard Specification for Mortar for Unit Masonry*. United States: American Society for Testing and Material., 2–13. https://doi.org/10.1520/C0270-14A.

ASTM International. *Standard Test Method for Compressive Strength of Hydraulic Cement Mortars (Using 2-in. or [50-mm] Cube Specimens)* Annual Book of ASTM Standards (2016).

ATC. (1997). FEMA 273: *NEHRP Guidelines for the seismic rehabilitation of buildings. Basic procedures manual*.

BS 5628 *"Code practice for use of masonry: Structural use of unreinforced masonry."* (2005). London: British Standards Institution.

Cohen, E., & Laing, E. (1956). *Discussion to 'Arching action theory of masonry walls.* Journal of the Structural Division, ASCE, 82(5), 1067-28-1067–40.

CSA S304-14. (2014). *Design of Masonry Structures*, https://doi.org/10.1080/09613218309442127

Dafnis, A., Kolsch, H., & Reimerdes, H.-G. (2002). *Arching in Masonry Walls Subjected to Earthquake Motions*. J. Struct. Eng. https://doi.org/10.1061/(ASCE)0733-9445(2002)128:2(153)

Dawe, J. L., & Seah, C. K. (1989). *Behaviour of masonry infilled steel frame*s. *Canadian Journal of Civil Engineering*, *16*(6), 865–876. https://doi.org/10.1139/l89-129

Drysdale, R. G. (2005). *Mechanics of Rigid Arching*. In Masonry Structures Behaviour and Design (pp. 334–338). Canadian Masonry Design Center.

Flanagan, R., & Bennett, R. (1999). *Bidirectional behavior of structural clay tile infilled frames*. Journal of Structural Engineering, *125*(1985), 236–244. https://doi.org/10.1061/(ASCE)0733-9445(1999)125:3(236)

Flanagan, R. D., & Bennett, R. M. (1999). *Arching of Masonry Infilled Frames: Comparison of Analytical Methods*. Practice Periodical on Structural Design and Construction, *4*(3), 105–110. https://doi.org/10.1061/(ASCE)1084-0680(1999)4:3(105)

Frederiksen, V. T. (1992). *Membrane effect in laterally loaded masonry walls: a second order phenomenon*. In Proceedings of the 6th Canadian Masonry Symposium (pp. 537–547). Saskatoon, Saskatchewan.

Furtado, A., Rodrigues, H., Arêde, A., & Varum, H. (2016). *Experimental evaluation of out-of-plane capacity of masonry infill walls.* Engineering Structures. Procedia Engineering, 111, 48–63.

Gabrielsen, B., Kaplan, K., & Wilton, C. (1975). *A study of arching in non-reinforced masonry walls*. Scientific Services Inc., *SSI 748*(1).

Gabrielsen, B., & Wilton, C. (1974). *Shock tunnel tests of arched wall panels*. San Mateo, CA. Retrieved from http://www.dtic.mil/docs/citations/ADA006682

Griffith, M. C., Vaculik, J., Lam, N. T. K., Wilson, J., & Lumantarna, E. (2007). *Cyclic testing of unreinforced masonry walls in two-way bending.* Earthquake Engineering and Structural Dynamics, *36*(6), 801–821. https://doi.org/10.1002/eqe.654

Hendry, A. . (1981). *Structural brickwork*. Halsted Press. London.

Klinger, R. E., Rubiano, N. R., Bashandy, T., & Sweeney, S. C. (1996). *Evaluation and analytical verification of shaking table data from infilled frames*. In Eleventh World Conference on Earthquake Engineering (pp. 1–8).

McDowell, E. L., McKee, K. E., & Sevin, E. (1956). *Arching action theory of masonry walls*. Journal of the Structural Division, Proceedings, American Society of Civil Engineers, *82*(2), 915–918.

Moghaddam, H., & Goudarzi, N. (2010). *Transverse resistance of masonry infills*. ACI Structural Journal, *107*(4), 461–467.

Monk, C. B. (1958). *Resistance of structural clay masonry to dynamic forces: A design manual for blast resistance*.

Morandi, P., Hak, S., & Magenes, G. (2014). *In-plane Experimental Response of Strong Masonry Infills*. In 9th International Masonry Conference, July 7, 8, 9; 2014; Guimarães (pp. 1–12). Istanbul. https://doi.org/10.13140/2.1.4206.5280

MSJC. (2013). *Building Code Requirements for Masonry Structures*. Masonry Standards Joint Commitee.

Sepasdar, R. (2017). *Experimental investigation on the out-of-plane behaviour of concrete masonry infilled RC frames*. Dalhousie University.

Wang, C. (2017). *Experimental investigation on the out-of-plane behaviour of concrete masonry infilled frames*. Dalhousie University.

APPENDIX A OUT-OF-PLANE FLEXURAL STRENGTH CALCULATIONS

Infill Specification (IF-S-FS)	
Height	980 *mm*
Length	1350 *mm*
Thickness	90 *mm*
Net Thickness	34 *mm*
f'_m	8.8 *MPa*
f'_{mortar}	8.4 *MPa*
f_{tp}	0.8 *MPa*
f_{tn}	0.4 *MPa*
I_c, I_b	$17.2 \times 10^6 mm^4$

1. Moment capacity, tension controlled (CSA S304-14)

$$M_{rpa} = \phi_m f_{tp} S_p = 1.0x0.8x\frac{1000(90^2 - (90-34)^2)}{6} = \ 0.662\ kN \cdot m$$

$$M_{rn} = \left(\phi_m f_{tn} + P_f/A_e\right)S_n = (1.0x0.4 + 0)\frac{1000(90^2 - (90-34)^2)}{6} = \ 0.332\ kN \cdot m$$

2. Elastic Plate Analysis using Moment Coefficients

$$w_{f\ (Horizontal\ Bending)} = \frac{M_{rpa}}{\beta_{y1} h^2} = \frac{0.662}{0.05022x0.98^2} = 13.73\ kPa$$

$$w_{f\ (Vertical\ Bending)} = \frac{M_{rn}}{\beta_y h^2} = \frac{0.332}{0.0743x0.98^2} = 4.65\ kPa\ \ (Governs)$$

3. Failure line method

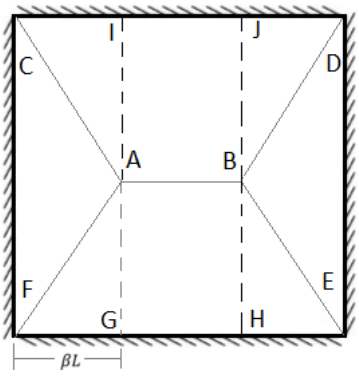

External Work (LoadxDeflection) = Internal Work (MomentxRotation)

$$\text{External Work} = 2 \cdot w_f \cdot \left(\frac{\beta L \cdot H \cdot \delta}{3}\right)_{C-F-G-I,D-E-H-J} + w_f \left(\frac{H \cdot \delta \cdot (L - 2\beta L)}{2}\right)_{G-H-I-J}$$

$$\text{External Work} = 0.6615 w_f \delta - 0.441 w_f \delta \beta$$

$$\theta_1 = \frac{\delta}{\beta L} \qquad \theta_2 = \frac{\delta}{H/2}$$

$$\text{Internal Work} = 4M_{rpa}\theta_1 \, H/2 + 4M_{rn}\theta_2 \beta L$$

$$\text{Internal Work} = 0.96\frac{\delta}{\beta} + 3.65\beta\delta$$

Equating Internal Work to External Work, β=0.375 yields the lowest pressure resistance of

$w_f = 7.92$ kPa

4. Yield line analysis

A similar solution to the Failure Line Method, but with an additional term in the internal work due to the crack along line A-B

$$\text{Internal Work} = 4M_{rpa}\theta_1 \, H/2 + 4M_{rn}\theta_2 \beta L + M_{rn}(L - 2\beta L)\theta_2$$

$$\text{Internal Work} = 0.961\frac{\delta}{\beta} + 1.823\delta\beta + 0.912\delta$$

Equating Internal Work to External Work, β=0.425 yields the lowest pressure resistance of

$w_f = 8.33\ KPa$

APPENDIX B OUT-OF-PLANE STRENGTH CALCULATIONS

Infill Specification (IF-S-FS)	
Height	980 *mm*
Length	1350 *mm*
Thickness	90 *mm*
Net Thickness	34 *mm*
f'_m	8.8 *MPa*
f'_{mortar}	8.4 *MPa*
I_c, I_b	$17.2 \times 10^6 mm^4$

1. Two-way arching using calculated deflection BS 5628 (2005)

$$g_{ov} = \varepsilon_{cv} h = \frac{f_{cv}}{E_m} h = \frac{f_{cv}}{850 \times 8.8} 980 = 0.131 f_{cv}$$

$$\Delta g_o = \frac{g_{ov} h}{4\gamma t} = \frac{0.131 f_{cv} \cdot 980}{4 \cdot 0.9 \cdot 90} = 0.396 f_{cv}$$

$$C = \phi_m f_{cv} (1-\gamma) t b = 1(f_{cv})(1-0.9)90(1000) \cdot 10^{-3} = 9 f_{cv}$$

$$w_{fv} = \frac{8C}{h^2}(\gamma t - \Delta g_o) = \frac{8(9 f_{cv})}{0.98^2}(0.9(90) - 0.396 f_{cv}) \cdot 10^{-3} = 6.07 f_{cv} - 0.0298 f_{cv}^2$$

Now add in the contribution from the horizontal direction

$$\Delta g_o = 0.399 f_{cv} = \frac{g_{oh} \mathrm{l}}{4\gamma t}; \quad g_{oh} = \frac{0.399 f_{cv}(0.9(90)4)}{1350} = 0.09576 f_{cv}$$

$$\varepsilon_{ch} = \frac{g_{oh}}{l} = \frac{0.09576 f_{cv}}{1350} = 0.0000709 f_{cv}$$

$$f_{ch} = \varepsilon_{ch} E_m = 0.0000709 f_{cv}(850 \times 8.8) = 0.528 f_{cv}$$

$$C = \phi_m f_{ch} (1-\gamma) t b = 1(0.528 f_{cv})(1-0.9)90(1000) \cdot 10^{-3} = 4.75 f_{cv}$$

$$w_{fh} = \frac{8C}{l^2}(\gamma t - \Delta g_o) = \frac{8(4.75 f_{cv})}{1.35^2}(0.9 \cdot 90 - 0.399 f_{cv}) = 1.688 f_{cv} - 0.00832 f_{cv}^2$$

$$w_f = w_{fh} + w_{fv} = 7.758 f_{cv} - 0.0381 f_{cv}^2$$

Take the compressive strength as the lower of 0.85 f'_m and f'_{mortar}.

$0.85 f'_m = 7.48$ *MPa*

$w_f = 57.16$ *kPa*

2. Two-way arching using experimental deflection BS 5628 (2005)

$\Delta g_o = 7.6\,mm$

$C = \phi_m f_{cv}(1-\gamma)tb = 1(f_{cv})(1-0.9)90(1000)\cdot 10^{-3} = 9f_{cv}$

$w_{fv} = \frac{8C}{h^2}(\gamma t - \Delta g_o) = \frac{8(9f_{cv})}{0.98^2}(0.9(90) - 7.6)\cdot 10^{-3} = 5.503 f_{cv}$

Now add in the contribution from the horizontal direction

$g_{oh} = \frac{7.6(0.9(90)4)}{1350} = 1.824\,mm$

$\varepsilon_{ch} = \frac{g_{oh}}{l} = \frac{1.824}{1350} = 0.001351$

$f_{ch} = \varepsilon_{ch} E_m = 0.001351(850\times 8.8) = 10.1 > 7.48 \therefore f_{ch} = f_{cv}$

$C = \phi_m f_{cv}(1-\gamma)tb = 1(f_{cv})(1-0.9)90(1000)\cdot 10^{-3} = 9f_{cv}$

$w_{fh} = \frac{8C}{l^2}(\gamma t - \Delta g_o) = \frac{8(9f_{cv})}{1.35^2}(0.9\cdot 90 - 7.6) = 2.898\, f_{cv}$

$w_f = w_{fh} + w_{fv} = 5.503 f_{cv} + 2.898 f_{cv} = 8.401 f_{cv}$

Take the compressive strength as the lower of 0.85 f'$_m$ and f'$_{mortar}$.

0.85f'$_m$=7.48 *MPa*

$w_f = 62.84\,kPa$

3. **MSJC 2013**

$\alpha_s = \frac{1}{h}(EI_c h^2)^{0.25} \le 50$

$\alpha_s = \frac{1}{980}(201172\times 17.1\times 10^6\times 980^2)^{0.25} = 43.5$

$\beta_s = \frac{1}{l}(EI_b l^2)^{0.25} \le 50$

$\beta_s = \frac{1}{1350}(850\times 8.8\times 17.2\times 10^6\times 1350^2)^{0.25} = 37.1$

$q_{ult} = 729(f'_m)^{0.75} t^2 \left\{\frac{\alpha}{l^{2.5}} + \frac{\beta}{h^{2.5}}\right\}$

$q_{ult} = 729(8.8)^{0.75}(90)^2 \left\{\frac{43.5}{(1350)^{2.5}} + \frac{37.1}{(980)^{2.5}}\right\}$

$q_{ult} = 56.8\,kPa$

4. Dawe and Seah (1989)

$$\alpha_s = \frac{1}{h}(EI_c h^2 + GJ_c th)^{0.25} \leq 50$$

$$\alpha_s = \frac{1}{980}(850 \times 8.8 \times 17.1 \times 10^6 \times 980^2 + 7352.6 \times 14.76 \times 10^7 \times 90 \times 980)^{0.25} = 43.8$$

$$\beta_s = \frac{1}{l}(EI_b h^2 + GJ_b tl)^{0.25} \leq 50$$

$$\beta_s = \frac{1}{1350}(850 \times 8.8 \times 17.2 \times 10^6 \times 1350^2 + 7352.6 \times 14.76 \times 10^7 \times 90 \times 1350)^{0.25} = 37.3$$

$$q_{ult} = 800(f'_m)^{0.75} t^2 \left\{\frac{\alpha}{l^{2.5}} + \frac{\beta}{h^{2.5}}\right\}$$

$$q_{ult} = 800(8.8)^{0.75}(90)^2 \left\{\frac{43.8}{(1350)^{2.5}} + \frac{37.3}{(980)^{2.5}}\right\} = 62.3\ kPa$$

5. FEMA 356

$$\frac{h}{t} = \frac{980}{90} = 10.89$$

h/t	5	10	15	25
λ_2	0.129	0.060	0.034	0.013

Using linear interpolation,

$$\lambda_2 = 0.05538$$

$$q_{ult} = \frac{0.7 f'_m \lambda_2}{h/t} \times 144 = 31.3\ kPa$$

6. Klinger et al. (1996)

$$x_{yv} = \frac{t f'_m}{E\left[1 - \frac{h}{2\sqrt{\left(h/2\right)^2 + t^2}}\right]} = \frac{90 \times 8.8}{8.8 \times 850\left[1 - \frac{980}{2\sqrt{\left(980/2\right)^2 + 90^2}}\right]} = 6.4355\ mm$$

$$x_{yh} = \frac{tf'_m}{E\left[1 - \frac{l}{2\sqrt{\left(l/2\right)^2 + t^2}}\right]} = \frac{90 \times 8.8}{8.8 \times 850\left[1 - \frac{1350}{2\sqrt{(1350)^2 + 90^2}}\right]} = 12.0704\ mm$$

$$M_{yv} = \frac{0.85f'_m}{4}\left(t - x_{yv}\right)^2 = \frac{0.85 \times 8.8}{4}(90 - 6.4355)^2 = 13058.26\ N \cdot mm$$

$$M_{yh} = \frac{0.85f'_m}{4}\left(t - x_{yh}\right)^2 = \frac{0.85 \times 8.8}{4}(90 - 12.0704)^2 = 11356.57\ N \cdot mm$$

$$q = \frac{8}{h^2 l}\left\{M_{yv}[(l-h) + h\ln(2)] + M_{yh}\left(\frac{x_{yv}}{x_{yh}}\right)\ln\left(\frac{l}{l - h/2}\right)l\right\}$$

$$q$$

$$= \frac{8}{980^2 \times 1350}\left\{13058.26[(1350 - 980) + 980\ln(2)]\right.$$

$$\left. + 11356.57\left(\frac{6.4355}{12.0704}\right)\ln\left(\frac{1350}{1350 - 980/2}\right)1350\right\} = 0.10729\ MPa = 107.29\ kPa$$

7. Angel (1994)

$$R_1 = 1$$

$$R_2 = 0.357 + 7.14 \times 10^{-8} E\left(\frac{0.145038\ kips}{1MPa}\right) I\left(\frac{1in}{25.4mm}\right)^4 \leq 1$$

$$R_2 = 0.357 + 7.14 \times 10^{-8} \times 850 \times 8.8\left(\frac{0.145038}{1}\right) 17.1 \times 10^6 \left(\frac{1}{25.4}\right)^4 = 0.443$$

$$\lambda = 0.154e^{-0.0985\frac{h}{t}} = 0.154e^{-0.0985\frac{980}{90}} = 0.0527$$

$$q = \frac{2f'_m}{h/t} R_1 R_2 \lambda = \frac{2 \times 8.8}{980/90} \times 1 \times 0.443 \times 0.0527 = 0.0377\ MPa = 37.7\ kPa$$

8. Moghaddam and Goudarzi (2010)

$$K = \frac{384E_f I_b}{l^3} = \frac{384 \times 201172 \times 17.1 \times 10^6}{1350^3} = 536900$$

$$\alpha = \frac{K}{\left(\frac{E_m tl}{h}\right)} = \frac{536900}{8.8 \times 850 \times 90 \times \frac{1350}{980}} = 0.579$$

$$\lambda = \frac{h}{t} = \frac{980}{90} = 10.89$$

$$q_r = min\{q_{cr}, q_{max}\}$$

$$q_{cr} = \left[0.85 - \left(0.12 + \frac{0.045}{\alpha}\right)\frac{f'_m}{E_m}\lambda^2\right]\frac{f'_m}{\lambda^2}$$

$$q_{cr} = \left[0.85 - \left(0.12 + \frac{0.045}{0.579}\right)\frac{8.8}{8.8 \times 850}\lambda^2\right]\frac{8.8}{10.89^2} = 0.06176\ MPa = 61.76\ kPa$$

$$q_{max} = \frac{0.18E_m}{\left(0.12 + \frac{0.045}{\alpha}\right)\lambda^4} = \frac{0.18 \times 8.8 \times 850}{\left(0.12 + \frac{0.045}{0.579}\right)10.89^4} = 0.484\ MPa = 484\ kPa$$

$$q_r = 61.76\ kPa$$

CALCULATIONS FOR INFILL WITH A 10 *MM* TOP GAP

Infill Specification (IF-S-TG)	
Height	980 *mm*
Length	1350 *mm*
Thickness	90 *mm*
Net Thickness	34 *mm*
f'_m	8.8 *MPa*
f'_{mortar}	10.4 *MPa*

1. Arching using calculated deflection BS 5628 (2005)

$$g_{ov} = 10\ mm$$

$$\Delta g_o = \frac{g_{ov}h}{4\gamma t} = \frac{10 \cdot 980}{4 \cdot 0.9 \cdot 90} = 30.25\ mm$$

*The center of the infill would need to deflect 30.25 *mm* in order for vertical arching to occur. Only calculate horizontal arching

$$g_{oh} = \varepsilon_{cv}l = \frac{f_{ch}}{E_m}l = \frac{f_{ch}}{850 \times 10.4}1350 = 0.153f_{ch}$$

$$\Delta g_o = \frac{g_{oh}l}{4\gamma t} = \frac{0.153f_{cv} \cdot 1350}{4 \cdot 0.9 \cdot 90} = 0.636f_{cv}$$

$$C = \phi_m f_{ch}(1-\gamma)tb = 1(f_{ch})(1-0.9)90(1000) \cdot 10^{-3} = 9f_{ch}$$

$$w_{fh} = \frac{8C}{l^2}(\gamma t - \Delta g_o) = \frac{8(9f_{ch})}{1.35^2}(0.9(90) - 0.636f_{ch}) \cdot 10^{-3} = 3.20f_{ch} - 0.0252f_{ch}^2$$

Take the compressive strength as the lower of 0.85 f'$_m$ and f'$_{mortar}$.

0.85f'$_m$=7.48 *MPa*

$w_f = 22.3\ kPa$

2. Arching using experimental deflection BS 5628 (2005)

$\Delta g_o = 3.3\ mm$

$C = \phi_m f_{ch}(1-\gamma)tb = 1(f_{ch})(1-0.9)90(1000) \cdot 10^{-3} = 9f_{ch}$

$$w_{fh} = \frac{8C}{l^2}(\gamma t - \Delta g_o) = \frac{8(9f_{ch})}{1.35^2}(0.9(90) - 3.3) \cdot 10^{-3} = 3.07f_{ch}$$

Take the compressive strength as the lower of 0.85 f'$_m$ and f'$_{mortar}$.

0.85f'$_m$=7.48 *MPa*

$w_f = 23.0\ kPa$

3. **MSJC 2013**

$$\alpha_s = \frac{1}{h}(EI_c h^2)^{0.25} \leq 50$$

$$\alpha_s = \tfrac{1}{980}(201172 \times 17.1 \times 10^6 \times 980^2)^{0.25} = 43.5$$

$\beta_s = 0$

$$q_{ult} = 729(f'_m)^{0.75} t^2 \left\{\frac{\alpha}{l^{2.5}} + \frac{\beta}{h^{2.5}}\right\}$$

$$q_{ult} = 729(8.8)^{0.75}(90)^2 \left\{\frac{43.5}{(1350)^{2.5}} + \frac{0}{(980)^{2.5}}\right\}$$

$q_{ult} = 19.6\ kPa$

4. Dawe and Seah (1989)

$$\alpha_s = \frac{1}{h}(EI_c h^2 + GJ_c th)^{0.25} \leq 50$$

$$\alpha_s = \frac{1}{980}(850 \times 8.8 \times 17.1 \times 10^6 \times 980^2 + 7352.6 \times 14.76 \times 10^7 \times 90 \times 980)^{0.25} = 43.8$$

$\beta_s = 0$

$$q_{ult} = 800(f'_m)^{0.75} t^2 \left\{ \frac{\alpha}{l^{2.5}} + \frac{\beta}{h^{2.5}} \right\}$$

$$q_{ult} = 800(8.8)^{0.75}(90)^2 \left\{ \frac{43.8}{(1350)^{2.5}} + \frac{0}{(980)^{2.5}} \right\} = 21.5\ kPa$$

CALCULATIONS OF STRENGTH REDUCTION FACTOR FOR INFILLS WITH PRIOR IN-PLANE DAMAGE

Infill Specification (IF-S-D2)	
Height	980 *mm*
Length	1350 *mm*
Thickness	90 *mm*
f'_m	11.0 *MPa*
f'_{mortar}	13.0 *MPa*
δ	19.1 *mm*
δ_{cr}	5.2 *mm*

1. Angel (1994)

$$R_1 = \left[1.08 - 0.015 \left(\frac{h}{t} \right) - 0.00049 \left(\frac{h}{t} \right)^2 + 0.000013 \left(\frac{h}{t} \right)^3 \right]^{\frac{\delta}{2\delta_{cr}}}$$

$$R_1 = \left[1.08 - 0.015 \left(\frac{980}{90} \right) - 0.00049 \left(\frac{980}{90} \right)^2 + 0.000013 \left(\frac{980}{90} \right)^3 \right]^{\frac{19.1}{2\times 5.2}}$$

$$R_1 = 0.78$$